Dissecting the Structure and Function Relationship in *Drosophila* Dendrite Development with the help of Computational Modelling

by / *von*

ANDRÉ FERREIRA CASTRO

from / *aus*

LISSABON, PORTUGAL

JOHANN WOLFGANG GOETHE-UNIVERSITÄT, FRANKFURT AM MAIN

BIOLOGICAL SCIENCES DEPARTMENT

FRANKFURT AM MAIN, 2020
(D30)

Dissecting the Structure and Function Relationship in *Drosophila* Dendrite Development with the help of Computational Modelling

by / *von*

ANDRÉ FERREIRA CASTRO

from / *aus*

LISSABON, PORTUGAL

PHD DISSERTATION SUBMITTED TO THE FACULTY OF BIOLOGICAL SCIENCES

DISSERTATION ZUR ERLANGUNG DES DOKTORGRADES DER NATURWISSENSCHAFTEN VORGELEGT BEIM FACHBEREICH BIOWISSENSCHAFTEN

JOHANN WOLFGANG GOETHE-UNIVERSITÄT, FRANKFURT AM MAIN

BIOLOGICAL SCIENCES DEPARTMENT

FRANKFURT AM MAIN, 2020

(D30)

Vom Fachbereich Biowissenschaften der Johann

Johann Wolfgang Goethe – Universität als Dissertation angenommen

Dekan:
Prof. Dr. Sven Klimpel

Betreuer im Fachbereich:
Prof. Dr. Amparo Acker-Palmer

Externer Betreuer:
Dr. Hermann Cuntz

Gutachter:
Prof. Dr. Amparo Acker-Palmer
Prof. Dr. Gaia Tavosanis

Datum der Disputation:

To my Mother, Sister, Grandmother and Anuschka.

Contents

Acknowledgements

First and foremost, I would like to thank Dr. Hermann Cuntz for the opportunity given to me to conduct my research.

Second, I would like to thank Prof. Dr. Gaia Tavosanis for her guidance and support during the experimental part of this project. To Prof. Dr. Peter Jedlicka and to Prof. Dr. Albert Cardona, for showing great generosity and much appreciated support. And to Prof. Dr. Amparo Acker-Palmer, for interesting and important feedback.

A special thanks to all my fellows from the Cuntz, Tavosanis and Moore labs. Particular acknowledgements to Dr. Felix Effenberger, Marvin Weigand, Lothar Baltruschat, Dr. Tomke Stuerner, Dr. Yun Jin Pai and Fatma Rabia Urun for providing me with stimulant discussions.

A very special thanks to Anuschka Berthelius for her support and companionship during my graduate studies.

Last but not least, I want to thank my family, without their unconditional and unwavering support I would have never achieved my goals in life.

Zusammenfassung

Keywords: **Dendrite function, Dendrite growth, space-filling, da neurons, Fly, Self-organization, Model, Mechanotransduction, Computational Neuroanatomy**

Abstract

The study of the relationship between shape and function in nature plays an important role in the natural sciences since the beginning of the scientific revolution. In neuroscience, at the beginning of the 20^{th} century the seminal drawings of Ramón y Cajal enabled neuroscientists to identify neurons as the structural and functional units of the nervous system. Using the back then recently developed Golgi staining method, Ramon y Cajal produced for the time excellent depictions of axons and dendrites, providing the observation of a complete dendritic tree for the first time. Ramon y Cajal hypothesised that axonal processes are components of a neuron specialized in distributing electrical signals to postsynaptic cells, interfacing with those cells through synapses. While dendrites are tree-like structures of nerve cells designed for receiving and propagating signals to the cell body.

Dendritic trees exhibit many different patterns and sizes, with their length varying from a few micrometers to a few millimeters depending on the cell type and or developmental stage. Their branched structures generate compartments for electrical and chemical computing. They also serve as a means for the integration of signals flowing from presynaptic cells, or for sensory neurons, the outside environment. Besides, their branching pattern expands the surface of the cell allowing for synaptic contacts with a larger number of neighboring cells without significantly increasing its volume. This facilitates the connectivity of billions of cells densely packed in small volumes.

Even one century after Ramón y Cajal's groundbreaking contributions to neuroscience, one of the most fundamental questions in the field is still largely open, namely understanding how the shape of a neuron is adapted to its specific biological function. A systematic investigation of this question is challenging both technically and conceptually because neurons have diverse molecular, morphological, connectional and functional properties.

Over previous decades, a significant amount of research in the field of neu-

roanatomy provided new concepts to tackle the aforementioned problem. For example, new high-throughput methods allowed for acquiring comprehensive information about certain individual cells' anatomy and physiology.

As a result, two non-opposing principles have emerged trying to explain the structure-function relationship in dendrites: the principle of computational optimization and the principle of wiring optimization. Both paradigms agree upon the fact that structure and function closely follow one another, but they propose different rationales to explain the structural patterns found across different cell types. On one hand, the computational paradigm argues that cell patterning is driven by the need for the implementation of different algorithms required for the information processing at the local level. On the other hand, the wiring optimization paradigm argues that morphological cell structure maximizes the probability of connections between neurons, while at the same time keeping dendrite wiring length and volume to a minimum, thus recognizing neurons as obedient players of a larger orchestra.

Recently, the question of whether an increased understanding of growth processes of dendrites could aid in dissecting of the fully developed cell-type-specific dendrite morphology and function came into the focus of research. Conceivably, quantifying the development of dendrites may elucidate the developmental mechanisms underlying dendritic pattering and wiring, providing the basis for a deeper understanding of the observed structure-function neuronal diversity found in nature.

In the light of the preceding, dendritic arborisation (da) neurons of the *Drosophila melanogaster* larva PNS have proven to be an excellent model system for the study of such growth and patterning processes. Structure and function in these cell classes are intimately intertwined as here, class type-specific dendritic arbour differentiation processes are required to satisfy a given physiological need. Also, there exists a remarkable genetic toolkit that enables one to selectively and reproducibly label, image and manipulate each one of these sensory neuron classes. In this thesis, I address the aforementioned open problem by linking single-cell patterning, information processing and wiring optimization in sensory da neurons to behaviour in *Drosophila* larva.

In particular, I study Class I ventral peripherical dendritic arborization (c1vpda) neurons. These are a class of proprioceptive neurons that relay infor-

mation on the position of the larva's body back to the CNS during crawling behaviour to assure proper locomotion. Their stereotypical comb-like shaped dendritic branches spread along the body-wall, and they get noticeably deformed during crawling behaviour. The bending of the dendritic branches is hypothesised to be a possible mechanism to transduce the mechanosensory inputs arising from cuticle folding. Interestingly, c1vpda neurons do not obviously gain from satisfying optimal wiring constraints since they are required to pattern into a specific shape to fulfil their function. Therefore, I considered the da system to study how the specific functional requirements may be combined with optimal wiring constraints during development.

Although the molecular machinery of dendrite patterning in c1vpda neurons is well studied, the precise elaboration of the comb-like shaped dendrites of these cells remains elusive. Moreover, even though a lot of work has been put into the description and quantification of growth processes of the nervous system, there are still few solid and standardised models of arbour staging and patterning. Importantly, the defining parameters that determine the dendrite elaboration program that in turn is responsible for creating the final arbour morphology are still unknown. As a result, unraveling possible universal stages of dendrite elaboration shared between different model systems and cell types is challenging.

Thus, in order to understand the development of the fine regulation of branch outgrowth that leads to the observed terminal arbour morphology in the mature cell, I collected *in vivo*, long-term, non-invasive high temporal resolution time-lapse recordings of dendritic trees during the differentiation process in the embryo and its maturation phase in the larva. For further analysis, I developed new algorithms that quantified the structural changes in dendrite morphology in the time-lapse videos. My approach provides a framework to analyse such developmental data, or any dataset comprising continuous morphological dynamical processes in an unbiased way. Using these newly developed methods, I examine the development of a sample of c1vpda cells. I identified five stages of differentiation in these data: initial stem polarization, extension, pruning, stabilization, and isometric stretching during larval stages.

The beginning of the growth process is marked by the polarisation of the main stem. Subsequently, during the extension phase, branches emerge

interstitially from the existing main stem. Later, higher-order branches sprout from pre-existing lateral branches, increasing arbour complexity. This is followed by a pruning stage where developmental intermediate dendritic branches are removed. This step leads to a spatial rearrangement of the dendritic tree. The end of the pruning step is followed by a stabilization period where arbour morphology remains virtually unaltered in the embryo. After hatching from the egg, c1vpda dendrites experience an isometric scaling, with their branching complexity and pattern being invariant across all larval stages.

After dissecting the c1vpda dendrites spatiotemporal differentiation process, I established a link between dendritic shape and behaviour. I measured intracellular Ca^{++} activity in the dendrite branches of l1 larvae during forward locomotion, while simultaneously recording branch deformation using a dual genetic line. I reported that post-embryonic c1vpda dendrites Ca^{++} responses increased in freely crawling larvae. Furthermore, I showed strong correlations between Ca^{++} signal and deformation of the comb-like dendritic branches during body-wall contractions.

Then, using a geometrical model, I provided evidence that the pruning stage could reorganise the dendrite morphology to maximise mechanosensory responses during body wall contraction. I showed that the angle orientation of each side branch correlates with the bending curvature and thus with the mechanical displacement of the cell membrane during locomotion. During the pruning phase, I observed a preferential reduction of less efficient branches with low bending curvature, influencing the mechanisms of dendritic signal integration of c1vpda sensory neurons. I proceeded to quantify branch dynamics at single tip resolution during pruning, providing evidence that a simple random pruning mechanism is sufficient to remodel the tree structure compatible with the observed way.

I used these time-lapse data to constrain a new computational noisy growth model with random pruning based on optimal wiring principles, that generates highly realistic synthetic c1vpda morphologies. This model requires few parameters to generate highly accurate temporal development trajectories and morphologies at the single-cell level. Utilising this powerful data and model enabled me to investigate upon the hypothesis that a noisy dendrite growth and random pruning mechanism synergise to achieve dendritic trees

efficient in terms of both wiring and function. My discoveries disclose how single neurons can create functionally specialised dendrites while minimizing wiring costs, elucidating how general principles of self-organization may be involved in the generation of these structures.

Keywords: **Dendrite function, Dendrite growth, space-filling, da neurons, Fly, Self-organization, Model, Mechanotransduction, Computational Neuroanatomy**

List of Figures

List of Tables

List of Symbols

Symbol	Units	Description
CNS		Central nervous system
PNS		Peripheral nervous system
da		Dendritic arborization
c1		Class I
c2		Class II
c3		Class III
c4		Class VI
vpda		Ventral peripheral dendritic arborization
ddaD		Dorsal dendritic arborization
ddaE		Dorsal dendritic arborization
d	μm	Diameter of the neurite
l	μm	Length of the segment
R_m	$\Omega\mathrm{cm}^2$	Specific membrane resistance
R_{in}	$\Omega\mathrm{cm}^2$	Specific input resistance
C_m	$\mu\mathrm{Fcm}^{-2}$	Specific membrane capacitance
R_a	Ωcm	Specific axial resistance
I_i	nA	Ionic current
f	Hz	Frequency
Temp	°C	Temperature
Na^+		Sodium ion
Ca^{++}		Calcium ion
K^+		Potassium ion
t-SNE		t-distributed stochastic neighbor embedding
MDS		Multi dimensional scaling
AEL		After egg lay
SOP		Sensory organ precursor
d		Dorsal

l	Lateral
v	Ventral
v′	Ventral
es	External sensory
ch	chordotonal
DV	Dorso-ventral
MST	Minimum spanning tree
Aca	Anterior canthi
Pca	Posterior canthi
ECM	Extra cellular matrix
DNA	Deoxyribonucleic acid
RNA	Ribonucleic acid
NompC	No mechanoreceptor potential C
MS	Mechanosensitive Channels
D	Dimension
Dscam	Down syndrome cell adhesion molecule
GFP	Green fluorescent protein
EM	Electron microscope
SEM	Standard error of the mean
NB	Neuroblast
GCM	Ganglion Mother Cell
ATP	Adenosine Triphosphate

Chapter 1

Introduction

In this first part, the topic of the present thesis is put into a larger context and the fundamental goals of the study described in the subsequent chapters of the manuscript are specified. In the final part of this chapter, an overview of the thesis structure is given.

1.1 Context

1.1.1 Natural Kinds in Biology

Aristotle is probably one of the first documented thinkers who overtly asserted that objects can be separated into natural kinds, i.e. groups that are generated by an objective property with an informative role in interpreting reality. This tenet holds that there are objective methods to categorise objects into groups corresponding to natural subdivisions found in nature, rather than reflecting subjective human priors (Okasha, 2016).

A ramification of the natural kinds doctrine can be found in the shape–function paradigm. This organizational scheme presumably originated alongside the start of human scientific thinking and supports the existence of a tight relationship between shape and function in nature. It enjoys a great degree of success across many scientific branches such as physics, chemistry and biology (Dresselhaus et al., 2007; Powell, 2010; Moody, 2011). Particularly, this paradigm finds its way into neuroscience through a subfield named neuroanatomy. This branch of neuroscience is concerned with the quantification of the morphological properties of neuronal structures and circuits, and to a greater extent relates these morphological characteristics to their functional implications (Burke and Marks, 2002; Denk et al., 2012).

In the early 1900s, Ramón y Cajal collected an extraordinary number of images of neuronal cells across different animal species using the Golgi staining method (translated

into English in Ramon y Cajal, 1995). After careful comparative observation of his drawings, Cajal considered the dendrite patterns of the observed neurons one of the defining characteristics which separate the nervous tissue from the remaining living tissues. These observations drove him to propose what is called the **neuron doctrine**, identifying neurons as the structural and functional units of the nervous system. This initiated a century-long project of classifying distinct neuronal cell types that has experienced unprecedented success in recent years (Zeng and Sanes, 2017; Hodge et al., 2019).

In a broader perspective, the neuron doctrine and the neuronal classification project can only be understood by taking into account evolutive processes. The evolution of progressively more complex functions has been made possible by the evolution of more complex and specialized structural patterns, hence more complex connectivity and greater structural differences between individual neurons. However, how neurons grow into the patterns that enable the diverse behaviours observed in nature, remains largely unknown (Lefebvre et al., 2015). Throughout this thesis, I will address this question, by linking single-cell patterning, information processing and wiring optimization to behaviour in *Drosophila melagonaster* sensory da neurons.

The nervous systems of any species are some of the most complex objects known to humankind. As a result, disclosing the relationship between structure and function is an extremely difficult task that poses conceptual and technological problems (Bota and Swanson, 2007; Tasic et al., 2016; Poulin et al., 2016; Zeng and Sanes, 2017; Koch and Segev, 2000). Nevertheless, experimental and theoretical observations disclose many structural and functional patterns, leading one to think that there must be underlying organizational principles that govern brain structure and allow the nervous system to function (Snider et al., 2010; Cuntz et al., 2012; Stepanyants et al., 2004; Wen et al., 2009; Chklovskii, 2004). Fortunately, the structural analysis of the nervous system is experiencing a new methodological expansion with the creation of sophisticated methods to image and reconstruct large regions of the nervous systems of different species. These methods have been proved extremely useful for understanding neuronal cell types function and their integration in networks, providing renewed hope to solve this quest (Zheng et al., 2018; Eichler et al., 2017; Wang et al., 2019).

1.1.2 Dendritic Structure - an Historical Primer

Historically, the role of single neurons in computations happening in the brain was miscalculated (Stuart and Spruston, 2015). Until recent decades, information processing in nervous systems was thought to be carried out at the circuit level: different computations being the result of different connectivity patterns with single neurons playing a smaller role in the process (McCulloch and Pitts, 1943; Gerstner, 2002).

Nonetheless, over the last decades, new experimental data were accumulated that made neuroscientists question these assumptions. Particularly the presence of voltage-gated ion channels in dendrites membranes and the recording of action potentials near the soma suggested that dendrites may be playing a bigger role in information processing than initially thought. Finally, the mathematical modelling of dendrite electrical properties, championed by Wilfrid Rall, made dendrites develop conceptually from a simple synaptic inputs collector to a much more sophisticated computational device (Häusser and Mel, 2003; London and Häusser, 2005; Gerstner, 2002; Koch and Segev, 2000; Silver, 2010; Brunel et al., 2014; Stuart and Spruston, 2015)

Today, it is understood that the geometry of a neuron's dendrite is vital not only to establish the connectivity required for the nervous system to operate normally (Chklovskii, 2004; Stepanyants et al., 2004; Stepanyants and Chklovskii, 2005; Wen et al., 2009) but as well to act in combination with the membrane's ion channel cocktail to perform the required computations on its inputs (Carr et al., 2006; van Elburg and van Ooyen, 2010; Abrahamsson et al., 2012; LeMasson et al., 2014; Gabbiani et al., 2002).

1.1.3 Basic Research - Structure and Function Relationship in Dendrites

Dendrites are complex structures that exhibit great variation in their morphological characteristics and structure. Due to this complexity, mechanisms of signal integration in dendrites are insufficiently understood. The first step to overcome this problem is a combination of a solid research question, a tractable model organism and the right technology to acquire the data necessary to test the hypothesis posed in the question (Herz et al., 2006).

Within the shape-function framework, one approach has proved itself very successful for cases where the computation is accomplished by a single identifiable neuron. This is the case for some invertebrate sensory neurons and neurons located in initial sensory processing areas. This approach, named hereafter **computational paradigm**, asserts that the coupling of a class type-specific dendrite geometry with specific ion channels provide the substrate for signal processing and integration in dendrites (Trussell, 1997; Gabbiani et al., 2002; Häusser and Mel, 2003; London and Häusser, 2005; Spruston, 2008).

Another approach, named **wiring optimization paradigm**, has been fruitful in distilling large principles and explaining structural patterns in brain wiring such as brain location (Van Essen, 1997), brain areas segregation (Rivera-alba et al., 2014), as well as axonal and dendrite shape (Mitchison, 1992; Chklovskii, 2004; Cuntz et al., 2012). This framework proposes that the dendrite's geometry maximizes the number of potential anatomical contacts between neurons while optimizing the total expenditure of metabolic constraints, cable length, and volume (Chklovskii, 2004; Stepanyants et al.,

2004; Stepanyants and Chklovskii, 2005; Wen et al., 2009).

Despite this daunting complexity, even if the dendrites were simply morphological clones of one another, it seems unlikely that the genome could encode the location of every synapse and therefore the location of every piece of a dendritic tree. This impracticability implies that general growth rules for connectivity and structure are genetically encoded, with self-organizing processes and dynamics providing the final stage of dendrite patterning (Hassan and Hiesinger, 2015; Hiesinger and Hassan, 2018). Identifying the growth rules and mechanisms behind neuronal structure formation and linking it to behaviour is one of the long-term goals in neuroscience.

1.1.4 Translational Research - Disease and Technology

In the literature, various studies address the relationship between aberrant dendrite structure and neuropsychiatric disorders (Kasai et al., 2010). Particularly atypical spine density and morphology, synapse and branch loss, and aberrant synaptic signalling and plasticity are noted to influence different neuropsychiatric disorders such as autism spectrum disorder, bipolar disorder, intellectual disability and schizophrenia (Copf, 2016; Emoto et al., 2016; Wang et al., 2019; Real et al., 2018; Forrest et al., 2018). Therefore, distinguishing and understanding these changes in neuronal morphology are fundamental for understanding neuronal structural pathology.

In addition to possible medical applications, understanding dendrite structure and connectivity has technological implications as well. On a more theoretical level, brain-inspired architectures have proved themselves very fruitful backbone designs to numerous machine learning algorithms and paradigms, providing a continuous source of inspiration to new ideas in the field (Guerguiev et al., 2017; Richards et al., 2019). It is worth mentioning that this association is symmetric, with recent developments in systems neuroscience using computer vision and other artificial intelligence algorithms to understand how information is processed in cortical areas of the brain (Yamins and DiCarlo, 2016). Ultimately, bio-inspired Artificial Intelligence aims at engineering high-speed and large-scale hardware that implements functionalities of brains to engineer intelligent machines and brain-computer interfaces (Floreano, Dario and Mattiussi, 2008; Indiveri et al., 2011).

1.2 Problem Statement

Although later progresses have disclosed dramatic new information on how dendrite mechanisms work at various scales, these endeavours have not sufficed to elucidate how dendritic arbours structure and physiology map to the behavioural level (London and Häusser, 2005; Hausser et al., 2017). This situation is the result of a combination of experimental and conceptual limitations, namely:

- **Dendrite structure quantification** is still an open problem in the field. There are limitations from data acquisition methods, disagreements of how to define a cell discretely as well as on the selection of the most pertinent morphometrics used to characterize the dendritic arbours branching patterns (Stepanyants et al., 2004; Brown et al., 2008; Snider et al., 2010; Sümbül et al., 2014; Zeng and Sanes, 2017; Kanari et al., 2018; Cembrowski and Menon, 2018; Cervantes et al., 2018).
- **Measuring dendritic activity during behaviour** is essential to dissect functional relevant dendritic mechanisms. However, the use of recordings or imaging collection from dendrites in an intact preparation remains a difficult hurdle to overcome (Spruston, 2008; Beaulieu-Laroche et al., 2018; Real et al., 2018).
- **Establishing a causal link between a dendritic mechanism and a certain behaviour** is the ultimate goal of dendrite research but, the most difficult since one needs to connect the cellular level to the behavioural context of the animal. Nonetheless, connecting these different levels across scales is fundamental for understanding the nervous system (Agmon-Snir et al., 1998; Gabbiani et al., 2002; Yeon et al., 2018; Forrest et al., 2018).
- **Theoretical frameworks** provide a rigorous background to interpret experimental data and to link different levels of explanation across scales. However, unifying the two dendrite structure-function paradigms has not yet been achieved. The wiring optimization paradigm is very successful in explaining structural patterns across scales. It provides an evolutionary plausible background to interpret the emergence of various neuronal structures, but it is very agnostic about the functional mechanisms that dendritic morphology may be involved. On the other hand, the computational paradigm allows the identification of different dendritic mechanisms for discrete subtypes, while showing difficulties in finding general principles based on what I have learned across different cell types (London and Häusser, 2005; Hausser et al., 2017).

1.2.1 Research Objectives

Taking into account what was previously mentioned, the main goal of this thesis is to address some of the fundamental issues associated with the structure-function relationship in dendrites. By studying one cell type in depth I aimed at setting a new standard in the field on what is possible to achieve while attempting to establish correspondence between dendrite structure and function.

Throughout this research, I used the da neurons from the *Drosophila melanogaster* larva as a model system because invertebrates have proven to be excellent animal models for connecting the function of dendrites to neuronal networks and behaviour (London and Häusser, 2005; Dewell and Gabbiani, 2017). This is partly due to the compactness of the

invertebrate nervous system and because it offers the possibility of sophisticated genetic manipulations and imaging. I particularly focused on the c1vpda proprioceptors which are thought to provide feedback about body position of the larva that is essential for coordinated locomotion (Hughes and Thomas, 2007a; Heckscher et al., 2012).

I reasoned that dendrite development and function are intimately intertwined, and to successfully elucidate the relationship it is necessary to study the temporal processes of cell patterning (Scott and Luo, 2001; Grueber and Jan, 2004; Jan and Jan, 2010; Dong et al., 2014; Lefebvre et al., 2015). Yet much is still unknown about the development of dendritic arbours, and little direct evidence is available on how changes in dendritic morphology affect neural function. Thus I recorded and processed high-resolution time-lapse images of dendritic differentiation in the embryo and its maturation in the larva. Afterwards, I probed the contribution of the c1vpda cells' characteristic comb-like dendritic geometry in sampling the mechanosensory inputs during crawling behaviour, by recording high-resolution calcium imaging in freely crawling larvae.

While the interactions of *Drosophila* larvae with their physical environment and neural morphology might differ from those of vertebrates, the dendritic mechanisms and adaptive requirements are similar between species. Thus, even though I used this less complex animal, I was able to identify patterns and possibly general principles of dendrite morphogenesis with broad applicability. Ultimately, a close combination of experimental and theoretical work will be required to make causal links between dendritic function and behaviour, which is essential for a deeper understanding of how our brains work (Cuntz et al., 2010; van Ooyen, 2011). The time-lapse data enabled me to create growth models that shed light on questions about dendritic pattern formation and how individual type of neurons control branching and minimise wire while doing so.

In particular, I focused on the following research questions (**Figure 1.1**):

1. Are c1vpda cells dendrites active during crawling? If so, is the stereotypical comb-like shape of c1vpda cells optimised for mechanical stimuli transduction?
2. Do c1vpda third instar (fully developed) neurons respect minimum wiring constraints?
3. What are the development stages that lead to dendrite patterning in c1vpda cells? Do c1vpda cells respect wiring minimization constraints during development?
4. C1vpda dendritogenesis is a process of stabilizing spontaneous variation during development, or is it a hierarchical cascade of precisely targeted and hardwired newly formed branches?

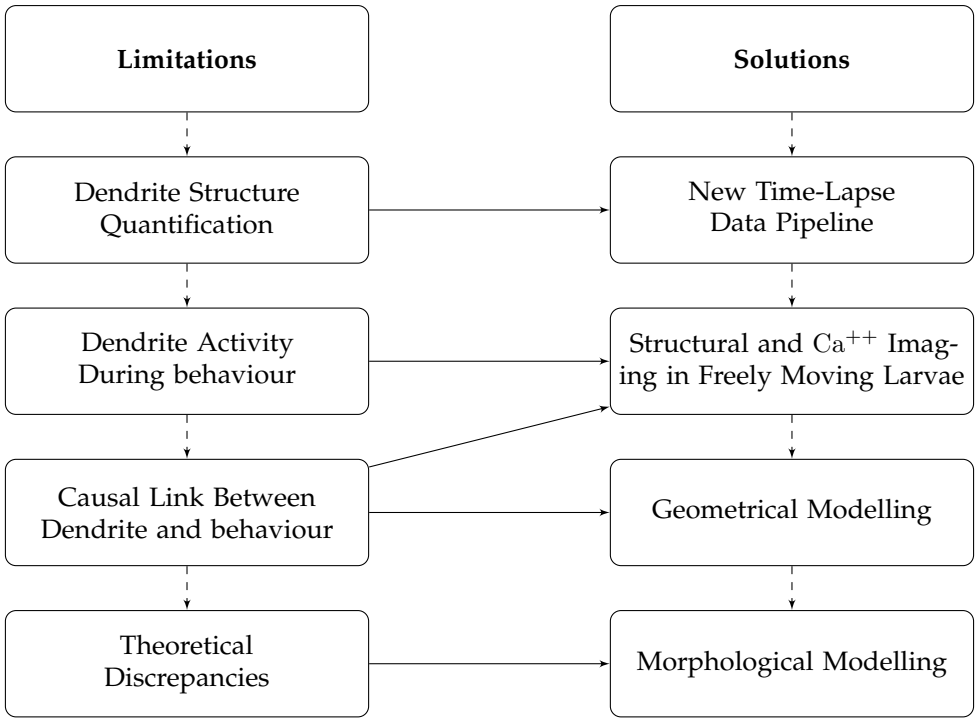

Figure 1.1: **Work Flow From the c1vpda Project**.
To fully comprehend the dendrite structure-function relationship it is required to address all the current limitations in the field. Thus, I designed an in-depth study where I could integrate different levels of explanation, data and modelling to thoroughly dissect the emergence of structure and function in the c1vpda cell.

1.2.2 Research Contributions

The work developed in this thesis comprises the following contributions:

- **Neuroinformatic Tool** - I developed a new semi-automatic computational pipeline to quantify high-throughput time-lapse data of the developmental process of different cell types. This pipeline was extensively tested on c1vpda and c3da neurons time series.
- **Neuroinformatic Tool** - I developed a new semi-automatic computational pipeline to quantify neuromorphology and gene expression of different cell types. This pipeline was extensively tested on a dataset with n>1000 C4 da neurons, with over 80 different types of mutants.
- **Poster & Talk** - *A framework for modelling the Growth and Development of Single Neurons Using Time-Lapse Data*. **Castro, A., F.**, Stuerner, T., Tavosanis, G.‡, Cuntz, H.‡. In 18th RIKEN Summer Programme (2017) - Exploring and Emulating the Brain. ‡ *Co-senior authors*
- **Poster** - *Dissecting the structure and function relationship in Drosophila dendrite development with the help of computational modelling*. **Castro, A., F.**, Baltruschat, L., Stuerner,

T., Tavosanis, G.‡, Cuntz, H.‡. In 27th Annual Computational Neuroscience Meeting (CNS*2018).
‡ *Co-senior authors*

- **Talk** - *Actin Dynamics in Dendritic arborization Neurons: A Computational Approach*. Stürner, T., **Castro, A.F.**, Philipps, M., Cuntz, H.‡, Tavosanis,G.‡. In 17th Annual Neurofly 2018. ‡ *Co-senior authors*

- **Talk** - *Dendritic Elaboration of a Fly Sensory Neuron*. **Castro, A., F.**, Baltruschat, L., Stuerner, T., Tavosanis, G.‡, Cuntz, H.‡. Young Investigators' Colloquium SoSe19, Goethe University. ‡ *Co-senior authors*

- **Talk** - *Actin Dynamics in Dendritic arborization Neurons: A Computational Approach*. Stürner, T., **Castro, A.F.**, Philipps, M., Cuntz, H.‡, Tavosanis,G.‡. In EMBO Workshop - Cell biology of the neuron: Polarity, plasticity and regeneration 2019. ‡ *Co-senior authors*

- **Talk** - *The Control and Effector Network of Neuronal Scaling and Neuron-Level Dendritic arbour Diversification*. Pai, Y.§, Delandre, C.§, Kwon, A., T., Tann, J., **Castro, A., F.**, Akimoto, S., Cuntz, H., Carninci, P., Moore, A., W. In Cold Spring arbour Neurobiology of *Drosophila* Meeting (2019). § *Co-first authors*

- **Publication** - *Development of Mechanosensory Dendrites Through Selective Pruning of Terminals*. **Castro, A.F.**, Baltruschat, L., Bahrami, A., Stuerner, T., Jedlicka, P., Tavosanis, G.‡, Cuntz, H.‡ (*in prep*). ‡ *Co-senior authors*

- **Publication** - *Comparative Computation Analysis of Actin-Binding Proteins in Vivo Unravel the Single Elements of Dendrite Dynamics*. Stürner, T., **Castro, A.F.**, Philipps, M., Cuntz, H.‡, Tavosanis,G.‡ (*in prep*). ‡ *Co-senior authors*

- **Publication** - *The Control and Effector Network of Neuronal Cell Size Expansion*. Pai, Y.§, Delandre, C.§, Kwon, A., T., Tann, J., **Castro, A.F.**, Akimoto, S., Cuntz, H., Carninci, P., Moore, A., W. (*in prep*).
§ *Co-first authors*

1.3 Manuscript Overview

In this final section, an outline of the structure of the manuscript is presented. In the next chapter, an overview of the state-of-the-art on various topics pertinent to this thesis is presented. First, the life cycle of the *Drosophila* larva will be addressed. Then the genetics and molecular basis of da neurons development will be reviewed.

Chapter 3 considers methods adopted to quantify and model dendrite structure. At the end of the chapter, the reader will be able to understand the complexity of dendritic trees

as geometrical objects and how one can resolve the structure and function conundrum using quantitative approaches to analyse dendrites.

In chapter 4, the publication based on the research accomplished during this thesis is presented. The development of c1vpda sensory neuron dendrites of the *Drosophila* larva throughout embryonic and larval stages is described and quantified. Combining high temporal resolution time-lapse data during development, calcium imaging recordings in freely moving larvae and data-driven growth models of the c1vpda patterning, the structure and function relationship of these cells is unravelled.

In chapter 5, the present manuscript is put in a larger context. The results and methods of the present thesis are contrasted against other efforts done in the field. Finally, the thesis is summarised and future directions and general improvements to the study are discussed.

In the final chapter of the thesis, the methods used in this study are described.

Chapter 2

Dendrite Development in *Drosophila* Larva PNS

A wide array of topics essential to this thesis are covered in the following chapter. First, the reader is going to be exposed to the field of *Drosophila* research, particularly to its advantages, and how neuroscience as a whole has benefited from using this animal model. Next, the development of the *Drosophila* will be reviewed, a particular focus will be put on the emergence of structure and function in da neurons, the cytology, genetics, developmental course and functional role of these neurons will be addressed. Certain structural components related to c1vpda sensory neurons, such as mechanosensitive (MS) ion channels will be particularly emphasised.

2.1 *Drosophila* Research in Neuroscience

The genetic toolkit available for *Drosophila melanogaster* is currently unpaired by any other animal model. The possibility for combining powerful genetic, molecular, and behavioural approaches with high-resolution imaging capabilities keeps attracting new scientists to the field. With a relatively short life cycle and small size, fly handling and experiments offer impressive advantages when compared with other animal models. Despite its structural simplicity, the fruit fly exhibits a rich behaviour repertoire supported by a complex yet tractable nervous system. Consequently, understanding the mechanisms employed by this life form may shed light on the inner workings of more complex organisms (Mohr, 2018).

In the first decade of the previous century, *Drosophila* genetic research was championed by Thomas Hunt Morgan, who initiated 50 years of inheritance studies using this organism. Morgan demonstrated that genes are carried on chromosomes and that they are the mechanical basis of heredity. Consequently, *Drosophila* became a major model organism in contemporary genetics helping to dissect the nature of mutation, recombination,

evolution, and development. The approaches and techniques developed at the time set the stage for the subsequent phase of research in the field, where groundbreaking biological mechanisms related to nervous system development were found (Bellen et al., 2010). Particularly in neurogenetics, these genetic tools started to be used in the 1960s. In those studies, genetic mutations have been associated to neuroanatomical defects and were used to understand the relation between the organization of the PNS, CNS and behaviour (Frenkel and Fernando Ceriani, 2011). To this day, seminal discoveries related to developmental neuroscience, microtubules dynamics and guidance, neuronal targeting, and even higher cognitive processes, such as learning and memory, were first resolved in *Drosophila* and then used to guide neuroscience research in more complex organisms, including vertebrate species (Bellen et al., 2010).

2.2 The *Drosophila* Larva Life Cycle

The *Drosophila melanogaster* is a holometabolous insect. After hatching from its egg, it has a larval and pupal stage of development before it reaches its adult form (**Figure 2.1**). The eggs are white in colour and oval in shape. Their length is smaller than $1mm$ and are enclosed in a hard extracellular case named chorion. From the anterior part of the chorion, two small hollow filament extensions emerge from its surface, allowing air exchanges with the exterior, and as well a micropyle, through which a spermatozoon can enter the egg. Inside the chorion, the eggs are besieged by a thin vitelline layer (**Figure 2.2**). Eggs hatch around 22-–$24hrs$ after egg lay (AEL), at 25°C (Ashburner, 2005; Tyler, 2000).

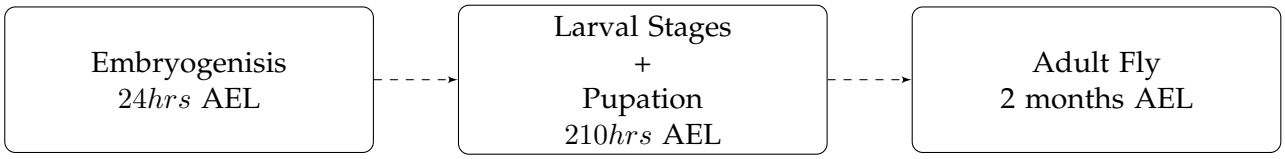

Figure 2.1: ***Drosophila melanogaster*** **Life Stages at 25°C**

After hatching from the egg, a small larva emerges. This stage is called the first instar, during which the larva feeds for $24hrs$ until it moults into a bigger larva, initiating the second instar phase. After feeding for another 24 hrs, the larva moults into the third and final instar stage, the largest of the larval forms. $30hrs$ later, the third instar larva moults into a pupa. At the beginning the pupa is a white stationary structure, that becomes increasingly darker with time. During this stage, the larva metamorphoses into the adult fly. After pupation, the adult fly may live for more than 2 months. Mating and fertilisation happens during this phase. Female flies lay eggs at a rate of around

dozens per day. In the following sections, I will present in more detail the *Drosophila*'s life cycle (Ashburner, 2005; Tyler, 2000).

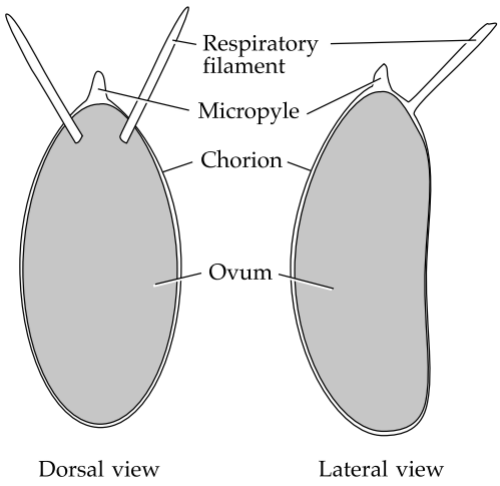

Figure 2.2: **Schematic Views of the *Drosophila* Egg.**
Left panel, dorsal view of the *Drosophila* egg. **Right panel**, lateral view of the *Drosophila* egg (from Ashburner (2005)).

2.2.1 Embriogenesis

The fertilization of the egg inside the female adult fly unleashes a period of deep alterations in the egg's structure, called embryogenesis. The following subsection presents a summary of the *Drosophila*'s embryogenesis, which is marked by a sequence of interconnected stages [1].

Cleavage Divisions – 0 - 2:50 hrs AEL

After fertilization, the zygote nuclei divide for fourteen cycles within the central area of the egg (**Figure 2.3**). Most insect eggs undergo superficial cleavage, a pattern of cleavage in which only the peripheral cytoplasm cleaves to generate cells, while the central yolky cytoplasm remains uncleaved. By the end of this stage, mitoses of the nuclei will bring their total number to approximately 5000 (Tyler, 2000).

During the first eight division cycles, hundreds of nuclei are produced. They then start migrating to the periphery of the egg, where the mitoses continue at an increasingly slower pace. By the ninth division, a couple of nuclei have already reached the surface of the embryo, with most of the remaining nuclei arriving at the periphery at the tenth cycle. After the fourteenth cycle, the embryo goes from being a syncytial blastoderm, i.e. when no other cell membranes exist besides that of the egg itself, to a cellular blastoderm (Ashburner, 2005; Tyler, 2000; Gilbert, 2000; Vijayalakshmi, 2012).

[1] Time intervals of embryonic stages are for development at 25ºC and correspond to the maximum interval range given at Tyler (2000)

Figure 2.3: **Embryonic Cleavage Divisions.**
Top to bottom, snapshots of the *Drosophila* egg during the fourteen mitotic divisions (from Gilbert (2000)).

Gastrulation – 2:50 - 3:10hrs AEL

Following cleavage, the phase of gastrulation proceeds by transforming the blastoderm into a multilayered embryo. During this stage, the germ layers primordia: mesoderm, endoderm and ectoderm, are formed by the infolding of a midventral cell block (**Figure 2.4**). Gastrulation creates a multilayered band of germ layers on the ventral side of the egg that curves around the egg's posterior tip. This band is called the germ band (Tyler, 2000; Campos-Ortega and Hartenstein, 1997; Leptin, 1999).

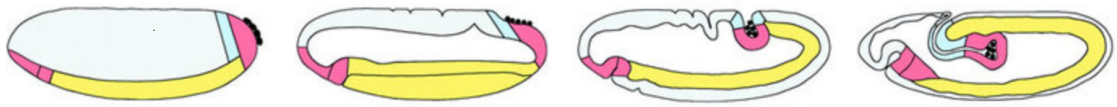

Figure 2.4: **Embryonic Stages of Gastrulation and Germ Band Elongation.**
Left to right, snapshots of the *Drosophila* embryo during gastrulation. Colours mark regions of mesodermal (yellow), endodermal (pink) and ectodermal (light blue and sky blue) primordia. Germ band approximately doubles in length along the anterior-posterior axis, while narrowing along the dorsal-ventral axis (modified from Leptin (1999)).

Germ Band Elongation and Neuroblast Segregation – 3:10 - 7:20hrs AEL

Soon after the initiation of the gastrulation stage, the germ band starts to elongate. During this stage, the width of the ventral germ band primordium is reduced in half, while it extends around the posterior end of the embryo, folding over the dorsal side of the egg (**Figure 2.4**). Initially, the germ band elongates very quickly then elongation slows down to attain its maximal extension, around twice its initial length (Tyler, 2000; Campos-Ortega and Hartenstein, 1997).

Already during the fast phase of germ band elongation, neuroblasts (NB) start to segregate from the ectodermal layer. For a time period of 2hrs, different subpopulations of neuroblasts emerge and they will start dividing shortly afterwards to generate neurons and glia. NBs undergo repeated asymmetric divisions, giving rise to another NB and a smaller ganglion mother cell (GMC). The GCM cell will divide again, producing neurons and/or glial cells (Homem and Knoblich, 2012; Campos-Ortega and Hartenstein, 1997; Wolpert et al., 2002; Volker Hartenstein, Shana Spindler and Fung, 2008; Grueber et al., 2002b).

Germ Band Shortening – 7:20 - 10:20hrs AEL

After germ band elongation, another morphogenetic process named germ band shortening occurs, with profound structural consequences for the epithelium. Here, the embryonic thoracic and abdominal segment boundaries form along the anterior-posterior axis, establishing the continuity of various sections (**Figure 2.5**). The shortening of the band supports the formation of the tracheal tree, and the gonads (Campos-Ortega and Hartenstein, 1997; Schöck and Perrimon, 2002).

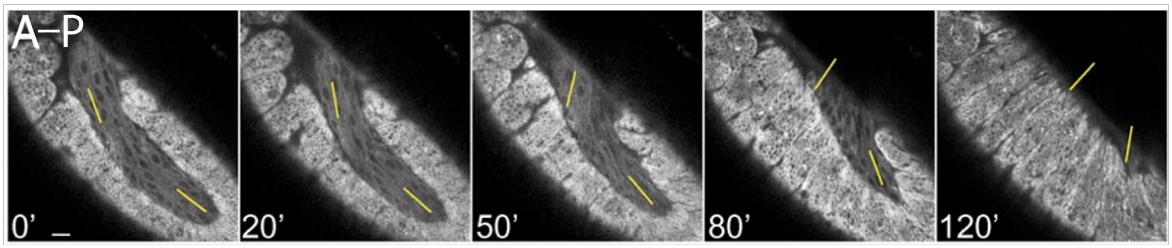

Figure 2.5: **Time-lapse of Germ Band Shortening.**
Left to right, illustrative time-lapse of *Drosophila* embryo during germ band shortening. In all panels, anterior is left, posterior is right and dorsal is up, or in the upper right corner. DV axis is represented by yellow lines and observation time after the beginning of germ band shortening is indicated in the left lower corner. Scale bar $20\mu m$ (modified from Schöck and Perrimon (2002)).

Dorsal Closure and Head Involution – 10:20 - 13hrs AEL

During germ band shortening the embryo is still open dorsally, only filled by the amnioserosa. The dorsal closure of the embryo arises by fusion of the dorsal epidermal primordium (**Figure 2.6A**). The contraction of the amnioserosa and the two lateral epidermal cell sheets provide the tensile force necessary for the germ band to close (Kiehart et al., 2017; Campos-Ortega and Hartenstein, 1997). As the germ band closes, the involution of the head happens concomitantly. The aforementioned morphogenetic stage involves the migration of the epidermis over the head segments, which are drift inside the embryo (**Figure 2.6B**). The head tissues remain internal until metamorphosis when they come together to form the adult head (VanHook and Letsou, 2008; Gompel

and Chyb, 2013).

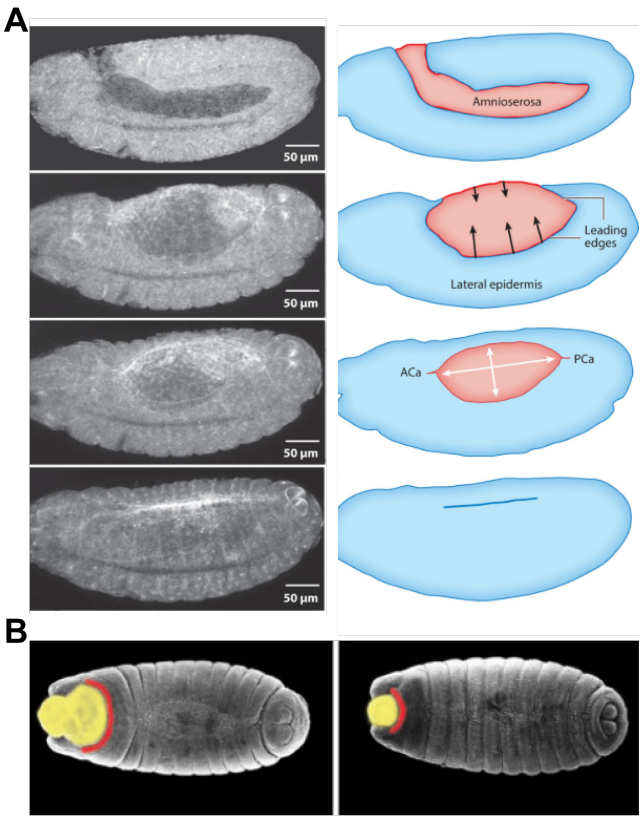

Figure 2.6: **Embryonic Dorsal Closure and Head Involution.**
A, Top to bottom, illustrative confocal images (left) and respective schemes (right) of germ band dorsal closure (ACa and PCa denote anterior and posterior canthus, respectively, modified from Kiehart et al. (2017)). The embryo is laterally oriented. **B**, Head segments (yellow) moving inside the embryo (modified from VanHook and Letsou (2008))

Differentiation and Hatching – 13 - 24hrs AEL

After head involution in completed morphogenesis is fundamentally accomplished. Throughout the last stage, the cuticle gets thicker and its specialisations become noticeable. Besides, all sensilla differentiate, sensory axons reach the CNS and the muscles have become connected with their respective motor axons. Shortly before hatching, around $22hrs$ AEL, larvae show severe head swings, contractions and body swirls. These mechanical forces help the larva to hatch.

2.2.2 Larval Stages

After $24hrs$ of embryonic development and differentiation a first instar larva hatches from the egg. The larva at this stage of development is small relative to the size of its third instar counterpart. During larval stages, it will ingest about three to five times their weight until pupation starts (Ashburner, 2005).

Larval Anatomy

The *Drosophila* larvae have oval-tubular, yellowish bodies anatomically divided into different sections. On the anterior-posterior axis, one can distinguish a head, three thoracic segments, eight abdominal segments, and a telson spanning from the anus (**Figure 2.7**). These thoracic and abdominal segments are extended and contracted sequentially during crawling behaviour and are delimited by rows of denticle belts that provide traction between the larva's body and the medium (Fushiki et al., 2016). In each segment, one can distinguish sensory bristles spread over the cuticle.

Internally, the nervous system of a *Drosophila* larva contains about 10,000 neurons (Eichler et al., 2017). Data collected using light microscopy didn't find qualitative differences in the neuroanatomy between first and third instar larvae. Nonetheless, scaling and also neurogenesis continues across larval stages in at least some brain regions (Almeida-Carvalho et al., 2017).

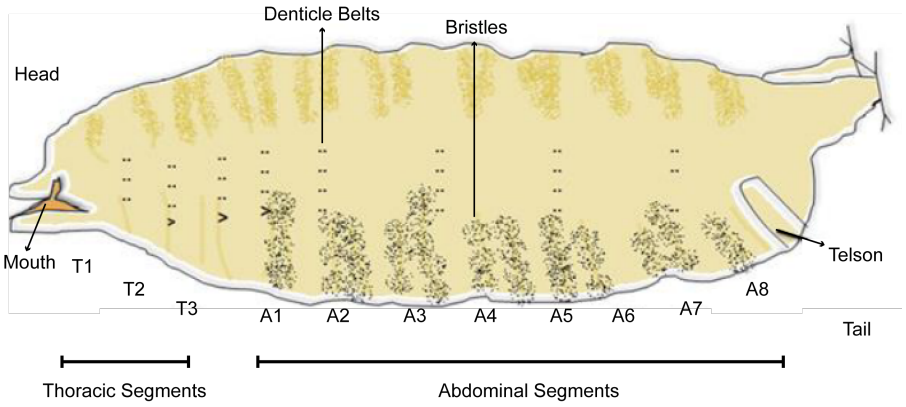

Figure 2.7: **Basic External Larva Anatomy Diagram.**
Schematic diagram of the external anatomy of a laterally oriented *Drosophila* larva (modified from Vijayalakshmi (2012))

.

Ecdysis – l1-l2 49hrs AEL and l2-l3 72hrs AEL

The development of the larva is marked by two moulting events before pupariation, which initiate the second (around $49hrs$ AEL) and third instar (around $72hrs$ AEL) of larval stages. These moulting episodes are concluded by ecdysis, i.e. the shedding of the old cuticle. Larval ecdysis in *Drosophila* is preceded by a set of morphological, physiological and behavioural events, such as appearance of new mouthparts, tracheal inflation, old trachea detachment and collapse, inflation of the new trachea, and, finally, strong body movements to facilitate the detachment of the old mouth hooks and cuticle (**Figure 2.8**, Park et al. (2002); Ashburner (2005)).

I1-I3 Behaviour

The nervous system of the larva is fully functional upon hatching to support feeding, and all the behaviours necessary to accomplish this goal. A recent study report that first instar larvae scored quantitatively lower in a battery of behavioural tests when compared with their third instar counterparts (Almeida-Carvalho et al., 2017). The assay included the following behaviours: free locomotion speed, feeding, responsiveness to substrate vibration, gentle and nociceptive touch, burrowing, olfactory preference and thermotaxis, light avoidance gustatory choices and associative learning. However, qualitatively, first instar larvae showed similar results in almost all cases as the third instar larvae, showing that changes in body size, and the size and number of neurons, seem largely inconsequential for larval behaviour.

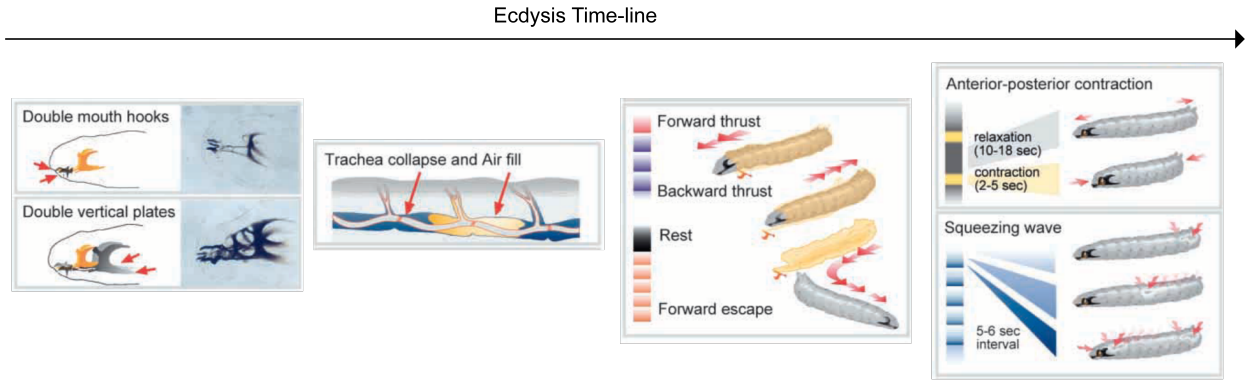

Figure 2.8: ***Drosophila* Larva Ecdysis.**
Timeline depicting the morphological, physiological and behavioural changes preceding ecdysis in *Drosophila* (modified from Park et al. (2002))

.

2.2.3 Pupariation and Pupation – 120-210hrs AEL

At around $120hrs$ AEL, when the larvae reach a critical mass of about $0.3mg$, a small release of ecdysteroid hormone in the absence of juvenile hormone, triggers the wandering stage (Ashburner, 2005). During this stage, the body of the third instar larva decreases in size and adheres to a firm medium. The cuticle hardens and then it transforms into a puparium, enclosing the immobile animal. Next, the larva moults a fourth time detaching itself from the inside of the puparium to give place to metamorphosis. In the course of this process, larval organs are self-destructing and the imaginal discs and histoblasts are differentiating to their adult form. By the end of this stage, eclosion happens and the adult fly is fully formed. The timing of eclosion is controlled by circadian rhythm (Ashburner, 2005; Tyler, 2000).

2.3 Development of the Embryonic and Larval PNS

To generate appropriate behaviour, the larva transduces sensorial information from the environment using the PNS, which then relays the information to the CNS (Grueber et al., 2003a; Singhania and Grueber, 2015). Each one of the different sensory modalities has their correspondent sensilla, which connect to somatosensory neurons located on the epidermis. These cells can also innervate the body wall of the larva. Neurons of the PNS of the larva are arranged stereotypically across segments, with the location of organs and neurons being constant in different animals (**Figure 2.10**).

2.3.1 Proneural Clusters - Emergence of Sensillum

A chain of highly conserved cell to cell interactions generates most of the *Drosophila*'s sensorial organs from proneural clusters. The latter are large clusters of adjacent ectodermal cells that will be able to generate sensory organ precursors (SOP). For each of one of these clusters, only one cell will have neural capacity (Campos-Ortega and Hartenstein, 1997). The expression of a family of transcription factors called proneural genes will determine if an undifferentiated cell in the cluster becomes the SOP, or not (**Figure 2.9A**).

After the SOPs are determined, their number in each proneural cluster is reduced by lateral inhibition. The proneural genes activate the Notch/Delta signalling pathway in the cells in which they are expressed, inhibiting proneural gene expression in all but a few cells, sending the remaining into an epidermal fate (Singhania and Grueber, 2015; Campos-Ortega and Hartenstein, 1997).

Then, the SOPs will undergo asymmetric cell divisions to generate cellular diversification. Terminal cell fates can differ depending on the lineage. However, a canonical SOP lineage can account for the asymmetric division process that leads to almost all of the different types of sensilla, including external sensilla, chordotonal organs, and type II multidendritic sensilla (**Figure 2.9B**). The canonical lineage starts with the SOP dividing into two pII daughters: pIIa and pIIb. PIIa divides once more and gives rise to the outer accessory cells. Finally, the pIIb gives rise to the sensory neuron(s) and inner accessory cells in two consecutive cell divisions (Homem and Knoblich, 2012; Singhania and Grueber, 2015).

A crucial factor in generating diversity in asymmetrical cell division is the protein Numb. This protein is found asymmetrically segregated into one side of the cytocortex of the mother cell. This will cause selectively segregation of Numb during cell division. Therefore, following cell division daughter cells with the Numb protein will suppress Notch signalling, while other daughter cells will be receptive to Notch signalling cells due to the absence of Numb, resulting in two distinct cell fates (**Figure 2.9C**; Santiago

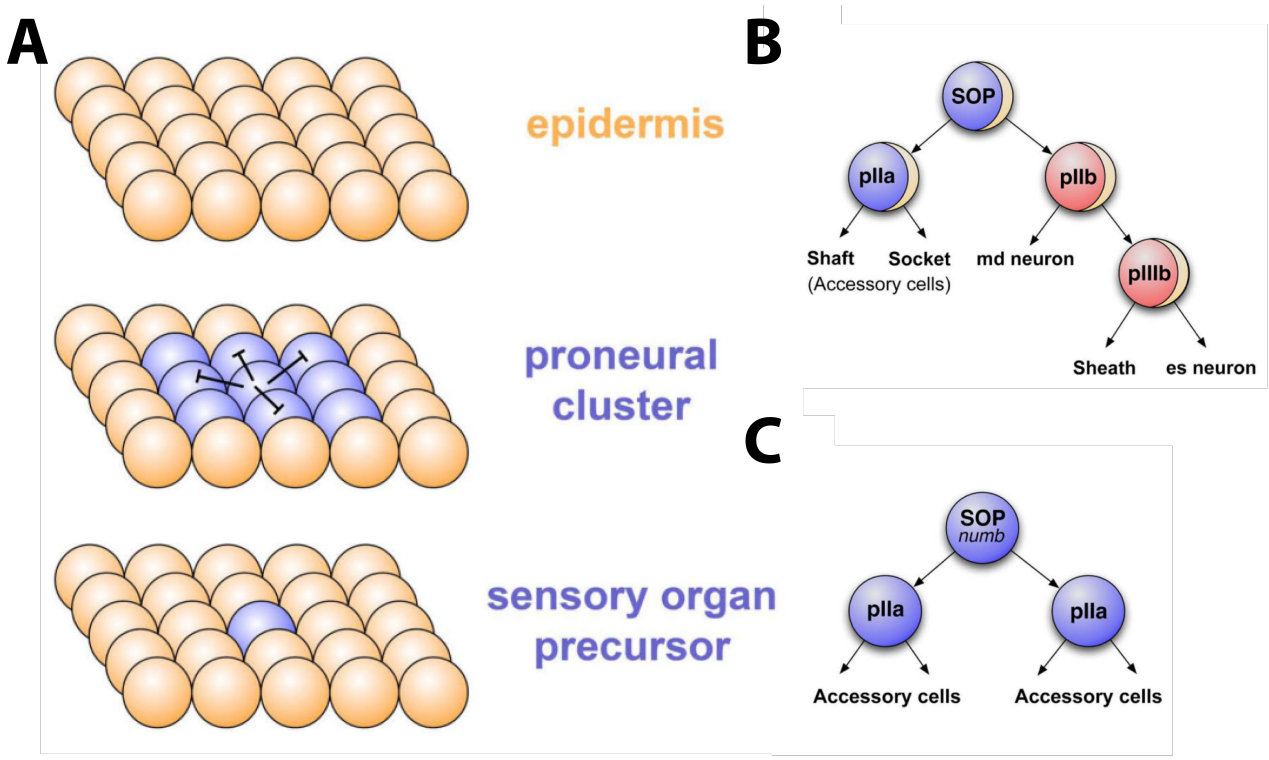

Figure 2.9: **Sensory Organ Precursors Specification and Lineage.**
A, Proneural clusters (blue spheres) in a field of epidermal cells (orange). From the proneural cluster, a single sensory organ precursor emerges through lateral inhibition. **B**, representative wildtype external sensory organ precursor lineage. **C**, similar as in **B** but for a lineage without numb. In the absence of numb the SOP divides into two identical pIIa cells. (modified from Singhania and Grueber (2015))

.

and Bashaw (2014); Haberle and Lenhard (2016).

2.3.2 PNS Neurons Organization

The PNS consists of two types of sensory neurons. Type I neurons innervate the sensory organs to which they are related by lineage and are ciliated. Type II neurons have multiple dendrites and, with one exception, are not connected to sensilla. These sensory organs are organized in dorsal, lateral and ventral clusters (**Figure 2.10**, Grueber et al. (2003a)). Besides their location on the epidermis these cells are divided into the following groups:

1. **Type I**

    - External sensory (es) organs
    - Internal chordotonal (ch) organs

2 **Type II**

    - Bipolar dendrite (bd) neurons
    - Tracheal dendrite (td) neurons
    - Dendritic arborization (da) neurons:

        Class I - propriocepters

        Class II - unknown function (but express Mechanosensitive (MS) ion channels)

        Class III - light touch

        Class IV - multimodal: touch and nocioception

2.3.3 Dendritic arborization Neurons

The four types of dendritic arborization cells are among the best-studied models for dendrite development. These sensory neurons are located between the epidermis and the muscle of the larva, where they spread their intricate branching dendritic structures. A single axon spans from the da cells relaying information into the CNS. All four types of da neurons are involved in mechanosensory processes, with the class IV being multimodal cells also involved in nociception (Kim et al., 2012a; Cheng et al., 2010; Vaadia et al., 2019; He et al., 2019; Liang et al., 2017).

From the four classes of da neurons, the class I cells have the simplest dendritic morphology (**Figure 2.10**, left panel). All three class I neurons, labelled as vpda, ddaD and ddaE (A-F is an alphabetic suffix that orders the cells from ventral to dorsal within each cluster) innervate both the dorsal and the ventral region of the fly larval body wall (Grueber et al., 2002a). The ddaE and ddaD project their fan-shaped dendritic trees anteriorly and posteriorly, respectively. On the other hand, the vpda spreads sensory processes in both directions from one primary dendrite that branch in a comb-like fashion (Grueber et al., 2002a).

Class I neurons are involved in relaying proprioceptive information to the CNS, feedbacking the contraction-extension status of the segments of its body to coordinate locomotion. Mutant larvae in which the function of class I neurons is impaired showed clear defects in length stride and crawling speed. It is thought that the specific localization of class I neurons, and their dendrite pattern are optimized to sample mechanosensory

inputs important to proprioception (Hughes and Thomas, 2007a; Kim et al., 2012a; Cheng et al., 2010; Vaadia et al., 2019; He et al., 2019; Liang et al., 2017).

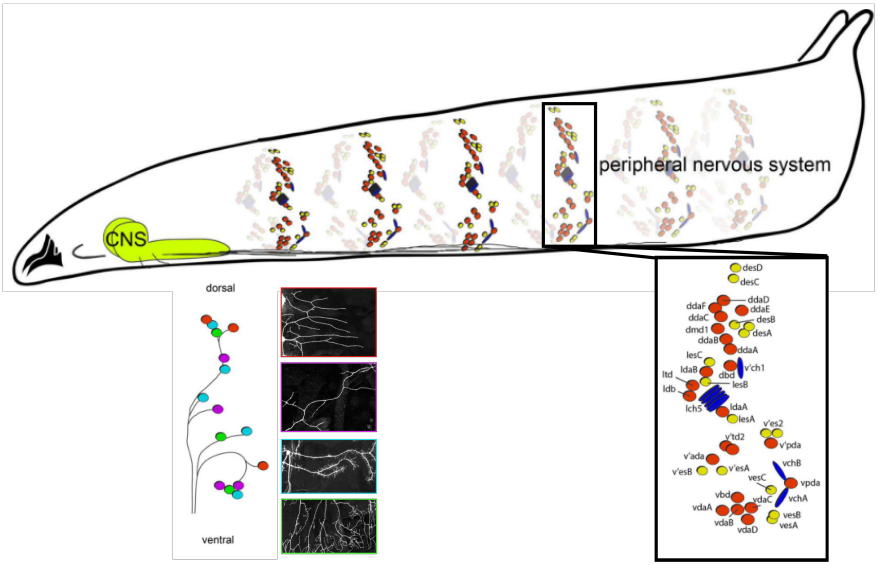

Figure 2.10: **Organization of the *Drosophila* Larva PNS.**
Top panel, illustrative representation of a *Drosophila* larva. **Lower left panel**, scheme of da cells location in a segment and respective representative morphologies. Colour scheme: red - class I, purple - class II, light blue - class III, and green - class IV. **Lower right panel**, scheme showing PNS location and stereotypy in the larva. External sensory organs are indicated by yellow circles, chordotonal organs by blue ovals, and multidendritic neurons by red circles (modified from Singhania and Grueber (2015))

.

2.4 Dendrite Cytology

Dendrites are tree-like structures, irregular in thickness, which are covered by a plethora of excitable channel. They are specifically designed for collecting information from other neurons, glia, circulating hormones and sensory information. The membrane that delimits neurons is similar to the ones from other biological cells, being defined by a lipid bilayer structure that provides a hydrophobic barrier impermeable to water-soluble substances (Kandel et al., 2012).

In order to fulfil their functional roles in the nervous system, dendrites come in many different sizes and patterns. This diversity in cell types is regulated by transcription factors that control the expression of genes endowing a cell with its morphological and functional properties (Kandel et al., 2012).

2.4.1 Dendrite Organelles

As in other cells, dendrites contain numerous subcellular structures that support the cell function and maintenance (Kandel et al., 2012). These structures include:

- **Endoplasmic reticulum** is a network of membranes called cisternae, where proteins and membrane lipids are synthesised and exported.
- **Polyribosomes** are clusters of free ribosomes that are spread throughout the cell and where cytoplasmic proteins are synthesized.
- **Mitochondria** main function is to supply energy to a neuron by processing oxygen in order to generate adenosine triphosphate (ATP). This molecule is later spent in various cellular processes.
- **Golgi Apparatus** is involved in packing and transporting, proteins and lipids into membrane-bound vesicles. Afterwards, these vesicles can be used in different parts of the neuron or can be sent into the extracellular space through exocytosis.

2.4.2 Dendrite Cytoskeleton

The shape of a dendrite is determined by its cytoskeleton. During early morphogenesis, cytoskeletal regulators control structural proteins to build dendrites At later stages they provide refinement mechanisms to shape dendrite patterning. In general, cytoskeletons are made by three filamentous structures: microtubules, neurofilaments, and actin/microfilaments. However, in dendritic trees, microtubules and actin filaments have the most important structural role (Kandel et al., 2012; Coles and Bradke, 2015; Konietzny et al., 2017; Han et al., 2017):

- **Microtubules** are long structures that provide the structural backbone of a dendrite. Microtubules are made of protofilaments and can measure up to $0.1mm$ in length. Protofilaments consist of multiple pairs of α and β tubulin subunits that bind to each other along the protofilament.
- **Actin** filaments are linear polymers with a helical repeat around every $26nm$. They are the thinnest of the aforementioned types of protein polymers. They form dense and dynamical mesh networks with actin-binding proteins in the vicinity of the dendrite's membrane, providing structural stability and adaptability to the cell. These networks undergo morphological changes causing dendritic branches and spines to elongate and retract.

The dynamics of polymerisation and depolymerisation of microtubules and actin filaments endow the cell with structural plasticity, which is thought to play an important role in changes of synaptic connectivity, and in cognitive processes such as memory and learning (Kandel et al., 2012). In addition to serving as structural scaffolds, microtubules and actin filaments act as tracks along which organelles and proteins are moved around the cell (Coles and Bradke, 2015; Konietzny et al., 2017; Han et al., 2017).

2.4.3 Dendrite Ion Channels

Electric signalling in dendrites is generated by the influx or outflux of different ionic currents through ion channels across its membrane. The membrane potential and resting state ionic gradients dictate the direction of the ion fluxes. Ion channels have a fundamental role in electrical signalling by selecting specific ions to permeate the dendrite membrane in response to electrical, mechanical, or chemical signals. These channels act at extremely rapid rates, providing the fast transitions in membrane potential necessary for information processing. These changes in membrane potential may cause different actions in the cell such as action potentials, muscle flexing and hormonal release. (Kandel et al., 2012; Zheng and Trudeau, 2016; Sterling and Laughlin, 2015).

Ion channels can be distinguished by many different properties. However, the standard criterion used to classify ion channels is their gating mechanism. According to their gating mechanism, ion channels can be divided into three superfamilies (Zheng and Trudeau, 2016):

- **Voltage-dependent ion channels** - have a class of transmembrane proteins in the constitution of their pores called voltage-sensing domain. This subdomain of the channel changes its conformity when triggered by variations in membrane potential, causing the pores of the channel to open.
- **Ligand gated ion channels** transduce changes in the concentration of a chemical into electrical signals in dendrites. They open their pores in response to changes in the concentration of neurotransmitters, neuromodulators, intracellular second messengers, cellular metabolites, and signalling lipids.
- **Mechanosensitive ion channels (MS)** respond to physical stresses in the lipid bilayer, associated intracellular, or extracellular components, by opening its pores when a force threshold is reached. By doing so, they convert mechanical forces such as, tension, contraction, or bending into electrical or chemical signals.

Mechanosensitive Channels in *Drosophila*

MS channels generate current transients in response to a stepped mechanical stimulation (Zheng and Trudeau, 2016). These mechanical stimuli reaching MS channels from a receptive field can either attenuate or exacerbate, depending on the physical properties of the dendrite membrane, cytoskeleton, and connection with the ECM.

The gating mechanisms of MS channels remained elusive until recent studies of the insect NompC channel (Liang et al., 2013) reported a possible mechanism for this family of channels for the first time. It was suggested that a gating spring connecting the first

transmembrane helix of the channel with the supporting microtubule mesh seemed to be the point of force delivery to this membrane protein.

However, MS channels belong to many structurally unrelated families with possibly slightly different gating mechanisms being used (**Figure 2.11**). Therefore, I will introduce general concepts and frameworks important to understand the dynamics of two of the most important MS channels families present in *Drosophila* (Zheng and Trudeau, 2016; Kim et al., 2012a; Saotome et al., 2017; Yan et al., 2012; Zhao et al., 2016):

1. **TRP Channels** - involved in nociception, pain, sensing bristle deflections, vibrations by ciliated cells, proprioception, sound and touch perception.

2. **Piezo Channels** - generate robust fast-decaying cationic currents and it functions as a mechanical nociceptor in *Drosophila* larvae.

To change the resting state, the pores of the channel should be biased by the external force to change their geometry in the same dimension as the applied force. This mechanical principle is the foundation of all MS gating mechanisms, regardless of the number of dimensions in the system. Formally, the mechanosensitive molecule of the channel can exist in two states: the closed and the open, separated by energy G_o, with probabilities P_c of being closed, and P_o of being open, following the Boltzmann distribution[2] and with W_e the external stimuli (Zheng and Trudeau, 2016):

$$P_o/P_c = e^{(G_o - W_e)/kT} \tag{2.1}$$

In the resting state, $W_e = 0$ and the energy G_o deviates the P_c into a higher value, meaning that the probability of the ion channel to open is low. Only when an external force is applied to the system $W_e > 0$ the P_o increases with the magnitude of the W_e. Although the magnitude of the external stimuli is hard to measure experimentally, in the future new studies focusing on the structural details of specific MS channels will elucidate the loci of force application and the magnitude required for gating (Zheng and Trudeau, 2016; Kim et al., 2012a; Saotome et al., 2017; Yan et al., 2012; Zhao et al., 2016).

[2] All energies in the Boltzmann formalism are normalized to kT.

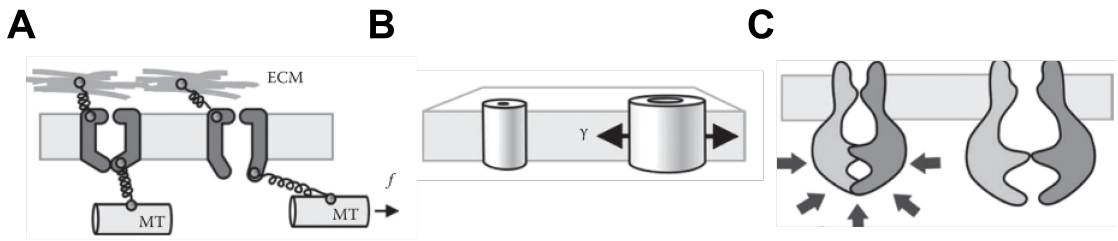

Figure 2.11: **MS Gating Mechanisms.**
A, gating by 1D linear force (f) applied to the channel gate by displacement of a microtubule acting like a tether. **B**, gating by fluctuations in 2D tension (γ) of the surrounding membrane where the channel is embedded. **C**, gating by density fluctuations in 3D of the cytoplasm surrounding the channel (modified from Zheng and Trudeau (2016))

.

2.5 Dendrite Development in the da System

During early development, the dendrite of a neuron will polarise from its soma (Singhania and Grueber, 2015; Hill et al., 2012). Afterwards, during morphogenesis, cell type-specific transcriptional mechanisms regulate the expression of gene patterns unique to a given da class. Extrinsic factors in combination with the expression of class-specific gene patterns will determine a neuron stereotypical size and shape. Although the geometry of the distinct da neurons varies, their general functional role is constant: they must cover the appropriate dendritic field to properly receive sensorial inputs, and their dendritic tree must have a specialised structure that enables input transduction and processing. (Jan and Jan, 2010; Lefevre et al., 2017; Cheng et al., 2010).

2.5.1 Master Regulators of da Morphology

In this subsection, I will focus on the morphological effects of the master regulators of the distinct da classes. The genes controlled by these transcription factors control are the most important one in the regulatory pathways that endow da neurons with cell type-specific cell fates. This shortlist is behind exhaustive since many other transcription factors and their combinatorial networks are involved in da dendrite morphogenesis and specification of final arbour morphology (Corty et al., 2009; Puram and Bonni, 2013; Dong et al., 2014; Jan and Jan, 2010; Lefebvre et al., 2015). Next, I will enumerate the transcription factors that are involved in the code that specify cell identity and da dendritic arbour complexity (**Figure 2.12**):

- **Spineless** is fundamental for dendrite morphology diversity in da sensory neurons and is expressed in all da classes (Kim et al., 2006). In loss-of-function mutants, all four da classes grew dendrites with similar morphologies, regressing to a primordial dendrite shape. It is hypothesised that spineless may contribute to

create a morphogenetic *tabula rasa* allowing other transcription factors to generate diverse dendrite patterns (Jan and Jan, 2010; Dong et al., 2014).

- **Abrupt** decreases the dendrites, size and complexity and is only expressed in class I da neurons (Parrish et al., 2006). Ectopically expressing Abrupt in larger class II, III or IV cells, simplified their dendrite pattern (Parrish et al., 2006; Li et al., 2004; Sugimura et al., 2004). This suggests that simple class I dendrite structure may be important for their functional role, and/or for resources conservation.

- **Cut** increases branching complexity and number of particularly small, actin-rich branchlets. Cut is expressed in different levels across class II, III and IV da neurons, but not in class I (Grueber et al., 2003a). The regulation of the expression level of this transcription factor acts like a knob which controls the branching intensity of da cells (Grueber et al., 2003a).

- **Knot/Collier** suppresses the formation of actin-rich branchlets and enhances the formation of microtubulin based branches (Jinushi-Nakao et al., 2007; Crozatier and Vincent, 2008). Knot/Collier is only expressed in class IV da cells, and it works in combination with Cut to control different aspects of the cytoskeleton generating the class-specific dendritic arbour of these cells.

Although the cell's intrinsic factors such as the transcription factors are the main actors in dendritic morphogenesis, it is to be noted that extracellular signals act in combination with them to ensure correct territory innervation (Kim et al., 2012b; Han et al., 2012) and growth direction (Matthews et al., 2007; Hattori et al., 2013).

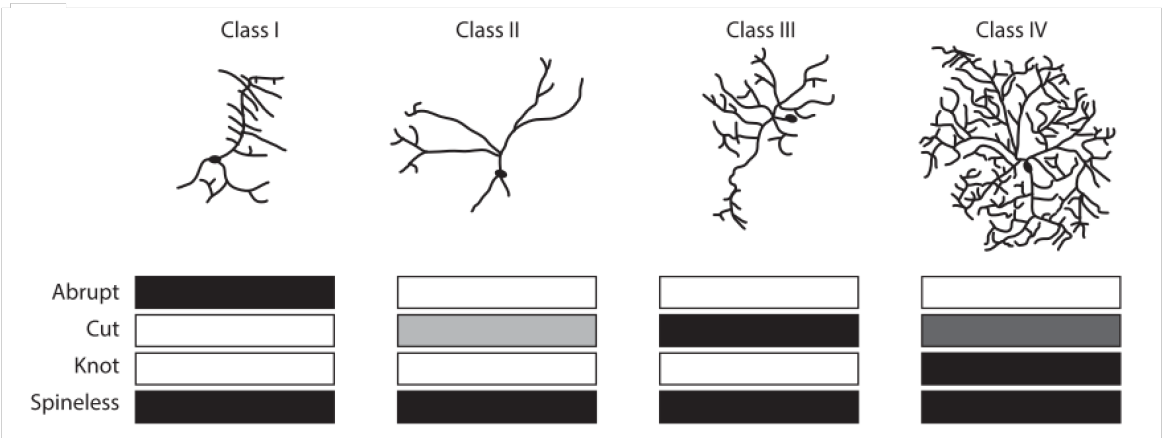

Figure 2.12: **Transcription Factors Behind da arbour Pattern.**
Different expression levels and combinations of the transcription factors necessary to generate da neurons dendritic morphology. From white to black increases the level of transcription factor expression (modified from Corty et al. (2009))

.

2.5.2 Da Dendrites Patterning

In order to fulfil their functional role, da neurons need to optimise dendrite spacing and coverage while saving wire. Dendrites also need to adapt to changes in the body size of the larva during development. I briefly discuss the developmental and molecular mechanisms that organize the patterning and wiring of da dendritic fields (for comprehensive reviews: Lefebvre et al. (2015); Puram and Bonni (2013); Jan and Jan (2010); Corty et al. (2009); Dong et al. (2014); Lawrence Zipursky and Grueber (2013)):

Dendrite Self-Avoidance

To avert sampling sensorial inputs from the same area of the spanning field with distinct dendritic branches, dendrites from the same cell avoid each other (Corty et al., 2009). Repulsive dendrite growth allows maximal coverage of the cell's territory while minimising wire (Lefebvre et al., 2015; Cuntz et al., 2012). A contact-mediated mechanism endows branches from the same dendrite with the ability to recognize each other when in close vicinity of one another, and then to selectively repel each other (**Figure 2.12B**). Throughout development branch interactions cause mutual retraction and growth direction rerouting, filling the space in an efficient manner (Garrett et al., 2018; Fuerst et al., 2008; Matthews et al., 2007; Soba et al., 2007; Simmons et al., 2017; Tadros et al., 2016; Hughes and Thomas, 2007a).

The molecular mechanism enabling dendrite self-avoidance is the stochastic expression of a small subset of Dscam isoforms. Dscam diversity provides each dendrite with the ability to recognizing itself by isoform-specific homophilic binding. This unique identity allows neurites that express the same set of isoforms to repel each other, resulting in self-avoidance. As adjacent cells have a low probability of expressing the same set of Dscam isoforms due to alternative splicing mechanisms, self-avoidance is assured (Hattori et al., 2007).

Dendrite Tiling

Similar to self-avoidance, dendritic tiling is a phenomenon in which the dendrites of class III and IV da neurons innervate the epidermis in a nonredundant manner, displaying little overlap and ensuring that their receptive fields are fully covered (Gao et al., 2000; Grueber et al., 2003a). Tiling can be achieved by homotypic repulsion by competitive interactions between branches of neurons belonging to the same class (**Figure 2.12A,D**) or different functional type (**Figure 2.12E**). In seminal studies, ablation of dendrites resulted in the innervation of the newly vacant receptive field by neurites of adjacent cells of the same type (Sugimura et al., 2003). However, unlike with Dscam and self-avoidance, not as much is known about the cell surface molecules responsible for tiling. Nonetheless, some molecules have been involved in class IV da neuron tiling

in the past years. One of these molecules was Flamingo. In Knock-down mutants of Flamingo the class IV dendritic branches overextend and overlap with neighbouring class IV cells (Gao et al., 2000; Kimura et al., 2006).

Dendrite Scaling

During development, dendrites can change in size by several orders of magnitude in a larva. To keep up with the epidermis surface growth, da neurons need to increase their size proportionally to preserve their receptive fields. This phenomenon is named dendritic scaling (**Figure 2.12C**). However, very little is known about the specialized mechanisms to support their scaling demands (Dong et al., 2014; Lefebvre et al., 2015; Jan and Jan, 2010). However, it was reported that microRNA bantam is required for dendrite growth to synchronize with the growth of the surrounding tissue. The epithelial cells surrounding class III and IV da cells expressing microRNA bantam signal the dendrites to grow concomitantly with the epidermis stretch during the larval stage. This microRNA inhibits the phosphoinositide 3-kinase target of rapamycin kinase pathway in dendritic arborization neurons, capping their dendrite expansion. (Parrish et al., 2009). The other da classes exhibit dendritic scaling although the mechanisms underlying it remain unknown.

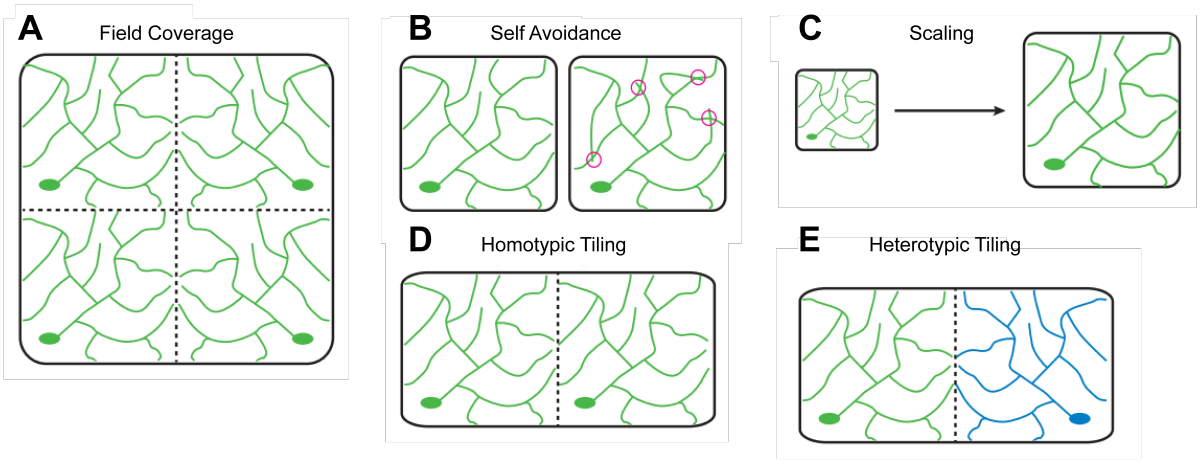

Figure 2.13: **Dendrites Distinct Patterning Strategies.**
A, non-redundant receptive field coverage by neurons of the same class. **B**, left panel, neuron self-avoids itself generating efficient field coverage. Right panel, neurons don't self avoid. **C**, illustrative dendrite scaling during growth. **D,E**, different types of tiling where neurons cover their respective fields without overlapping adjacent dendrites (modified from Dong et al. (2014))

2.6 Summary

In this chapter, important concepts necessary for the interpretation and understanding of the experiments and results of this thesis were introduced. A particular focus was put on the topic of *Drosophila* larva development. Initially introducing the *Drosophila*'s life cycle, the chapter moves on to explain the development and organisation of the larva PNS. Afterwards, the reader was exposed to basic dendrite cytology structure, notably to MS ion channels that are expressed in class I neurons. Finally, the state of the art on da neurons dendrite patterning was summarised.

Chapter 3

Dendrite Shape

This chapter focuses on the morphological features of dendritic trees. It will start with the description of methods for obtaining reconstructions of neuronal structures and their digitisation. Afterwards, an overview of quantitative methods for analysing and modelling dendrite shape will be provided. The main focus lies on the description of morphological complexity and how one can use these descriptors to develop models that can elucidate dendrite development.

3.1 Dendrite Geometry Quantification

Ramón y Cajal's drawings in the early 1900s marked a new era in neuroscience (Ramon y Cajal, 1995). The level of detail in the representations of dendritic trees in those illustrations allowed a deeper understanding of neuronal function and structure. However, as both technology and theory advanced in the field, the need for increasingly more precise and detailed data was required. Particularly in the advent of computational modelling in neuroscience, the rigorous quantification of neuronal structure became fundamental as the accuracy and predictive power of any model relies upon the precise fit of its parameters by real data (Halavi et al., 2012; Jacobs et al., 2009). Next, I will cover techniques used for obtaining high-quality 3-D digital representations of dendritic trees, named reconstructions.

3.1.1 Neuronal Reconstruction

The workflow for obtaining digital reconstructions of neuronal structures is similar across studies: cell labelling, followed by tracing of those images into a digital format. There are many labelling techniques in use in order to visualise dendrites with light microscopes. All of them have their own advantages and disadvantages, therefore their use, or not, will be dependent on external factors such as animal model, or type of experiment (Halavi et al., 2012; Jacobs et al., 2009). Labelling methods can be divided in:

1. **Injection methods**:

    - Biocytin
    - Cobalt chloride
    - Horseradish peroxidase

        Advantages – increases contrast; enables electrophisiological recordings

        Disadvantages – invasive

2 **Staining methods**

    - Immunohistochemistry
    - Golgi impregnation
    - Lipophylic dye

        Advantages – increases contrast.

        Disadvantages – imprecise because it stains areas around the tissue of interest.

3 **Genetic methods**

    - Green fluorescent protein (GFP)

        Advantages – high-resolution.

        Disadvantages – few animal models have an extensive genetic toolkit.

In connectomics studies, where high-resolution data of subcellular structures is required, using EM is the norm. It is important to note that EM does not require any pre-imaging labelling method. The dissection and identification of the different neuronal structures are made a posteriori during tracing (Schlegel et al., 2017; Helmstaedter, 2013).

After images of the labelled cells are collected, the tracing of the image stacks to a digital format ensues. This step is done using computer-microscope interfaces, or with purpose-made external software where the acquired image stacks have to be imported to. Tracing involves obtaining the Cartesian coordinates of all the segments of the neuronal structures, as well as their diameters and connectivity matrix. This process is called skeletization (Halavi et al., 2012; Jacobs et al., 2009).

Tracing can be an extremely time-consuming operation, being one of the biggest data processing bottlenecks in a scientific project (Schlegel et al., 2017). This problem gets exacerbated by the fact that with advances in imaging techniques neuroscientists are accumulating enormous amounts of imaging data, due to the speed increase which these images can be obtained (Eichler et al., 2017; Zheng et al., 2018).

To overcome this issue, many software and packages allow the user to reconstruct image stacks in an automatic, or semi-automatic manner (see Halavi et al. (2012); Cuntz et al. (2010); Schindelin et al. (2012); Peng et al. (2014)). Until very recently, tracing technology was lagging behind in comparison to the imaging technology, but progress has been made in developing high-throughput automated digital reconstruction algorithms (Helmstaedter, 2013; Halavi et al., 2012). This progress is mostly based on variants of convolutional neural networks, which have been developed and incorporated into tracing algorithms to tackle a variety of visualisation and image analysis problems (Sümbül et al., 2014; Wang et al., 2019; Peng et al., 2015; Januszewski et al., 2018; Kornfeld and Denk, 2018; Chen et al., 2015; Falk et al., 2019).

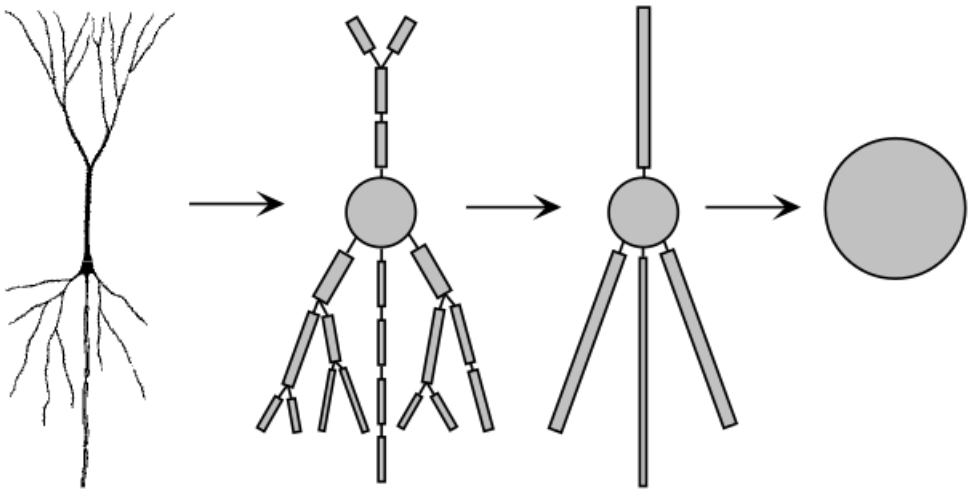

Figure 3.1: **Dendritic Tree Skeletization.**
From left to right, reconstructions of a pyramidal cell with increasingly lower resolution. The rightmost panel represents a point neuron that disregards morphological data from the cell (modified from Dayan and Abbott (2001))

.

Automated Reconstructions and CNN's

Convolutional networks, or CNNs, are neural networks that use a mathematical operation called convolution in at least one of their layers. These networks have been successfully employed to process image data, with significant improvements over other machine learning systems, such as feedforward networks. By employing convolution in its layers, CNNs need to store fewer parameters, reducing memory requirements of the model, improving its statistical efficiency and minimizing the amount of operations needed to compute the output (Goodfellow et al., 2016; Lecun et al., 2015). These networks are trained to enhance images of labelled cells, using as a training set previously manually skeletonized dendritic arbours. After the image stacks have their quality enhanced, simple thresholding methods suffice to automatically reconstruct the morphology.

Formally, **convolution** is an operation on two functions of a real valued argument that produces a third function, which is the result of how the two input functions' shape are modified by each other. For the continuous case:

$$f(x) = \int_{-\infty}^{\infty} s(a)w(x-a)da \tag{3.1}$$

In image reconstruction applications, the input x is a multidimensional array of pixels of an image of a labelled neuron, and the kernel w is a multidimensional array of parameters that are adapted by the learning algorithm at each iteration. The ouput $f(x)$ is named the feature map. Since data is processed in a computer, x will be discretised. Therefore, one can define the discrete convolution as:

$$f(x) = \sum_{a=-\infty}^{\infty} s(a)w(x-a). \tag{3.2}$$

CNN's topology is a very important factor for its success in accomplishing any task. The topology of a network may range from a few layers, named shallow CNNs, to dozens of layers, named deep CNNs. However, regardless of its topology a canonical layer CNN usually consists of three stages, and final step at the end of the network (**Figure 3.2**):

1. **First stage** – the layer performs several convolutions in parallel on the input data to produce a set of linear activations.
2. **Second stage** – each linear activation is run through a nonlinear activation function, this stage is named the detector stage, or rectifier.
3. **Third stage** – a pooling function is used to smooth the output of the layer, reducing the sensitivity to noise.
4. **Final stage** – this final layer is optional, but it is utilised in most CNNs used to automatic reconstruct biological images. Having a fully or densely connected layer is used to classify the input image into different classes based on the training data.

The workhorse of most CNNs is the stochastic gradient descent learning algorithm. With SGD one tries to minimize a given function $y = f(x)$, $x, y \in \mathbb{R}$, by moving x in small steps with opposite sign of the derivative $f(x)'$ using a small set of samples, named minibatch, to compute the gradient (Goodfellow et al., 2016; Lecun et al., 2015).

Nevertheless, although ML-based segmentation algorithms have dramatically improved the reconstruction bottleneck, some problems still persist after these methods are used

on real data. Unless for very specific cases, when the quality of the images collected is very high, there will be remaining errors that still require human proofreading involving visual inspection of the quality enhanced image stacks. A fully automated, an all-purpose, high-speed, high-resolution, reconstruction algorithm is yet to be designed.

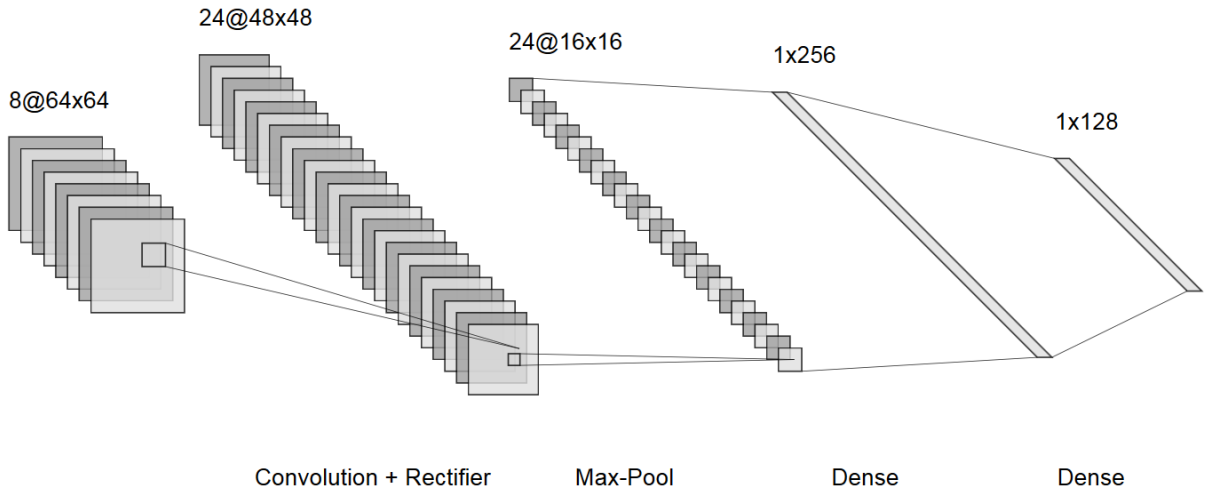

Figure 3.2: **Illustrative Example of a CNN Topology.**
From left to right, distinct layers of information processing: convolution, rectifier, pooling and a fully connected layers at end of the network.

3.2 Dendritic Tree as a Graph

Reconstructions are continuously being accumulated and stored into digital format, with the most complete database being NeuroMorpho.org (Ascoli et al., 2007). However, after images are traced, the morphological information stored in those files still needs to be quantified. Particularly in this thesis, the analysis performed to quantify neuronal structures is based on a formalism that represents dendritic trees using graph theory. At an abstract level, graphs are mathematical objects that represent binary relationships between discrete elements in a rigorous way (Jost, 2007). A graph Γ is a pair (V, E) of a finite set V of vertices or nodes, and a set E of unordered pairs, called edges, or links, of different elements of V. Thus, when there is an edge $e = (i, j)$ for $i, j \in V$, one says that i and j are connected by the edge e and that they are neighbours, $i\ j$. A special type of graph in which the edges do not form loops is called a tree, i.e., $\forall e \in E, e \neq (i, i)$.

The vertices of the graph are the equivalent of the branch and termination points of the reconstructed dendritic tree, and the edges between vertices, represent the connectivity matrix of the segments of a neuronal structure. Dendrites fall into a specific category of trees which have a root – the soma in the real cell – therefore all edges directionality lead away from the root. By convention the index 1 is attributed to the root of the dendritic

tree (**Figure 3.3**). Using graph theory, their branching structure can be well described with the corresponding directed adjacency matrix *dA*, a squared matrix of size $N\mathrm{x}N$, where N is the number of nodes in the tree (Cuntz et al., 2011).

The scarcity of multifurcations or self-loops in real dendrites led me to only consider binary graph trees as appropriate representations of real cells. Therefore, the diagonal of the adjacency matrix never contains an entry, and columns only have one. Since the root of the tree has no parent nodes, the first row is empty. All other rows have exactly one entry. For example, the following binary tree with $N = 8$,

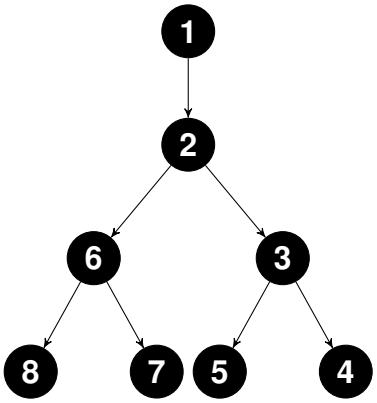

will have the following adjacency matrix:

$$\begin{pmatrix} 0 & 0 & 0 & 0 & 0 & 0 & 0 & 0 \\ 1 & 0 & 0 & 0 & 0 & 0 & 0 & 0 \\ 0 & 1 & 0 & 0 & 0 & 0 & 0 & 0 \\ 0 & 0 & 1 & 0 & 0 & 0 & 0 & 0 \\ 0 & 0 & 1 & 0 & 0 & 0 & 0 & 0 \\ 0 & 1 & 0 & 0 & 0 & 0 & 0 & 0 \\ 0 & 0 & 0 & 0 & 0 & 1 & 0 & 0 \\ 0 & 0 & 0 & 0 & 0 & 1 & 0 & 0 \end{pmatrix}$$

.

3.2.1 Morphometrics

The graph representation of real trees allows useful morphometrics to be extracted in a rigorous way. This morphological information is then used to address distinct research questions related to cell development, circuit formation, cell classification and information processing in the nervous system (Kanari et al., 2018; Schröter et al., 2017; Nanda et al., 2018; Cervantes et al., 2018; Zeng and Sanes, 2017; Schierwagen, 2008; Polavaram et al., 2014; Bota and Swanson, 2007). The subfield of neuroscience that carries the quantitative study of neuronal structures is called **neuromorphometry**, and

it can be roughly divided into four main categories: **topological**, **geometric**, **functional** and **dynamical** morphometrics (Brown et al., 2008). I will introduce some of the used measures in the field of neuromorphometry. However, the review I present here is not exhaustive; it rather reflects a choice of the measures most commonly used to quantify morphology, and which are illustrative of the aforementioned divisions.

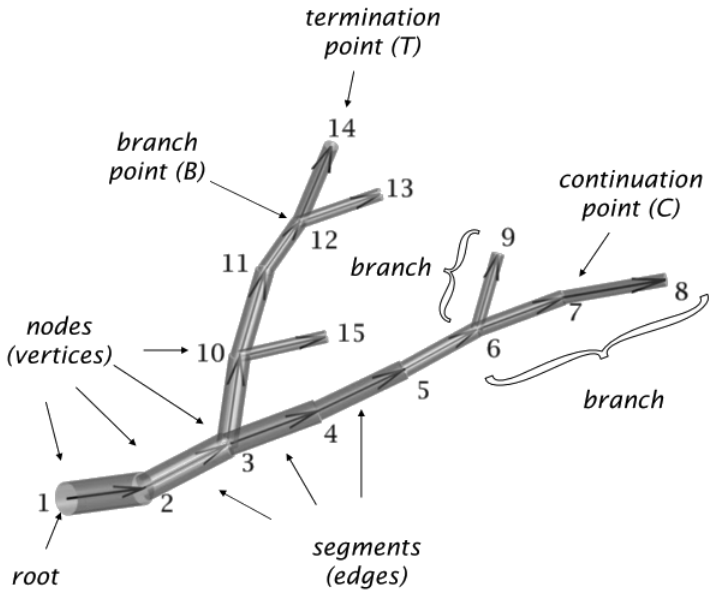

Figure 3.3: **Scheme of Dendritic Tree Translated into a Graph**
There are three types of vertexes, the *root*, the *branch point* and the *terminal tips*. The elements connecting the vertexes are *intermediate segments* and *continuation points*. The *root* is the point of origin of the tree, located at the soma of the real cell. The *branch point* is the vertex into which one segment enters and two segments exit. At a bifurcation, the parent segment gives rise to two daughter segments. A part of the tree composed of a certain subset of connected branches and vertexes is called the *subtree* (modified from Cuntz et al. (2011)).

Topological Morphometrics

Topological morphometrics focus on quantifying the branching pattern of a dendritic tree structure without considering their metric properties (**Figure 3.4**). For example, one of the most used measures to describe the structure of dendrites has been the *partition asymmetry*, that characterises the topological complexity of a tree based on the normalised difference between the degree of two daughter subtrees at any given branch point, without considering the branches' length (Uylings and Van Pelt, 2002). The partition asymmetry index A_p is defined as:

$$A_p = \frac{|r - s|}{r + s - 2} \tag{3.3}$$

with r and s indicating the number of terminal tips of each subtree, where $r \geq s$, and indicates the relative difference in the number of branch points $(r-1)$ and $(s-1)$ between

the subtrees. The partition asymmetry index ranges from 0 (completely symmetric) to 1 (completely asymmetric).

Another topological morphometric that does not consider the embedding of the tree in a metric space, is the Strahler ordering (Robert E, 1945). Originally, this measure was used in hydrology to quantify water basins' patterns. The algorithm starts by attributing the number order 1 to the terminal nodes of the tree and it increases the order number when branches of the same order merge on their path to the root. The Strahler number is defined as the number reached at the root of the tree after the procedure is exhausted. The Strahler ordering captures the overall branching complexity of the tree in a single value, making a comparison between trees straightforward. Table 3.1 presents some of the most used topological measures used to quantify dendrites.

Measure	Definition
Number of stems	Total number of segments leaving from the dendritic root
Number of branch points	Total number of branch points in the tree
Branch order	Topological distance from the dendritic root
Degree	Termination points downstream of the node under investigation
Partition asymmetry	Topological complexity of a tree
Strahler Order	Measure of topological complexity of a tree relating the order and asymmetry in that tree

Table 3.1: **List of Frequently Used Topological Measures to Quantify Dendrite Structure** (Cuntz et al., 2014).

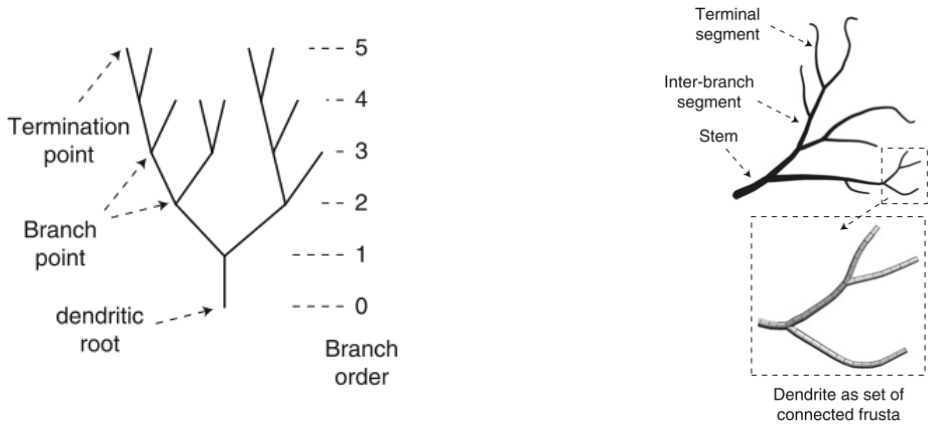

Figure 3.4: **Topological and Metrical Measures Terminology**
Left image - Topological analyses quantifies the connections and branching pattern of a dendritic tree. **Right image** - Metrical analysis quantifies the tree's geometry embedded in a metric space (modified from Cuntz et al. (2014)).

Metrical Morphometrics

Contrary to topological measures, metrical morphometrics consider the spatial embedding of a tree in a metric space (Jost (2007), **Figure 3.4**). These measures quantify

parameters such as length, curvature, surface area, volume and diameters of dendrites. Some examples of metrical morphometrics are presented in table 3.2:

Measure	Definition
Total length	Summed segment lengths of all segments in a tree
Path length	Summed consecutive segment lengths of a path between a given origin and a tip
Segment length	Path length of the incoming segment toward a node
Membrane Area	Surface area of the bi-lipid dendrite membrane
Dimension	Width, height, and depth of the bounding box
Segment diameter	Thickness of branch
Taper rate	The uniform decrease in diameter across a dendritic branch
Surface	Dendritic field area
Cable density	Ratio between total length and dendritic field area
Segment Tortuosity	Ratio between a segment length and the distance between the ends of it
Isoneuronal distance	Distance between a tip and the closest node not belonging to its path
Branching angle	Angle between a parent node and its daughter nodes
Fractal Dimension	Fractal dimension used as a measure of dendrite space-filling

Table 3.2: **List of Frequently Used Measures to Quantify Neuronal Geometry** (Cuntz et al., 2014).

Functional Morphometrics

Experimental and modelling studies have reported that neuroanatomical differences influence the electrical response of a neuron (Koch and Segev, 2000). Dendritic morphology, along with ion channels composition, appears to be correlated with differences in the firing patterns of certain cell types, including neocortical and hippocampal pyramidal cells (Mainen and Sejnowski, 1996; van Elburg and van Ooyen, 2010).

Structural morphometrics may act as proxies of differences in the electrotonic structure of a neuron. For example, longer and/or thinner dendritic branches have an influence on the attenuation of electrical signals arriving into the cell. The influence of dendrite structure on synaptic integration is well understood, with cable theory providing a solid framework to predict these effects (Segev et al., 1994). A measure emerging from this scheme that quantifies the efficiency between any particular synaptic input site and the cell body, while taking the physical properties of the neuron into consideration is the electrotonic distance (Segev et al., 1994; Koch and Segev, 2000). This measure is defined as the physical distance x scaled by the length constant λ[1] :

$$X = \frac{x}{\lambda}. \tag{3.4}$$

Similarly, the electrotonic length of a finite cable (i.e. dendrite) is the total length l scaled

[1]The voltage decreases to e^{-1}, that is, to 37% of its original value, at λ and to e^{-2}, or 13% of its original value at 2λ, and so on

by the length constant

$$L = \frac{l}{\lambda}. \tag{3.5}$$

A more general expression for X between two points i and j, applicable to cables of varying geometry or membrane properties, is

$$X = \int_{x_i}^{x_j} \frac{dx}{\lambda(x)}. \tag{3.6}$$

Besides the functional morphometrics that relate the physical structure to the electrical properties of the cell, there are others that link the morphology of neurons to their connectivity potential (Wen et al., 2009). One measure that specifically quantifies morphology and connectivity is the critical percolation density (Costa and Edson Tadeu Manoel Monteiro, 2003). The percolation density is calculated as the average density at which a path leading from the left to the right side of a lattice along dendritic branches suddenly emerges.

Dynamical Morphometrics

The development of better microscopy technology and computer software to track and measure dendritic arbours, made *in vivo* high-resolution time-lapse imaging of dendritogenesis possible (Hua and Smith, 2004; Hossain et al., 2012; Cline, 2001; Dailey and Smith, 1996; Nithianandam and Chien, 2018). Together these new methods of labelling, imaging, and quantification represent an emerging field termed *dynamical morphometrics* that allows precise characterisation of neuronal growth behaviour. In theory, any aforementioned topological, or metrical morphometric can be tracked through time, creating a time series which can be analysed to characterise and quantify diverse developmental and dynamical processes.

Another way to track dendrite differentiation during development is to use descriptors that categorise different morphologies and rank them based on their similarity. These distance tree algorithms can thus be used as a metric to quantify the similarity between morphologies during developmental studies, as well as for classification purposes as well (for a complete review see Cuntz et al. (2014)). Table 3.3 with some of these distance trees measures:

Measure	Definition
Edit distance	T1 to T2 by deletion and insertion of vertices
Shape Diffusion Index	Synthesized using the diffusion-limited aggregation
Persistence distortion distance	Minimal bottleneck distance between the PD's
Blastneuron	Alignment of the branches by topology and path shape
ACT	Sequence-based Tree Alignment
Topological Morphology Descriptor	Spatial structure of any tree as a "barcode"

Table 3.3: **List of Tree Distance Algorithms** (Cuntz et al., 2014).

3.3 Modelling Dendritic Structures

The use of computational tools in neuroscience has been proven extremely successful (Graham et al., 2011; Sterling and Laughlin, 2015; Jost, 2007; Dayan and Abbott, 2001; Sporns, 2011). At large, the field of computational neuroscience has two main objectives:

1. Store, disseminate and mine neuroscience databases (Ascoli et al., 2007).
2. Create and analyse computational, or theoretical, models of the nervous system (Graham et al., 2011; Jost, 2007; Dayan and Abbott, 2001).

In the following sections, I will focus on the latter.

3.3.1 Computational Modelling

In the last decades, computer models have proven themselves as a major tool in the advancement of neuroscience. By formalising the nervous system to a set of abstract equations or computer algorithms, they help to distill the structure and function relationship. As a result, these models can be used as explanatory or predictive tools to solve open problems in the field in an unambiguous way, and even to explore conditions that are very difficult to analyse experimentally (Graham et al., 2011; Jost, 2007; Dayan and Abbott, 2001).

However, there is still a disbelieve in the utility of some of these tools, particularly in the experimental community. This is due to the fact that models are in themselves complex and sometimes the relationship to the modelled system is not obvious due to its abstraction level. The trade-off between incorporating sufficient biological details and reducing this complexity to make the model tractable is an important factor when developing these tools. Finally, some of the parameters incorporated are hard to determine experimentally, and estimates need to be used or even complete guesses in some cases, shrinking the predictive power and reliability of a model enormously. To avoid this difficulty, a model must be constrained by empirical data at as many levels as possible (Graham et al., 2011; Jost, 2007; Dayan and Abbott, 2001).

3.3.2 Developing a Computational Model

The scientific question being addressed by the model will dictate the scale at which it has to be built, the level of details to be incorporated and the dynamics ruling the interactions of its elements. The very first step when building a model is to create a conceptual framework that attempts to capture the fundamental parameters and interactions that explain the function of that neuronal system. This process involves simplification and abstraction (Dayan and Abbott, 2001; Graham et al., 2011). Subsequently, the following three other steps need to taken into account when creating a model from scratch:

- **Informal or Formal Model** – informal models are less precise than formal models because they are conveyed using flow charts or images, whereas formal models are described in mathematical equations or computer algorithms. In theory, both can help hypothesis testing by predicting results that can be examined experimentally, however, formal modelling forces the modeller to be precise and self-consistent providing a much bigger predictive power to the model (Van Ooyen et al., 2014).
- **Level of Explanation or Scale** – understanding the nervous system requires comprehension of phenomena happening at many different levels and at spatial scales ranging from meters to nanometers. For each one of these scales, there are different computational models for how the elements at that specific level function and interact. These models range from biophysical plausible multi-compartmental models of single cells, that aim for studying the emergence of properties in the system due to the interactions of elements at a lower scale–bottom-up approach–to high-level neural fields that describe the spatiotemporal evolution of firing activity of populations of neurons, with disregard for the biophysical details from where they emerge from–top-down approach (Gerstner et al., 2015).
- **Phenomenological or Mechanistic Models** – formal models can be placed in a continuum ranging from phenomenological to mechanistic. As a rule of thumb, top-down strategies are phenomenological and bottom-up approaches are mechanistic. In a mechanistic model, the parameters and variables have direct biological interpretation and are fitted with real data. The simulation of the model, or solving its equations, give direct insight on how the neurobiological system, or behaviour, operates. Therefore, these models have superior predictive and explanatory power. However, one not always has access to all the relevant variables of the system, or incorporating all those variables would make the model untractable. When this is the case, phenomenological modelling is the best tool to apply. By replicating experimental data without explicitly model all the biological parameters, or underlying biological processes, a phenomenological model can provide insights on how the system works, and even be precursor of a mechanistic model of the same phenomena (Van Ooyen et al., 2014).

As models prove themselves useful explaining certain phenomena, they can be improved and generalised in order to accommodate more data. This maturation process usually follows a three-stage pattern (**Figure 3.5**). In the first demonstration stage, a model is the formal quantification of a series of experiments and it works to reassure the experimentalist that the results extracted from the experiments are correct and sound. The reference stage follows, where modelling is fundamental to the research design itself. Once the demonstration model reports good results in explaining the data, it can be improved incrementally in a loop of experiments →model generalization →new

experiments. Finally, when a reference model reaches a certain level after testing and improvement, it can not only give new insights about a given neural system but also lead new experiments in order to collect new data based on predictions gathered while simulating the model (De Schutter, 2009).

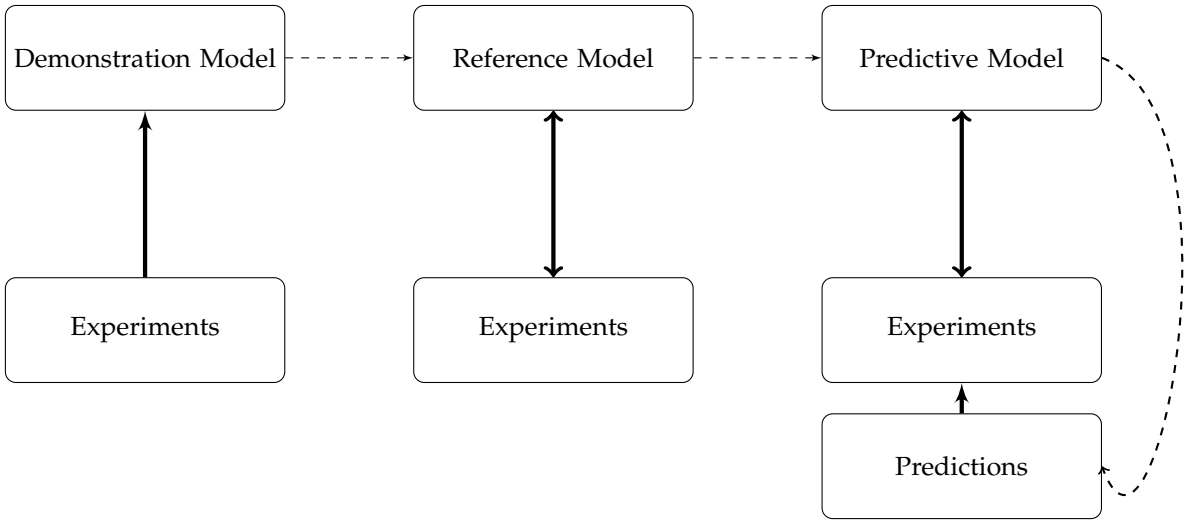

Figure 3.5: **Stages of Maturity of a Computational Model**.

3.3.3 Generative Models of Dendrite Growth

For classification purposes, a descriptive approach to dendrite morphometry may suffice. The quantification of dendritic shape using a combination of discriminative measures is enough to categorise different mature cell types and infer some functional roles (Zeng and Sanes, 2017). However, when one only analyses the morphology of developed cells, general principles of structure-function relationship are hard to distil because large variation exists in their morphologies due to distinct growing environments. To overcome this problem, a new approach was created which tried to invert the problem: instead of inferring principles by analysing anatomical characteristics, synthetic morphologies are generated *in silico* based on certain principles/mechanisms, and then compared with real cells. If the synthetic cell and the real counterpart match, it is plausible to assume that the underlying principle is indeed at play in nature (Cuntz et al., 2014; Graham et al., 2011).

To formulate a generative model of neurite shape, the modeller needs to take the parameters to be reproduced into account, e.g. branch angle, diameters, tapering and branch length. This is important because the choice of these variables will dictate what data is necessary to acquire and later compared with the synthetic cells. Moreover,

it will influence what underlying principles/mechanisms may be used to generate the morphologies, e.g. wiring minimisation, self-referential forces, or maximization of connectivity. Finally, it is crucial to decide if static morphometrics are enough to generate the synthetic cells, or if more information in the form of dynamical and/or functional morphometrics are required in order to constrain the model. Remembering the aforementioned postulates, generative models can be divided into three distinct categories. In the following section I will present an overview of the types of generative models of dendrite growth, starting from the most phenomenological to the more mechanistic (**Figure 3.7**):

1. **Reconstruction Models** – the simplest of the three models. Usually, these algorithms are designed to generate morphologies that replicate the shape of real cells at a static developmental time point, normally the adult stage. In the first step, from a given dendritic tree different morphometrics are quantified and statistical distributions are fit to those data. While analysing the data the modeller makes assumptions about the correlations between the variables (**Figure 3.6A**). Based on these assumptions, the algorithm then proceeds to generate realistic morphologies by sampling from the distributions of real data (Van Ooyen and Willshaw, 1999; van Ooyen, 2003; Uylings and Van Pelt, 2002; Graham et al., 2011; Ascoli and Krichmar, 2000).

2. **Growth Models** – seek to explain the spatiotemporal differentiation of dendritogenesis. Such developmental algorithms need to specify how distinct morphometrics evolve through time, in order to make predictions about the growth process (Graham et al., 2011; Nanda et al., 2018; Ganguly et al., 2016; Graham and van Ooyen, 2006). To properly constrain these models the modeller needs dynamical morphometrics. Some of these algorithms take the effects of branch self-avoidance into account (Memelli et al., 2013) or interactions between different dendrites on final arbour pattern (Van Ooyen and Willshaw, 1999; Torben-Nielsen and De Schutter, 2014; Van Ooyen and Willshaw, 2000; van Ooyen, 2003; Luczak, 2006; Vanherpe et al., 2016; Koene et al., 2009). Remarkably, growth models can incorporate functional assumptions, such as wiring minimisation (Cuntz et al., 2008, 2012, 2010) or connectivity maximisation (Stepanyants and Chklovskii, 2005; Rivera-alba et al., 2014; Van Ooyen et al., 2014), in order to generate highly realistic morphologies. The latter approach has significant advantages over other growth models because fewer parameters are used to generate the synthetic dendrites, while at the same time providing an overarching explanation for the structure-function relationship in those cells (**Figure 3.6B**).

3. **Biophysical models** – the most detailed of the generative models of dendrite growth (Graham et al., 2011). Final arbour pattern is derived using biophysical pa-

rameters known to be involved in dendrite outgrowth, including their production rate, local interactions and transport along the cell (Kuznetsov, 2010; Kobayashi et al., 2010; Krottje and Ooyen, 2007; Van Ooyen et al., 2001; van Veen and van Pelt, 1992; Li et al., 1995; Suter and Miller, 2011). These molecules can occupy intracellular or extracellular space. This class of model is often hard to constrain because the data required to do so is not available or difficult to obtain due to technological limitations. Moreover, simulating algorithms with this level of detail is computationally costly due to the vast number of parameters and their interactions (**Figure 3.6C**).

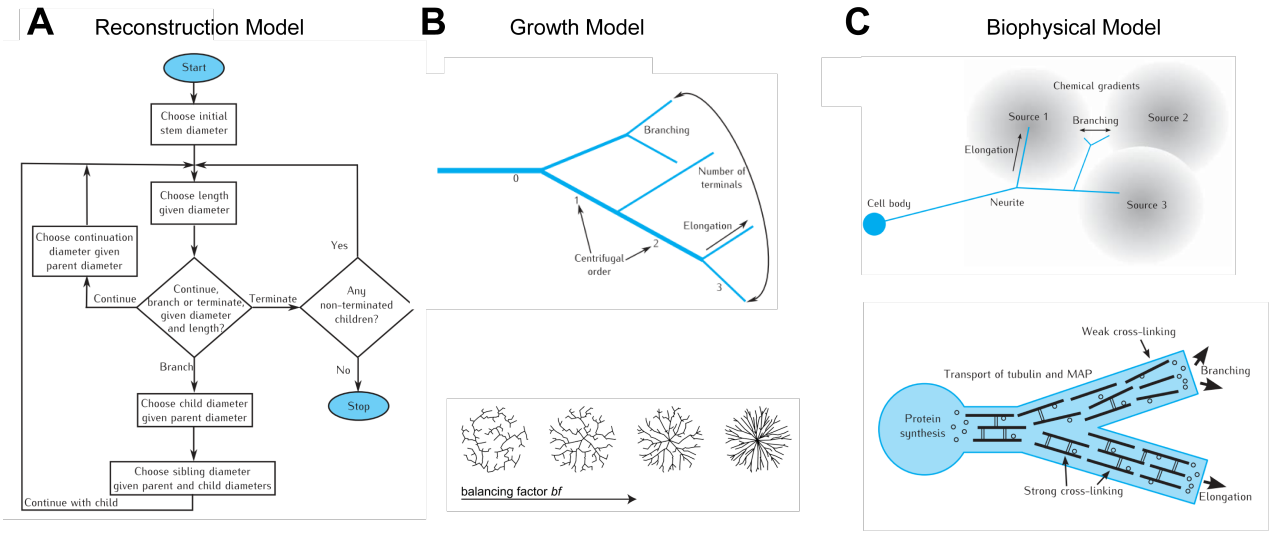

Figure 3.6: **Examples of Generative Models of Dendrite Shape**
A, an example of a sampling algorithm behind a reconstruction model. **B**, top panel, statistical growth model. This particular approach still works as a sampling algorithm, but each iteration generates a new dendritic tree, mimicking spatiotemporal differentiation. Lower panel, a functional growth model that tries to generate dendritic morphologies based on wiring optimization. **C**, top panel, biophysical model of dendrite outgrowth embedded in extracellular diffusible molecules. Lower panel, illustrative intracellular biophysical model where microtubule density and location increases the likelihood of branching (modified from Cuntz et al. (2010); Graham et al. (2011)).

3.4 Summary

In this chapter, the field of dendrite shape was reviewed, particularly the topic of dendritic structure quantification and modelling. The chapter started with an introduction to the topic of biological imaging tracing - the process of converting anatomical data into digital format. Afterwards, it was explained how dendritic structures can be quantitatively measured using different types of morphometrics. The chapter closed with an

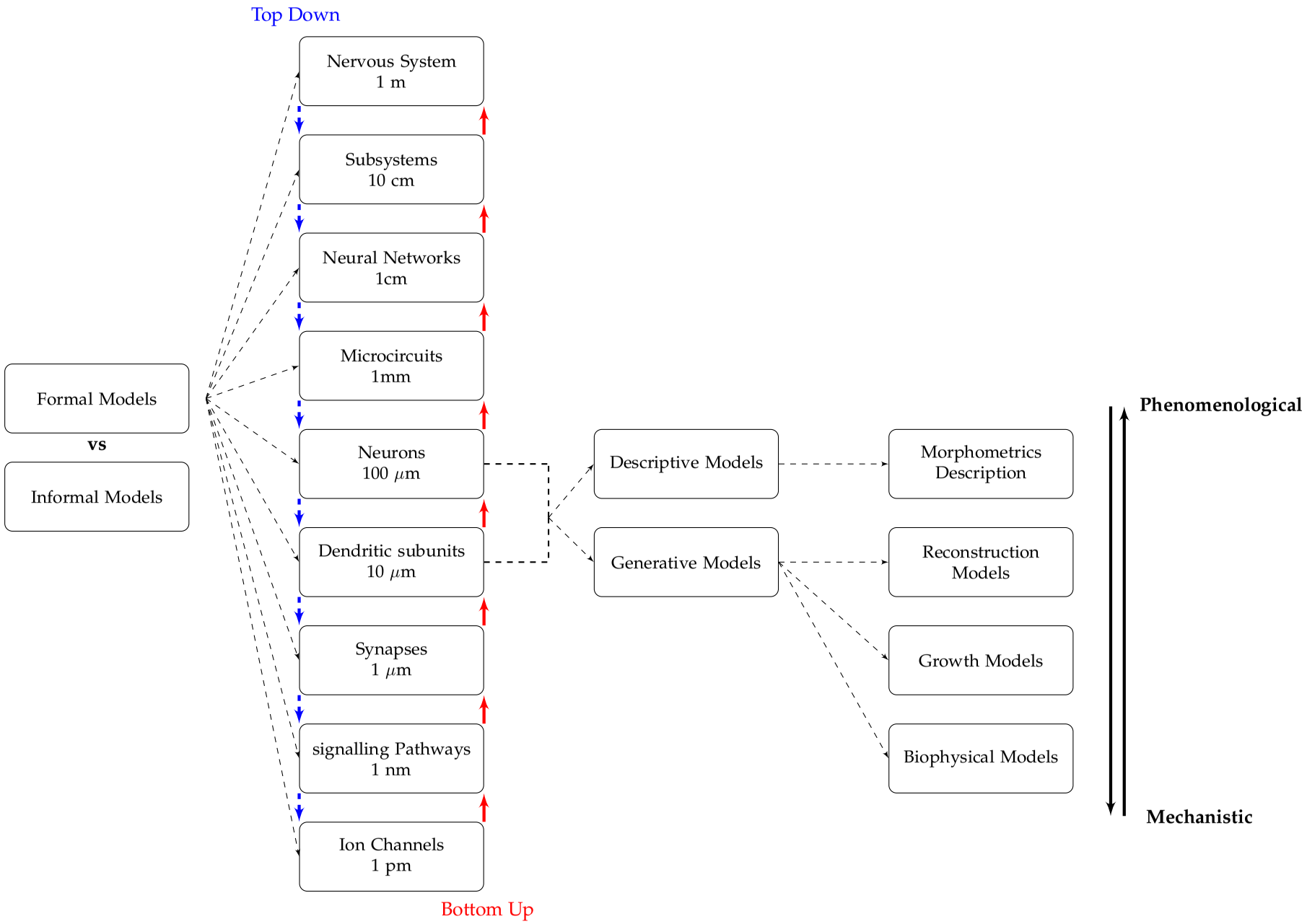

Figure 3.7: **Flow Chart of the Building Steps Underlying a Computational Model of Dendrite Structure**.

overview of how these measures are being used to create computational models that elucidate the link between structure and function in dendrites.

Chapter 4

Results: Balancing Wire and Function in c1vpda neurons

In this chapter, the results from the study are presented. Here, long-term structural time-lapse movies and functional imaging in freely moving *Drosophila* larvae were combined to quantify the stages of dendrite morphogenesis of c1vpda proprioceptive cells throughout development. How specific cell type functional requirements may be combined with optimal wiring constraints was analysed. Using the data collected, computational growth models that elucidated the different stages of dendrite development and their mechanosensory role were constrained.

4.1 Introduction

One of the biggest open questions in neuroscience is understanding how single neurons are adapted for specific functions (Carr et al., 2006). Even though recent technological advances have allowed new discoveries about dendrite function at various levels (London and Häusser, 2005; Stuart and Spruston, 2015) these efforts have fallen short on clarifying the structural and functional mechanisms that regulate dendritic arbour patterning (Lefebvre et al., 2015). This is largely due to not only experimental but also conceptual limitations (Hausser et al., 2017).

The *Drosophila* provides an excellent animal model for connecting the structure of dendrites to function (Dewell and Gabbiani, 2017). This is due to the small size of their nervous systems, and because they offer the possibility of sophisticated genetic manipulations and imaging (Akin et al., 2019; Allen et al., 2006; Cuntz et al., 2003; Farrow et al., 2003; He et al., 2019; Kohl et al., 2013; Vaadia et al., 2019). Particularly in the four classes of da neurons of the *Drosophila* larva PNS the generation of type-specific dendritic arbours is required to fulfil their physiological functions. For that reason, this model system is one of the best to investigate the molecular and genetic basis of the

dendrite structure-function relationship (Jan and Jan, 2010).

Recent experiments in freely behaving *Drosophila* larvae made important contributions in understanding the functional role of class I da proprioceptors (He et al., 2019; Vaadia et al., 2019). Evidence suggests that during crawling, the terminals of the different class I da neurons were sequentially deformed by the contraction of the body wall of the respective hemisegment where the cells were located (Heckscher et al., 2012). This structural deformation of terminals correlated with the activation of these neurons. It was hypothesised that this provided a peristaltic wave position encoding feedback mechanism during crawling (Vaadia et al., 2019). It was further reported, that da class I activation is correlated with dendrite bending during crawling. This sensitivity to membrane curvature is thought to be important in transducing the mechanosensory inputs by increasing the opening probability of MS channels expressed in those cells (He et al., 2019).

These findings are supported by previous studies where genetic manipulation of the sensory neurons' shape (Hughes and Thomas, 2007a) or null mutations of MS channels (Cheng et al., 2010) interfere with their sensory function, thus impairing crawling behaviour. Taken together, evidence suggests that the relay of proprioceptive information to the neuronal circuitry of motor control depends on precise dendritic morphology and specific localization of class I neurons in the body segments (Fushiki et al., 2016; Grueber et al., 2007).

Although the causal link between da class I deformation and behaviour is established, the temporal processes of cell patterning that lead to terminal arbour morphology remain largely unknown. The simple and stereotypical comb-like shape of c1vpda dendrites provides an ideal platform to question whether dendritic structure is optimised for mechanical signal transduction and if so, how do these cells pattern to perform this specific function? Do they form as the result of the assembly of an intrinsic deterministic program, or are they shaped by stochastic processes?

Additionally, being a set of proprioceptive neurons that respond to contractions in the larva body during crawling, c1vpda neurons do not obviously gain from satisfying optimal wiring constraints. Therefore, I used this system to study how the specific functional requirements may be combined with optimal wiring constraints during the developmental growth process that leads to the dendritic morphologies of the cells.

I combined long-term time-lapse imaging of dendrite development, theoretical modelling, functional imaging, *in silico* simulations and generative computational modelling to describe the spatiotemporal patterning of the c1vpda cell's dendrites. I identified and quantified the morphological dynamics of the different developmental stages of dendrite elaboration. In addition, I showed that calcium transients in c1vpda dendrites

correlate with the contraction of the body wall during forward crawling. Notably, I demonstrated that c1vpda cells can develop specialised dendrite patterns that support a well-defined function while respecting minimal wiring principles by combining noisy exploration of branch growth in their dendritic fields with random branch pruning.

4.2 Results

Each hemisegment of the larval body wall is innervated in the ventral and dorsal areas by class I neurons. This cell type present the lowest level of dendrite complexity of the four da classes. Specifically, the c1vpda cell innervates the ventral region of the fly's larval body and it is located in a flat 2D receptive field between the epidermis and the muscle. It has one laterally orientated primary dendrite stemming from the soma. Its terminals spread regularly along its length and perpendicularly towards the body wall (Grueber et al., 2002a)

Dendritic growth is the process that ultimately leads to cell type-specific morphologies. To successfully elucidate the structure-function relationship it is necessary to study the temporal processes of cell patterning (Jan and Jan, 2010; Lefebvre et al., 2015; Sugimura et al., 2003; Williams and Truman, 2004). Thus, my first goal was to investigate how the stereotypical comb-like shape of c1vpda neurons develop. And to understand how this process is combined with minimisation principles throughout development.

4.2.1 Long-term Time-lapse Imaging Reveals c1vpda Growth Stages

I addressed these questions by resolving the spatiotemporal dynamics and developmental mechanisms of the c1vpda cell growth program. The static evaluation of fully developed c1vpda cells would not allow the observation of the timing between consecutive branching events and elongation, avoiding the complete understanding of how dendrites of this da class acquire their distinct shape. Previous studies shed light on the developmental process of c1ddaD and c1ddaE during embryonic and larval stages (Gao et al., 2000; Sugimura et al., 2003) and metamorphosis alike (Shimono et al., 2009; Williams and Truman, 2004). However, as this was never done for c1vpda during embryonic and larval stages, I examined the development stages of the c1vpda cells more closely.

In order to resolve the cell differentiation process within a developmental continuous process, dendrite formation was studied by long-term, non-invasive time-lapse imaging since embryonic stages ($16hr$ AEL) until 3rd instar ($72hr$ AEL) (**Figure 4.1A**, top panel).

Initial dendrite formation started at around $16hrs$ AEL and was studied by time-lapse reconstructions using $30mins$ and $1hr$ intervals (see **Methods-Chapter 6**) in the embryo (**Figure 4.1A**, left panels). The polarisation of the soma started at around $16hrs$ AEL

with a simple growing tip sprouting from the soma, innervating the hemisegment dorsally and running parallel to the other ventral cells (**Figure 4.1A**, left panels). Within $1hr$, additional lateral branches emerged from the initial main stem extending in an anterior-posterior orientation.

Subsequently, an extension phase could be observed where new secondary branches kept sprouting from the initial stem with the same orientation as previous side branches and higher-order branches grew from existing side branches. Branches underwent repeated cycles of splitting and elongation until a peak number of branches was achieved at around $18.5hrs$ AEL (**Figure 4.1B**, middle panels). In concordance with c1ddaE and c1ddaD growth dynamics (Gao et al., 2000; Sugimura et al., 2003), dendrite complexity increased by interstitial branching and not through growth cone splitting (**Figure 4.1A**, middle panels).

To quantify the growth process during this stage, I analysed the developmental trajectories of key morphometrics. Namely the number of branch points, total dendrite length and surface of the dendrite spanning area during development in relation to one another. During the extension phase dendrite's cable length increased linearly with the available spanning area ($R^2 = 0.92$; **Figure A.1A**, right panel). New branches were added in a linear manner with the increase of the total length ($R^2 = 0.86$, **Figure A.1A**, left panel) and surface area alike ($R^2 = 0.73$; **Figure A.1A**, middle panel).

Surprisingly, after the peak number of branches was reached at around $18.5hrs$ AEL, the c1vpda cell went through a pruning phase, characterised by a reduction of branches and arbour pattern simplification (**Figure 4.1A, middle panels**, arrows). At around $20.5hrs$ AEL, dendrite structure stabilised after the number of branches decreased to approximately the same number of branches found in the first instar stage.

During the pruning phase, the dendrite's cable length decreased linearly with the reduction of branches ($R^2 = 0.77$; **Figure A.1B**, left panel). However, the pruning of branches add a small effect in decreasing the surface area of the cell ($R^2 = 0.21$, **Figure A.1B**, middle panel) and so did the reduction of dendrite cable ($R^2 = 0.41$, **Figure A.1B**, right panel). The previous relationships suggest that higher-order branches located in the inner part of the dendrite spanning area were the ones being retracted the most (**Figure 4.1B**, arrows). These branches have a small influence in defining the area where c1vpda dendrites spread on due to their location in the dendritic field.

The pruning phase was followed by a pre-hatching stabilisation period (**Figure 4.1A, right panels**). In this phase, virtually no new branches were added despite of the small increase of the total length ($R^2 = 0.33$, **Figure A.1C**, left panel) and surface area ($R^2 = 0.27$, **Figure A.1C**, middle panel). Dendrite cable length slightly increased linearly with the available spanning area ($R^2 = 0.74$, **Figure A.1C**, right panel), but at a lower

rate than during the initial extension phase.

I imaged the post-hatching dendrite development at the time points of $30hrs$, $50hrs$ and $72hrs$ AEL. The cells continued growing concomitantly with the expansion of the body wall (**Figure 4.1B**), with the dendrite's cable length increasing linearly with the available spanning area ($R^2 = 0.97$, **Figure A.1D**, right panel). However, this phase was also characterised by the stabilisation of the shape and complexity of the c1vpda dendrites, with new branches hardly emerging regardless of the increase of dendrite cable ($R^2 = 0.17$, **Figure A.1D**, left panel) or new available surface area ($R^2 = 0.09$, **Figure A.1D**, middle panel).

The observed dendrite pattern at $30hrs$ AEL was fundamentally the same as the one observed at $72hrs$ AEL, suggesting an isometric scaling of these neurons during larval stages (**Figure 4.1B**). The conservation of dendrite shape throughout larval stages suggests the need for functional conservation (Almeida-Carvalho et al., 2017). In sum, the time-lapse data indicates that c1vpda neurons' dendrite pattern is essentially developed and refined during initial embryonic stages. In subsequent larval stages, these cells scale isometrically in coordination with the increase of the size of the larva's body (Parrish et al., 2009).

4.2.2 Differentiation of c1vpda Dendrites Respect Wiring Minimisation Principles

To gain insight on the morphological maturation process of these cells, I quantified the dendrite structure of the reconstructed image stacks obtained from the time-lapse imaging using 49 distinct morphometrics (see **Methods-Chapter 6**). In a t-distributed Stochastic Neighbour Embedding (tSNE) (van der Maaten, 2008) plot of the entire dataset based on morphological similarity it is evident that developmental time was a strong source of variation in the data (**Figure 4.2A**). Since the underlying developmental trajectories of the key morphometrics were not readily apparent on the 2D tSNE representation, I plotted the number of branch points, total length and surface area of c1vpda cells during development (**Figure 4.2B** and **C**).

A mathematical scaling law relating the total length of dendritic wiring to the number of branch points and surface of planar dendrites was previously derived (Cuntz et al., 2012). It was shown that optimal wiring predicts a $\frac{1}{2}$ power law between the above mentioned morphometrics (see **Methods-Chapter 6**). Equipped with this simple equation, I examined the way c1vpda cells wire during development. As predicted, I found a square root relation between dendrite length and surface area (**Figure 4.2D**, left panel), and a square root relation between total length and number of branch points.

Afterwards, to strengthen the hypothesis that c1vpda cells minimise wire, I tried to

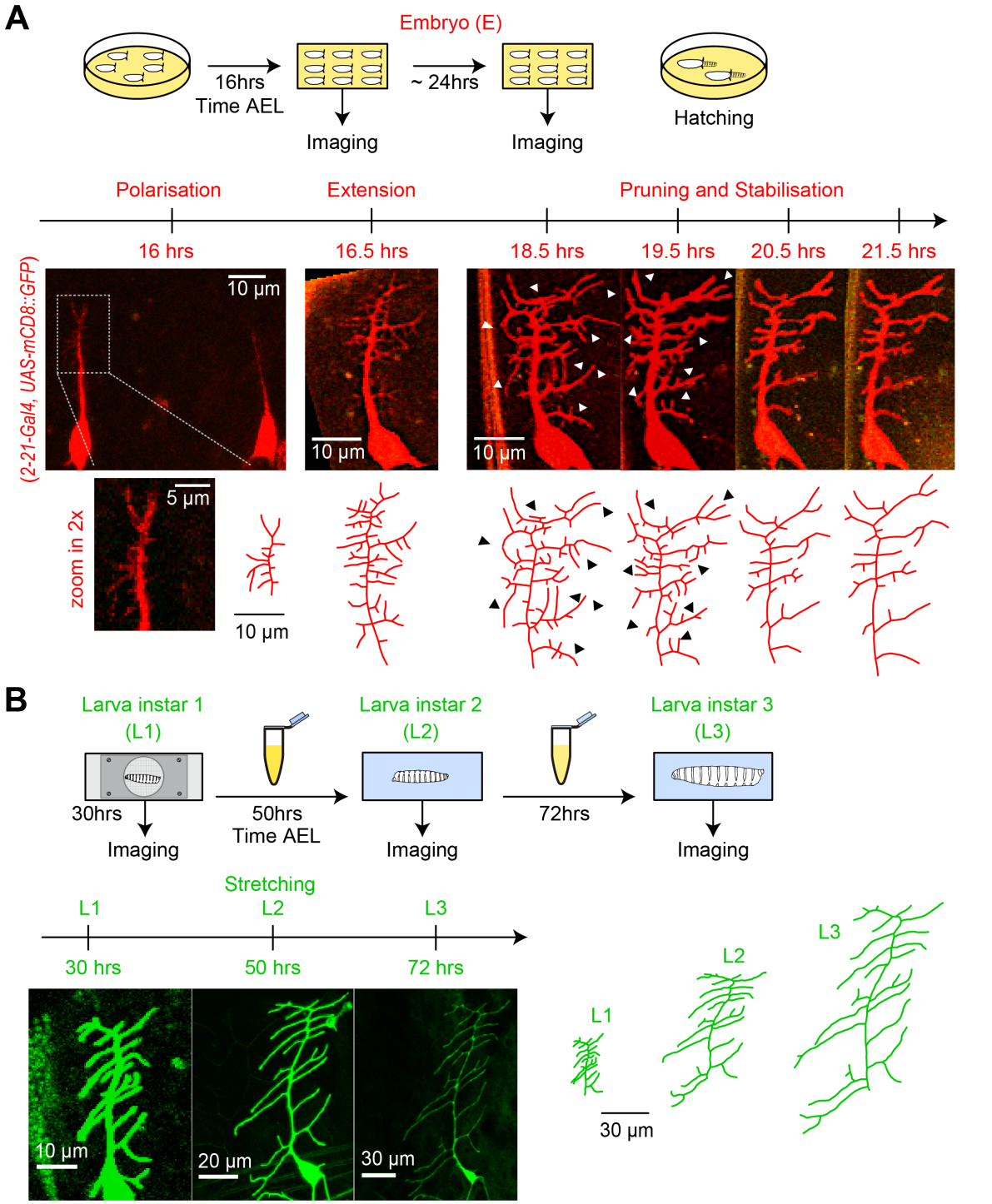

Figure 4.1: **Stages of c1vpda Dendrite Morphology Throughout *Drosophila* Embryonic and Larval Development.**

A, sketch (top row) illustrating the imaging conditions. Timeline and maximum intensity projections (middle row) of image stacks as well as reconstructions (bottom row) of representative c1vpda dendrites. White arrows and corresponding black arrows indicate pruning areas (see main text). **B**, Imaging of Larval stages, similar to **A**. Times shown are AEL.

replicate the scaling relationships of the key morphometrics using minimum spanning trees (MST) **Methods-Chapter 6**). Synthetic trees were generated using a formerly described minimum spanning tree (MST) based algorithm (Cuntz et al., 2008, 2010). In order to facilitate comparing both datasets, artificial and real morphologies were normalised to a standard surface area of $100\mu m^2$. As a result, I could then show that the number of branch points and the total length of the artificial trees scaled linearly with the real counterparts, with the experimental data being well fitted by the synthetic data ($R^2 = 0.98$; **Figure 4.2D**, right panel).

Taken together, the results in this section indicate that throughout differentiation during development, c1vpda neurons respect minimum wire constraints. Surprisingly, not only mature cells do so, but so do the embryonic ones. They grow to fill the target space optimally, using the least amount of wiring to achieve their mature shape.

Embryonic pruning of branches increases dendrite perpendicularity

Having established that the specification of c1vpda dendrite patterning fundamentally occurs during embryonic stages, I turned to examine how the observed pruning phase reorganizes the tree structure. I reasoned that the pruning of a dendritic tree could have economical benefits, by minimising the amount of wire used to perform a given function. Instead, it could improve the effectiveness of the cell by refining the branching pattern to enhance functionality. Since I previously demonstrated that the cells optimise wire throughout their developmental course, I moved on to investigate if the pruning phase had functional implications.

Visual inspection of a typical time series of a c1vpda cell being pruned (**Figure 4.1A**, middle panels) and the morphometric relationships observed during that phase suggested a possible retraction preference of smaller, non-perpendicular, higher-order branches. It was recently reported that mature c1vpda neurons spread dendrites perpendicularly to the body wall of each hemisegment to sample cuticle folding during crawling behaviour (Vaadia et al., 2019). This motivated me to understand if the pruning step increased the c1vpda arbour morphology perpendicularity.

To investigate the effects of the pruning step on overall arbour directionality, I first quantified the morphology of c1vpda cells during pruning. I began by considering the side branches that emerged from the initial main stem, leaving the main stem out of the analysis. To estimate how the side branches of the cells are directed towards the body wall, I used a new measure named *perpendicularity* (see **Methods-Chapter 6**) to capture the angles distribution of the overall dendritic tree before (**Figure 4.3A**) and after pruning (**Figure 4.3B**).

After quantifying the orientation of the side branches, I characterised the side branches

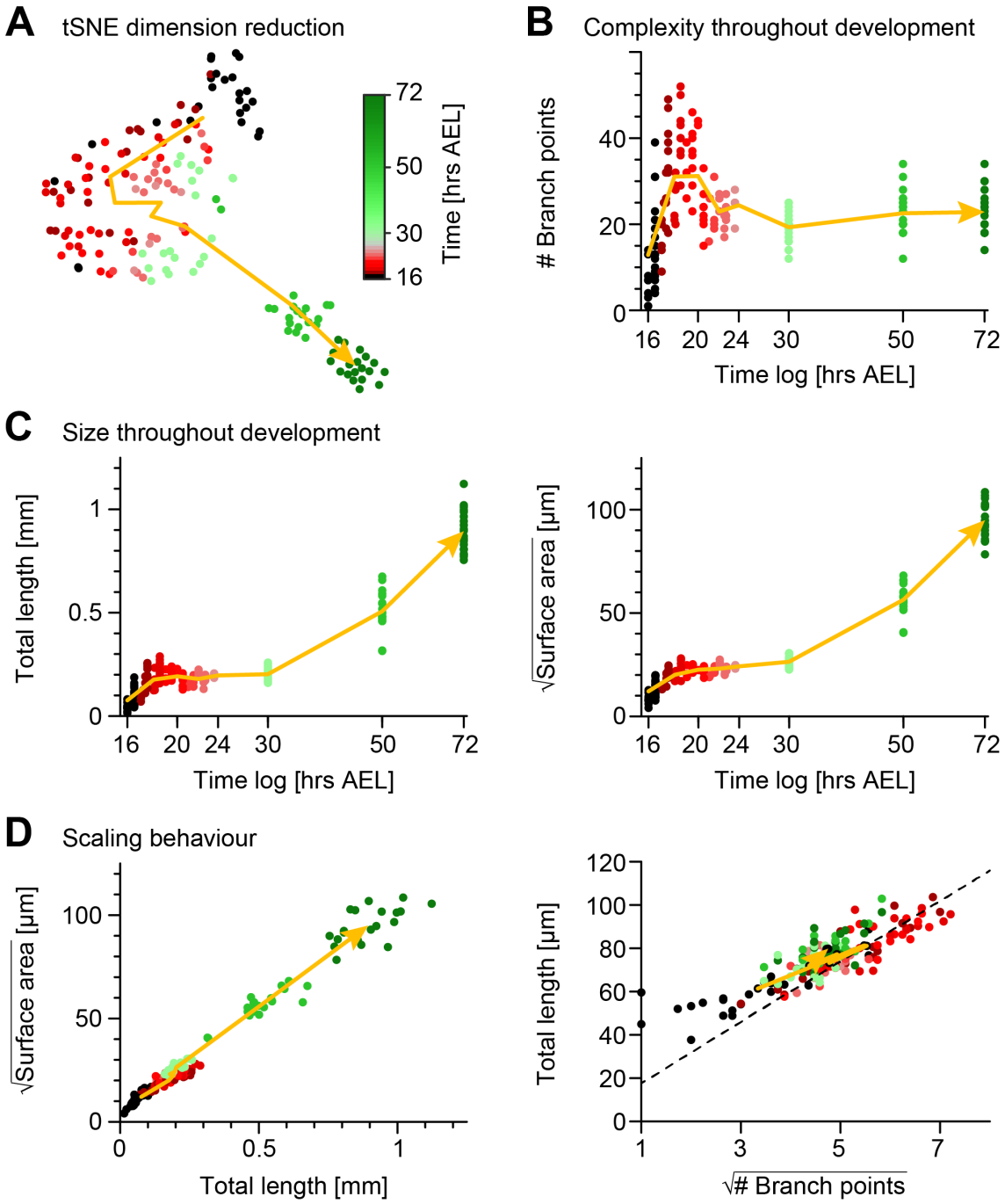

Figure 4.2: **Differentiation of c1vpda Dendrite Throughout Development.**

A, tSNE plot showing the entire dataset using a $49-$dimensional morphometric quantification. **B**, Changes in the number of branch points during development. **C**, Changes in the total length of dendrite cable (left) and square root of the surface area (right) during development. **D**, Scaling behaviour of the square root of the surface area against total length (left) and total length against number of branch points (right). Both show the linear relationships predicted from the optimal wiring equations (Cuntz et al., 2012; Baltruschat et al., in preparation). The dashed line shows the average scaling behaviour of the simulated synthetic trees ($n = 1000$ simulations; see **Methods-Chapter 6**). In all panels, each dot represents one cell with the colour scheme indicating imaging time AEL. The yellow arrows show average behaviour of all neurons across two hour bins. Data from $n = 165$ reconstructions.

by ordering them using a new branching scheme named *Branch Length order* (see **Methods-Chapter 6**; **Figure 4.3**, trees representations; **Figure B.1**) to capture the stereotypical comb-like shape of the cells. The new branching scheme allowed us to distinguish the longer initial side branches sprouting from the main stem from the smaller higher-order branches in an unbiased way. This enabled us to compare their morphometry before and after pruning.

To scrutinise the consequences of pruning in the morphology of the cells, I plotted the relationship between Branch Length order, perpendicularity and actual branch length. In the right panels of Figure **4.3A**, it can be seen that at the peak of branching complexity, i.e. before pruning initiation, higher-order branches are characterised by smaller lengths (with a median of $1.6\mu m$) and lower median angles ($37.31°$) than first-order branches ($6\mu m$, $64.72°$, respectively, $p < 0.001$, $p < 0.001$ by bootstrap).

I then analysed the morphology of the same cells after pruning (Figure **4.3B**, right panels). Notably, the median branch length and angle before and after pruning of first-order branches remained approximately at similar values ($6.1\mu m$ and $63.93°$). The same trend was observed for higher-order branches ($2\mu m$ and $41.67°$).

However, the drastic reduction in the total number of branches was asymmetrically distributed between the different branch orders. By comparing Figure **4.3A** and Figure **4.3B**, it can been seen that the retraction of higher-order branches (number before pruning = 267 vs. number after pruning = 92, decrease of 64.9%) greatly exceeds the reduction magnitude of first-order branches (number before pruning = 162 vs. number after pruning = 131, decrease of 19.1%).

Importantly, this morphological effect of the pruning step has the direct consequence of reshaping the overall branch angle distribution profile of the dendrites by skewing it to higher angles. The reduction of the higher-order branches flattens the angle distribution of these branches but leaves the pronounced peak of the first-order branches at higher angles relatively unchanged (median angle before pruning = $49.41°$, median angle after pruning = $59.04°$, difference of the median = $9.99°$, $p < 0.05$, by bootstrap).

This comparison between the morphologies of c1vpda cells before and after pruning supports previous observations on the possibility of a preferential subtraction of smaller, non-perpendicular higher-order branches. The asymmetrical reduction of branches with different orders refines the overall dendrite shape, increasing its perpendicularity. This analysis provides a first step in the direction of understanding the patterning of c1vpda.

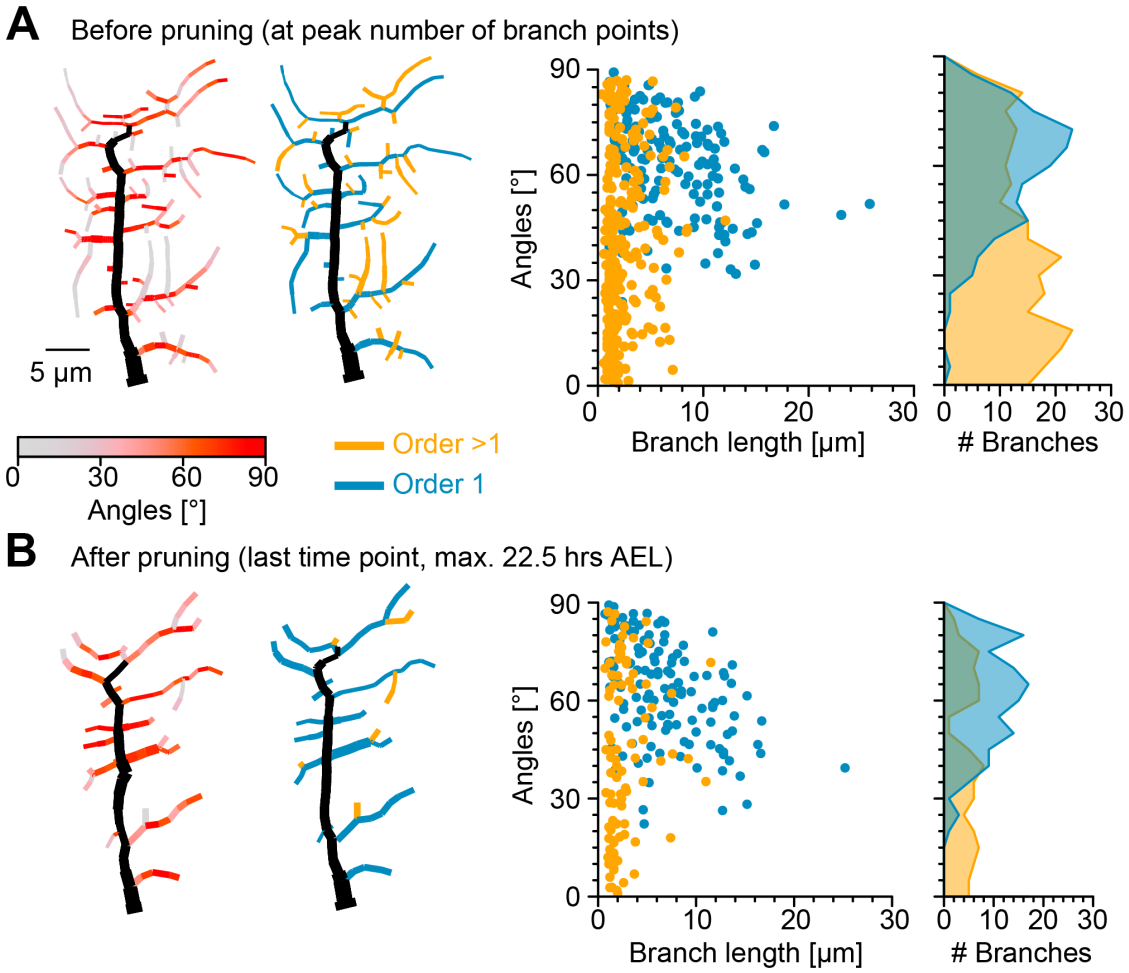

Figure 4.3: **Quantification of the Morphological Effects of Pruning.**

A, Illustrative c1vpda morphology before pruning. Morphology on the left side is colour coded by branch segment angles and morphology on the right is colour coded by Branch Length order (see text). On the right, histograms for branch length (one dot per branch) and number of branches per angle are shown separated by Branch Length order (blue: order 1, orange: order > 1, $n = 429$ branches). **B**, Similar visualisation but for dendrites after pruning ($n = 223$ branches).

4.2.3 C1vpda Dendrites may Optimize Mechanosensory Signal Transduction.

A recent study proposed dendrite curvature as the transduction mechanism of mechanosensory cues in class I neurons (He et al., 2019). Several findings are consistent with this hypothesis. First, it has been reported that MS channels change their pores conformation by sensing local changes in membrane tension when bending (Liang and Howard, 2018).

As mentioned in the introduction, disrupting the expression of MS channels on class I neurons leads to failure of activation of these cells (Cheng et al., 2010; Guo et al., 2016; He et al., 2019), causing locomotion impairments. Similar results were reported in C.elegans, (Yeon et al., 2018).

Finally, it was revealed that unique structural adaptations, amongst the da system, in the microtubule mesh of class I neurons, support their role in sensing and responding to mechanical stimuli (Delandre et al., 2016). The class I dendrites have dense arrays of microtubules, which are robustly connected to the epithelium by pads of electron-dense material (Delandre et al., 2016). These adjustments seem to support the mechanical forces required for mechanosensory signal transduction. Also other cells active in mechanotransduction have the same structure, corroborating the putative role of c1vpda cells as proprioceptors (Krieg et al., 2014; Liang et al., 2013, 2014).

However, it is not clear if class I dendritic branches are spatially arranged to maximize mechanical cues transduction through curvature. Particularly, for c1vpda cells, it is unknown whether the stereotypical comb-like shaped dendrite pattern, characterised by high perpendicularity of its side branches is shaped to optimize not only wire but to maximise membrane curvature (Vaadia et al., 2019). Interestingly, previous theoretical results on elastic properties of lipid bilayers showed that curvature is dependent on the tiltedness of the membrane (Helfrich, 1973).

This led me to first seek to demonstrate that c1vpda dendrites activation in freely forward-moving larvae follow branch deformation. Following a similar experimental setup (see **Methods-Chapter 6**; Figure **C.1**) as in Vaadia et al. (2019), I generated in strict collaboration with Lothar Baltruschat, from the German Center for Neurodegenerative Diseases in Bonn, a dual-expression line of larvae to label c1vpda cells with both calcium-sensitive GFCaMP6 (green) and static tdTomato (red) to relate c1vpda activation to segmental contraction and extension phases during crawling. I measured the calcium transients at the dendrites to precisely quantify the temporal correlation between segment contraction and dendrite activation.

I observed rises in GCaMP fluorescence in c1vpda neurons during segment contraction (Figure **4.4A**). The mean calcium response peak ($\frac{\Delta F}{F} = 2.35$) appeared shortly after the maximum segment contraction ($lag = -0.2s$). Moreover, both variables correlated very strongly ($r = 0.77$, $p < 0.001$, by Pearson coefficient). Calcium signals decreased as the peristaltic wave advanced to adjacent anterior segments (Figure **4.4A**; Figure **C.1A**). These data, support the finding that c1vpda neurons respond to body wall folding during segment contraction and that the transduction machinery for sensing locomotion may be localized to the dendrites of these cells.

After validating the functional link between body wall contraction and cell activation, I wondered if the c1vpda stereotypical dendrite shape is patterned to optimize signal transduction. I tested the effects of cuticle folding on the curvature of the lateral branches using a theoretical curvature model (**Methods-Chapter 6**, Figure **D.1**).

I designed a geometrical model in strict collaboration with Amirhoushang Bahrami,

from the Max Planck Institute of Biophysics in Frankfurt am Main, of tubular structures bending (see **Methods-Chapter 6**; **Figure D.1**). The tilting angle varied from $\theta = 90°$ for a branch spreading along the body-wall epidermis in the anteroposterior axis, e.g. some side branches, to $\theta = 0°$ for a tube spreading dorsally, e.g. the main stem. I then plotted the normalised branch curvature increase as a function of the tilting angle. As shown in **Figure 4.4B**, I observed a steady increase of the branch curvature with the increase of the respective tilting angle independently of branch length, or size of the tube. Theory, therefore, suggests that dendritic branches spreading perpendicularly to the body wall may increase signal transduction of mechanosensory inputs through membrane curvature (**Figure 4.4C**).

I then examined the functional implications of the pruning step on the bending curvature of the c1vpda dendrites. Lower angle branches show reduced curvature increase (Figure **4.4B**, **C**), so I reasoned that the retraction preference of branches with low perpendicularity angles could increase the overall cell's bending curvature. To test this hypothesis, I computed the bending curvature of c1vpda cells and plotted it against Branch Length order.

In Figure **4.4D**, left panel, it is shown that the distribution of bending curvature increase of first-order branches is further skewed towards larger magnitudes (median of the distro = 0.93), while the higher-order branches showed smaller median bending curvature increase (median of the distro = 0.71, difference between medians = 0.22, $p < 0.001$, by bootstrap). These differences in the distribution profiles of bending curvature between first and higher-order branches are a good qualitative match to the angle distributions found on the same dataset. These observations strengthen our hypothesis that the pruning of low angle branches may increase the fold change of bending curvature, by removing branches that show reduced curvature when the body wall contracts.

For that reason, I computed the relative bending curvature of branches in c1vpda morphologies before (median of 0.93 for first-order and 0.71 for higher-order branches with a difference between medians of 0.22, $p < 0.001$, by bootstrap) and after pruning (median of 0.93 for first-order and of 0.76 for higher-order branches with a difference between medians of 0.18, $p < 0.001$, by bootstrap; **Figure 4.4D**, left and middle panels). Similarly to the perpendicularity measured in **Figure 4.3**, the retraction of predominantly higher-order branches led to an overall higher median bending curvature (7.6% increase, $p < 0.001$, by bootstrap). The increment was caused by the pruning of low bending curvature branches (**Figure 4.4D**, rightmost panel).

Taken together, these data suggest that the patterning of the c1vpda dendrites is determined by functional constraints. The high morphological complexity before pruning, characterised by branches with low perpendicularity, would elicit less effective mechan-

otransduction. The angle orientation of the side branches correlates with the bending curvature, and, therefore, with the mechanical displacement of the membrane (Katta et al., 2015; Liang and Howard, 2018). This increases the opening probability of MS channels. These findings give support to the proposed mechanism where dendrite curvature may drive the activation of class I da neurons, by generating tension or compression in the dendritic membrane, or cytoskeleton (He et al., 2019; Krieg et al., 2014).

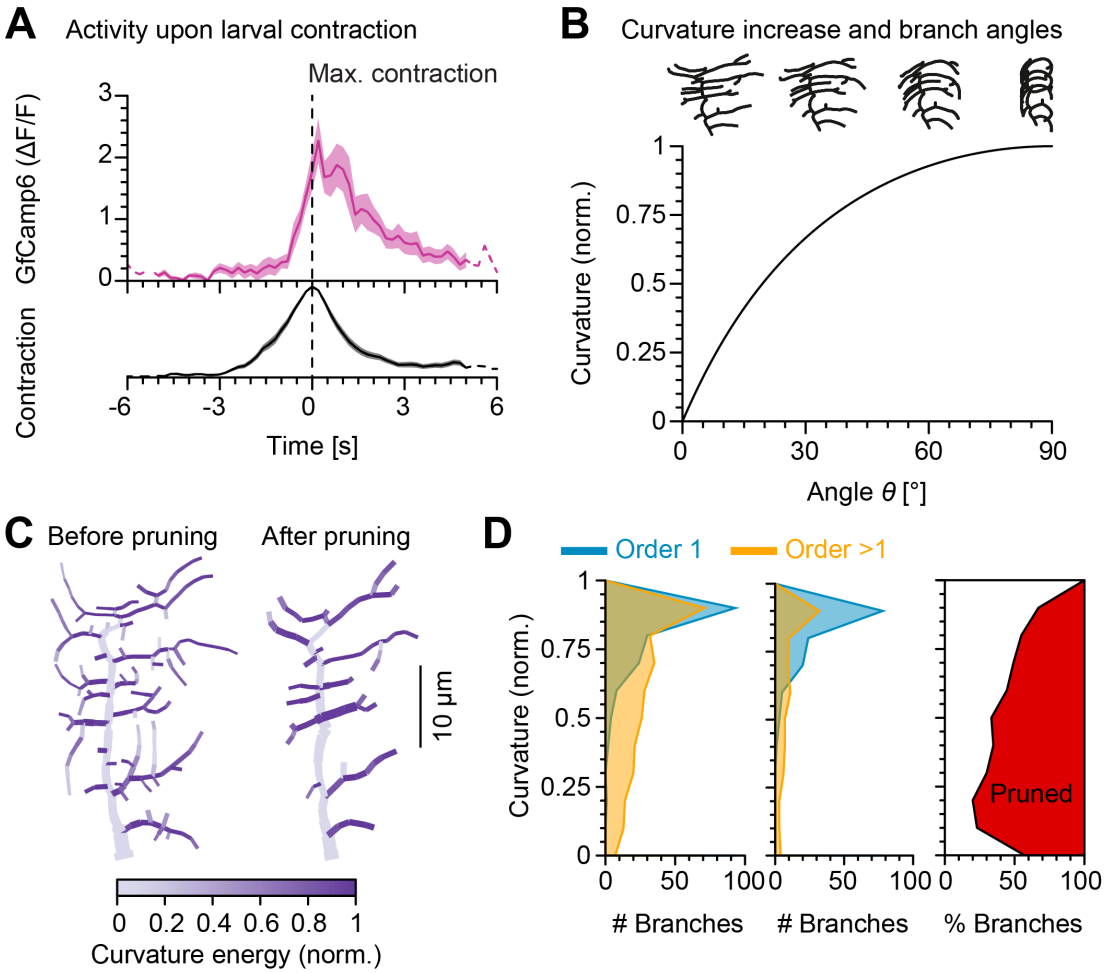

Figure 4.4: **Selective Pruning Increases Predicted Overall Bending Curvature.**
A, (Top) Mean Ca^{++} responses of c1vpda dendrites during crawling. Data from 6 animals, $n = 25$ cells; solid pink line shows average values where data comes from $n > 5$ cells and dashed pink line where $n < 5$ cells. SEM in pink shaded area. (Bottom) Average normalised contraction rate during crawling behaviour (similar plot as in top panel but in black colour). **B**, (Top row) Simulated contraction of a c1vpda morphology by wrapping around a cylinder. From left to right, resting state all the way to maximum contraction. (Lower panel) Relationship between normalised bending curvature experienced by a single branch as a function of its tilting angle θ. **C**, c1vpda Dendrite morphologies before (left) and after (right) pruning. Morphologies are colour coded by local curvature increase during segment contraction. **D**, Similar visualisation of the same data as in **Figure 4.3** but for curvature energy before and after pruning. Rightmost panel additionally shows the pruning (red shaded area) of branches by bending curvature increase.

4.2.4 *In silico* simulations and *in vivo* branch dynamics predict a stochastic pruning

After establishing a putative functional role of the pruning phase, the next to better understand how this stage reorganizes the spatial arrangement of the dendritic tree. The biological machinery behind branching dynamics is extremely complex (Akhmanova and Steinmetz, 2015; Chesarone and Goode, 2009; Coles and Bradke, 2015; Gomez and Letourneau, 2014). Instead of trying to comprehend the molecular or cellular components of branching dynamics during pruning, I wanted to address the morphological characteristics of the pruned branches. Is a selective pruning of higher-order branches, or one that is specific to branches with non-optimal angles most consistent with the analysed data?

To address this question I simulated *in silico* the selective pruning of four different types of terminal branches. Each scheme was applied on the morphologies before pruning and the results were compared with the real morphology after pruning (**Figure 4.5A**):

1. **Short branches first**.
2. **Low perpendicularity branches first**.
3. **higher-order branches first**.
4. **Random pruning of branches**, as a control condition.

When comparing the morphological differences between synthetic and real cells, it was observed that the random pruning scheme was the only yielding results not significantly different from the real trees. This suggests that the reshaping of the c1vpda dendrites may occur without resorting to a branch type-specific, deterministic pruning. Thus, I propose that a stochastic pruning mechanism may be sufficient to refine the structure in a self-organized manner (Hiesinger and Hassan, 2018).

In order to dissect the dynamics of the pruning phase, I performed time-lapse analysis at the single tip resolution (see **Methods-Chapter 6**). Branches were classified into one of the following five types (**Figure 4.5B**):

- **Pruned**.
- **Retracting**.
- **New**.
- **Elongating**.

- **Stable**.

When tracking the rates of extension and retraction of individual branches, I discovered that all types of branches maintained a relatively constant trend during pruning (**Figure 4.5C**, left panel). Both retraction and extension averaged approximately between 2 and $3\frac{\mu m}{hr}$ in all cases. This hints a branch type and time-invariant mechanism of branch polymerisation and depolymerisation in c1vpda cells.

In the right panel of **Figure 4.5C**, I observe an initial phase of intense branch dynamics when a short percentage of branches remained stable. This period lasted approximately half of the analysed time frame. During this interval, approximately half of the branches were pruned, while the number of new and elongating branches decreased (**Figure 4.5C**, right panel). Afterwards, the stabilisation phase ensued, characterised by a percentage increase of stable branches, and the decrease of pruned branches. By the end of this stage, the number of new branches almost disappeared. At the same time, the proportion of elongating branches increased back to compensate for the remaining retraction.

4.2.5 Computational growth model reproduces c1vpda dendrite development

In order to improve our understanding of the temporal patterning of c1vpda cells in the embryo, I formalised the stages of dendrite differentiation using computational modelling. In the past numerous models focusing on stochastic rules governing dendrite growth and branching have been proposed and applied to generate neuronal morphologies (Cuntz et al., 2010; Donohue and Ascoli, 2008; Eberhard et al., 2006; Koene et al., 2009; Torben-Nielsen and De Schutter, 2014). However, these models usually rely on large number of parameters that are not available from experimental data, and they tend to provide phenomenological insights rather than mechanistic understating of a given system (Goodhill, 2018).

Here, I implemented a generative model of dendrite patterning using the minimal set of parameters required to reproduce the c1vpda developmental stages and morphometrics. The model is constructed on a set of iterative local rules which represent dendrite branch growth of c1vpda cells, was based on previous morphological models that satisfy optimal wiring considerations through minimising total dendritic cable and conduction times from dendrite tips to the soma (Cuntz et al., 2010; Baltruschat et al., in preparation).

Dendrite patterning is simulated from the standpoint of individual branch dynamics, involving only three processes: branch elongation, interstitial branching and branch retraction (**Figure 4.6A**, see **Methods-Chapter 6**). In this model, new branches and elongating branches targeted points away from existing dendrites with some amount of stochasticity, while remaining within a small radius. Simultaneously, other branches

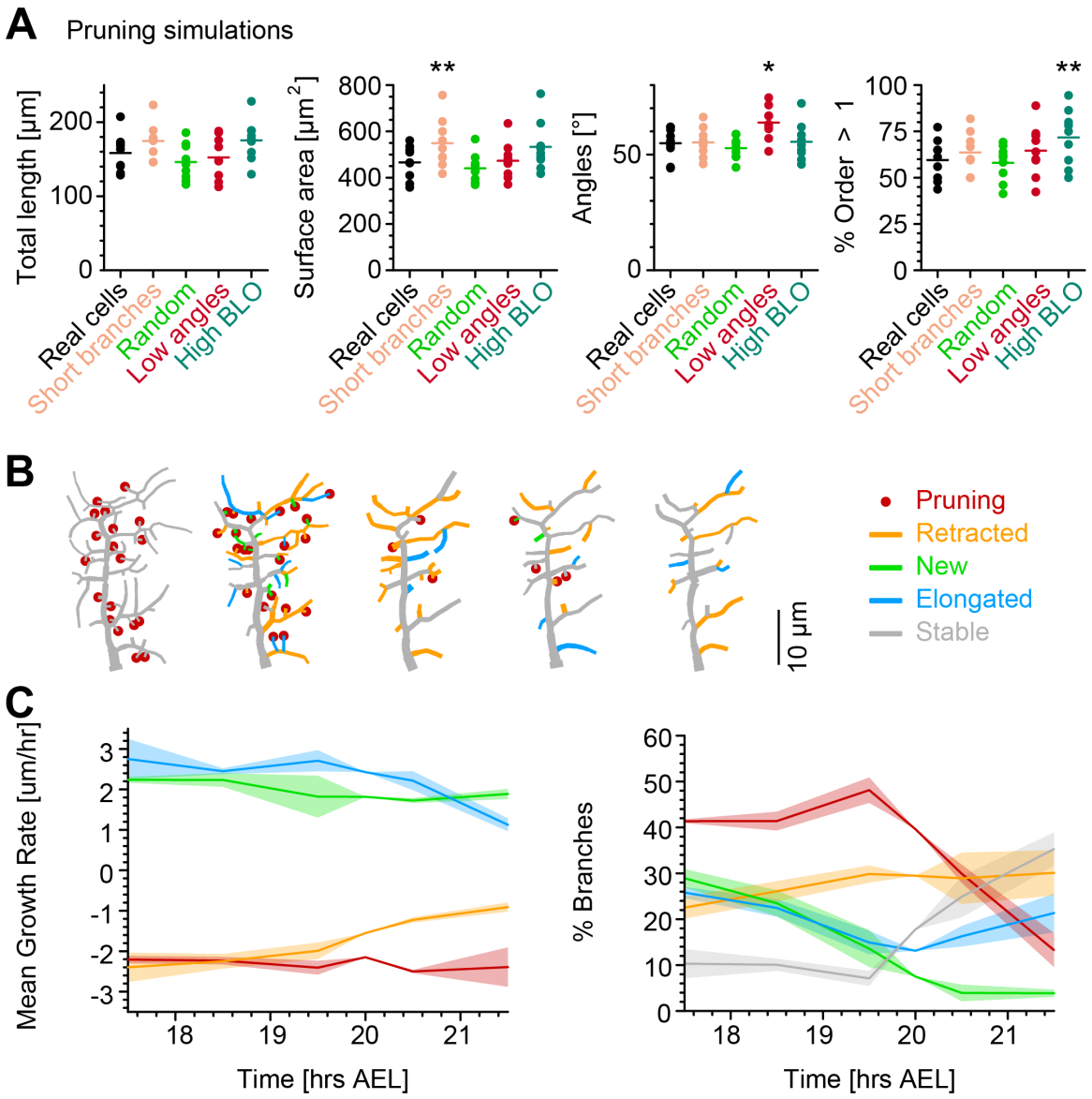

Figure 4.5: **In Silico Simulations and Single Branch Tracking Dissect Pruning Phase Dynamics.**
A, Key morphometrics comparing real cells after pruning with simulated pruning schemes applied on the morphology before pruning. Each dot is one morphology, bars indicate mean, and stars indicate p-values as follows: *< 0.05, **< 0.01 ($n = 429$ branches, $n = 9$ cells, from six animals). **B**, Sample c1vpda dendritic morphology during pruning with branches coloured by their respective dynamics, red circles - to be pruned; orange - retracting; green - newly formed; blue - elongating; grey - stable . **C**, (Left) Branch dynamics similar to **B** but quantified as growth rates ($\frac{\mu m}{hr}$) for all branches of all dendrites tracked during the pruning phase, $n = 1,139$; same colours as in **B**. (Right) Assignment of branches to the five types in **B** as a function of time. Shading represents SEM.

retracted and eventually could be pruned. The branch growth radius, retraction rate, and the distribution of new and retracting branches over time were obtained directly from the time-lapse data in **Figure 4.2B** and **Figure 4.5C** without recurring to any parameter fitting. The numerical simulations of the model dynamics were performed within the 2D physical boundaries and geometry of the spanning area of any given c1vpda dendrite, mimicking the combined effect of cell transmembrane and membrane molecules that facilitate cell-extracellular matrix adhesion, confining sensory neurons to a 2D space (Kim et al., 2012a; Meltzer et al., 2016).

All key morphometrics–number of branch points, total length and surface area– were consistently very well fitted by the growth model with random pruning at all simulated developmental stages (**Figure 4.6B** and **Figure E.1**). Importantly, the model reproduced the scaling relationships from **Figure 4.2D**, indicating that the resulting morphologies followed basic wiring constraints.

In addition, the model strengthened the hypothesis that a random pruning underlies arbour refinement in c1vpda cells. The model length and angle distributions before and after pruning matched the real data (**Figure 4.6C**, left panels, c.f. **Figure 4.3**) as well as the selective pruning of lower curvature branches observed in **Figure 4.4** (**Figure 4.6C**, rightmost panel).

These findings altogether indicate that a noisy growth in combination with random pruning of terminals is consistent with c1vpda dendritogenesis. Nonetheless, although the model successfully reproduced the growth dynamics of real cells, I noted that the branches from the model slightly under-estimated the perpendicularity angles of the first-order branches after pruning (median model = $60.18°$ vs. median real cells = $63.93°$). This suggests that cell adhesion molecules, such as Tenurin-m, possibly have a role in enhancing tips growth direction preference (Hattori et al., 2013).

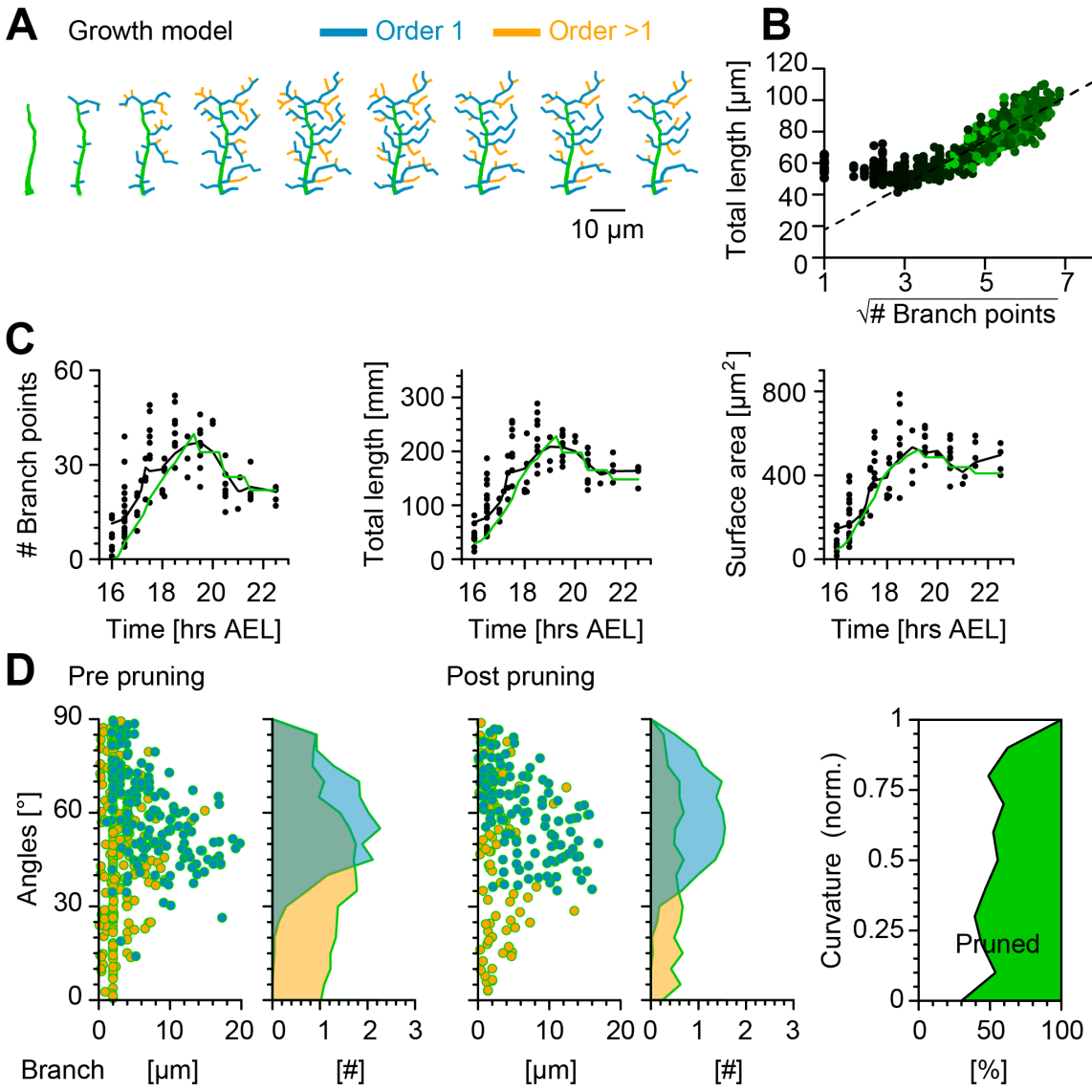

Figure 4.6: **Computational Growth Model With Stochastic Pruning Reproduces c1vpda Growth Dynamics.**

A, Synthetic dendrite morphologies of a sample c1vpda during embryonic development including the pruning phase. **B**, The dashed line shows the average scaling behaviour of the simulated synthetic trees ($R^2 = 0.98$, $n = 1000$ simulations; see STAR⋆Methods), similar as in **Figure 4.2D**. From left to right, Time course of the number of branch points ($R^2 = 0.88$), total length of dendrite cable ($R^2 = 0.95$) and surface area ($R^2 = 0.94$) of the model during development until pruning. In all subpanels, each black dot represents one reconstruction ($n = 90$), black lines represent the moving average of the real neurons and green lines represent the mean behaviour of the synthetic morphologies ($n = 1,215$). **C**, Representative visualisation of a random sample of synthetic trees before pruning (left, with same number of trees as in experimental data) histograms for branch length (one dot per branch) and number of branches per angle are shown categorised by Branch Length order (Blue: order 1, Orange: order > 1). Similar visualisation (middle) of dendrites after pruning. Rightmost panel shows the percentage of branches pruned (green shaded area) by curvature energy.

4.3 Summary

In this chapter, I investigated the emergence of an optimal wiring and function trade-off from noisy growth and random pruning during *Drosophila* class I ventral posterior dendritic arborization dendrite development. The results of these experiments can be distilled into the following finding:

- C1vpda dendrite growth does not compromise wiring constraints.
- Pruning of suboptimal branches in second dendrite growth phase.
- C1vpda dendritic Ca^{++} increases in response to larval contraction.
- C1vpda growth rules favour strong larval contraction responses.
- Random space-filling with pruning growth model explains C1vpda morphology

Chapter 5

Conclusions

This chapter summarises the contributions of the present dissertation and discusses directions for future work and possible extensions to the work presented in this thesis.

5.1 Summary and Contributions

5.1.1 Thesis Summary

In this thesis, I set out to investigate the assembly of a functional dendritic tree. Dendritogenesis is a complex developmental process and unravelling the mechanisms involved is very important not only for basic research but as well to medical purposes. In the Chapters 1, 2 and 3, I introduced the conceptual background, model system and experimental methods necessary to understand the study performed in this thesis.

In Chapter 4, I have shown that the spatiotemporal patterning of c1vpda sensory neurons can be accurately predicted by a stochastic growth model with random pruning. By combining long-term time-lapse imaging reconstructions and single branch tracking analysis, I was able to constrain the model without recurring to parameter fitting. I showed how a sequence of simply three steps: main stem polarization, non-overlapping stochastic growth of branches and pruning, reproduced a specialized dendrite phenotype that respects wire optimization principles.

5.1.2 Noisy Growth Underlies Class type-specific Shape and Wire Optimisation

Dendrite differentiation started with the polarisation of the main stem. The direction of the primary branch was found to be constant across cells. Cells from different hemisegments polarised dorsally, parallel to each other. This constancy of direction most likely serves a key role in defining the dendrite spreading during branch morphogenesis by biasing the branching direction (Yoong et al., 2019). During the subsequent extension phase, newly formed branches emerged interstitially from the existing main stem. The

newly lateral branches grew in anterior and posterior orientation spreading along the body-wall. Later, higher-order branches sprout from pre-existing lateral branches.

Next, I showed that the innervation of the receptive field generated a branched structure with two morphological distinct branches classes. The first group was composed of longer branches with their growing tips directed at the body wall. In contrast, the higher-order branches had smaller lengths with their growth direction mainly oriented dorsally. The segregation of branches in the aforementioned groups is likely to be achieved in a self-organized manner through noisy filopodial exploration and Dscam based self-avoidance (Grueber et al., 2003a; Matthews et al., 2007; Hughes and Thomas, 2007b; Soba et al., 2007).

Following the extension phase, I observed a pruning step that refined the spatial arrangement of the dendritic tree (**Figure 5.1**). The importance and impact of this novel stage was overlooked in previous studies (Sugimura et al., 2003; Williams and Truman, 2004; Yalgin et al., 2015). I reasoned that the pruning of the dendrite could have economical purposes, or it could improve the effectiveness of the cell instead. I demonstrate here that the latter is the case, with a simple random pruning selectively remodelling the tree structure influencing the mechanisms of mechanosensory transduction (**Figure 4.5**).

Subsequently to the pruning step, c1vpda neurons underwent a stabilization period. The stage was characterized by a small increase in cable length and surface of the spanning area, while the number of branches remained virtually unaltered. After hatching, a phase transition in the development of these cells was found. With the comb-like pattern and branching complexity of the dendrites persisting across all larval stages, the dendrites experienced an isometric scaling. During this stage, the cable and surface are increased following the larva's body growth (Parrish et al., 2009). The conservation of dendrite shape throughout larval stages suggests the need for functional conservation (Almeida-Carvalho et al., 2017).

Neurons need to wire to perform different tasks and throughout time dendritic morphologies are naturally selected to optimise a specific function (Sterling and Laughlin, 2015). However, no phenotype can be optimal at all functions and as a result, dendrites diverge structurally from one another. Particularly, each instantiation of a dendritic tree pattern occupies a small portion of a larger morphological space made up by all possible dendritic trees' structural configurations. At a larger scale, dendrites cluster in class-specific discrete locations of this morphological space (Zeng and Sanes, 2017).

However, besides performing a given function, neurons, and biological systems in general, need also to optimise dendrite cable or resources. The overproduction of useless resources carries a fitness cost to the organism, and as a result, a tradeoff between function and resources conservation arises (Szekely et al., 2013). This tradeoff

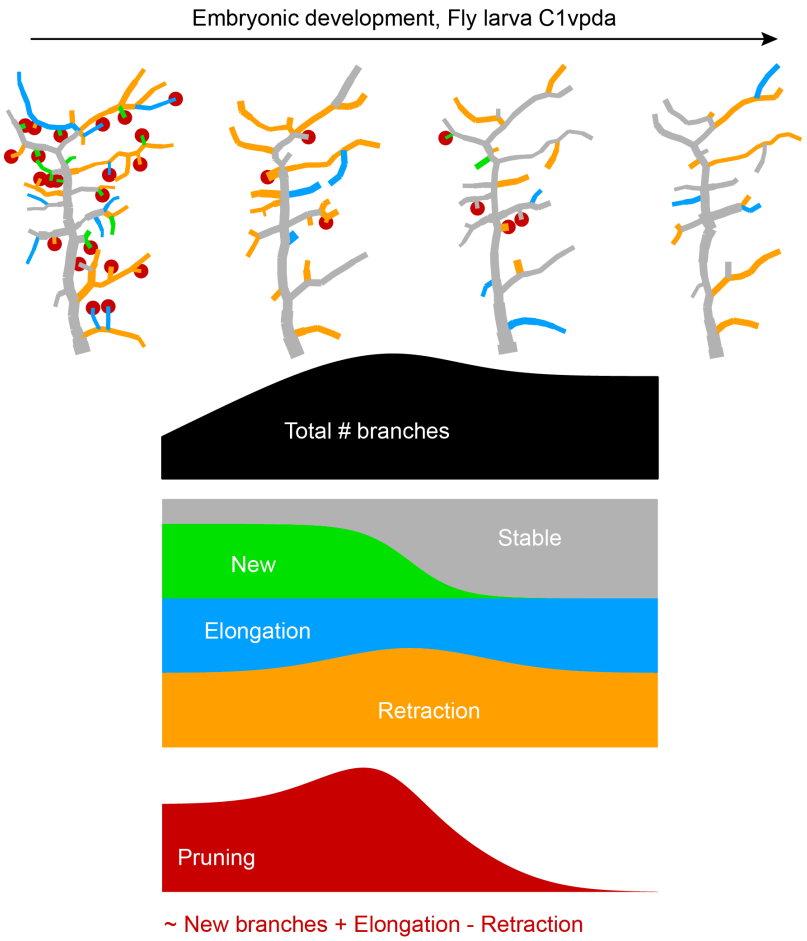

Figure 5.1: **Overview of C1vpda Branch Dynamics in the Embryo.**
Top panel, illustrative sample of c1vpda time series during pruning. **Bottom panel**, dendrite dynamics in the embryo that lead to final-arbour morphology. After polarisation of the main stem, during the extension phase, the number of new branches surpasses the number of pruned branches, increasing arbour complexity. During the pruning stage, the branch dynamics change. The number of pruned branches peaks and the number of newly formed branches reduces sharply. This leads to a spatial rearrangement of the dendritic tree. After the pruning step, a stabilization period occurs where the dendritic pattern remains virtually unchanged. This is marked by low numbers of pruned and newly formed branches and by the increase of the number of stable branches. Color scheme as in **Figure 4.5**.

between computation/function implementation and wiring optimization in dendrites raised the possibility that to optimize a vital function to the organism more resources must be spent achieving optimal structure-function relationship in detriment of wiring minimisation principles. Consequently, being a set of morphological stereotypical neurons, c1vpda neurons do not necessarily respect optimal wiring constraints because their dendritic structure-function relationship is highly specialised for its proprioceptive role. Here, I showed for the first time, to the best of my knowledge, how a stochastic growth process optimises function and structure. In the future, with continuing efforts to quantify type-specific dendrite patterning of different neurons one hope to formalise a general theory of how developmental stochastic processes allow dendritic computation and resources optimisation.

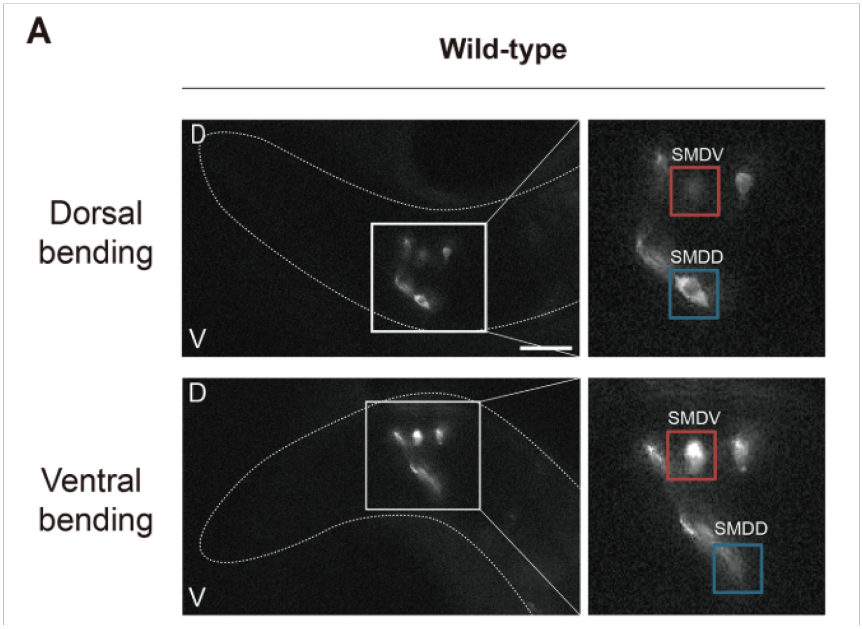

Figure 5.2: **Calcium Activity due to Head Bending in *C. elegans* During Proprioceptive Responses.** **A**, Illustrative images showing calcium signal increase in the somas' of SMDV and SMDD motor neurons of the *C. elegans* during dorsal and ventral head bending. **D** marks dorsal side, **V** marks ventral side and anterior is to the left of the images (modified from Yeon et al. (2018)).

5.1.3 Dendrite Curvature as a General Mechanism for Proprioceptive Responses

Before this study, it was unknown whether the stereotypical comb-like shaped c1vpda cells were wired to maximise membrane curvature. Based on theoretical predictions, I revealed how the first-order branches are better suited for mechanical sensory transduction arising from cuticle folding during crawling behaviour. Due to their direction preference running perpendicular to the body wall these branches experience larger curvature increase, raising the opening probability of the MS channels (Liang and Howard, 2018; Katta et al., 2015). I note that these results support a recently proposed hypothesis, which predicts that mechanosensory cells may become activated by membrane curvature increase (He et al., 2019).

Several findings are consistent with the aforementioned results. First, it was shown that class I da neurons have unique structural adaptations to support the forces required for mechanosensory signal transduction (Delandre et al., 2016). With these adaptions being found in other cells involved in mechanotransduction (Krieg et al., 2014; Liang et al., 2014). Finally, similar results were reported in C.elegans (Yeon et al., 2018; Inberg and Podbilewicz, 2018; Hall and Treinin, 2011), suggesting that dendrite curvature may provide the biophysical substrate of mechanosensory experience across multiple animal models (**Figure 5.2**).

5.1.4 Novel Generative Dendrite Growth Model

To further test the pruning hypothesis I developed and implemented stochastic growth models with pruning. In the past, numerous models focusing on stochastic rules governing dendrite growth and branching have been proposed and applied to generate neuronal morphologies (Cuntz et al., 2010; Donohue and Ascoli, 2008; Eberhard et al., 2006; Koene et al., 2009; Torben-Nielsen and De Schutter, 2014). However, they had many parameters that were hard to constrain due to the lacking of data (Goodhill, 2018). To avoid this problem, I parameterised the growth process of the C1vpda dendrites using single branch resolution tracking in order to constrain our models with a minimal amount of master parameters.

Branch dynamics and morphometrics at this stage were well fitted by a random growth and pruning model, suggesting that c1vpda morphogenesis is possibly a non-deterministic process, following other previously found results for other cell types (Ryglewski et al., 2017; Özel et al., 2015). The positioning and orientation of the main stem, iterative random exploration of the dendrite spanning area, combined with random pruning of branches sufficed to reproduced the experimental data.

Even though the generated synthetic morphologies were statistically close to the reconstructed cells, in the future, some improvements to the model can be made in order to strengthen the biological plausibility of the artificial cells:

- When comparing synthetic and artificial dendrites, I reported that the model slightly underestimated the perpendicularity of the lateral branches. In the future, it would be interesting to add the influence of external cues (e.g. Hattori et al. (2013)) on the elongation of dendritic branches of c1vpda neurons.

- The paucity of branch crossovers in c1vpda cells and the importance of self-avoidance in dendrite patterning (Grueber et al., 2003b; Grueber and Sagasti, 2010) led us to wish to parameterise self-referential forces in our model, as proposed by Memelli et al. (2013). However, to constrain self-avoidance parameters it would be required higher temporal resolution data to resolve the dynamics of branch self-avoidance. As a result, the time spent reconstructing the image stacks would not make the present project feasible in the period of time of a PhD thesis.

- The present model was only constrained using morphological data from one cell-type. In the future, it would be interesting to adapt the current model to study different cell classes and mutants to identify the fundamental neuromorphological parameters underlying the branching features of real dendrites.

5.2 Limitations and Future Work

5.2.1 Limitations of the Present Study

In the presented thesis I wished to acquire imaging data during the entire developmental process of c1vpda sensory neurons. Taking into account the reconstruction bottle-neck discussed in Chapter 3, to make this project feasible in the period of time of a PhD thesis the temporal-resolution of the reconstructed data already had to decrease. In future, through the emergence of new machine learning-based automated reconstruction algorithms, it might become possible to investigate the interactions of dendritic branches with higher-resolution. Thus, is turn would make it possible to constrain computational models that take into account self-avoidance and self-referential forces between dendritic branches.

Additionally, newer microscopes provide high-resolution, high-speed volumetric imaging enabling the investigation of new types of questions not possible before. On one hand, the calcium imaging in freely moving larvae could be improved as in Vaadia et al. (2019), where body-wide different types of proprioceptive neurons could be imaged during locomotion. Not only during forward crawling but as well during more complex behaviours such as head-turning. Also, the new volumetric microscopes, by allowing the acquisition of images at bigger depths may facilitate imaging experiments in the embryo, where neurons are sometimes located deep in the egg, and not accessible to regular light microscopes. In summary, the emergence and improvement of new microscopes will open up new imaging possibilities during different phases of development.

5.2.2 Open Questions

I consider that the objectives defined in Chapater 1 were reached. However, after this study, new open problems emerged. Next, I will enumerate open problems that may lead to new studies to further elucidate how dendrites pattern:

- What are the transcription factors, or external cues, underlying the initiation of the different developmental stages of c1vpda sensory neurons? In the future, the integration of different levels of analysis: genetic, molecular, structural and functional need to be incorporated in developmental studies to generate a clear picture of cell patterning (Zeng and Sanes, 2017; Lefebvre et al., 2015).

- Is dendrite branch curvature a general mechanism of proprioceptive mechanosensory signal transduction in insects and or nematodes? To answer this question comparative studies between different animal models would be required. Also, building a morphological that incorporates biophysical parameters such as ion channel dynamics would be necessary to formalise the problem.

- How to quantify self-avoidance interactions between dendritic branches? What are the parameters that describe best this dynamical process? Is dendritic branch self-avoidance annihilating or repulsive? The importance of self-avoidance to dendrite patterning has been extensively reported (for a review see Lawrence Zipursky and Grueber (2013)). However, there are no quantifications on the influence of self-avoidance mechanisms on branch dynamics during development. This problem prevents modellers to build more biological plausible growth models of dendrite patterning. Higher-temporal resolution time-lapse movies and high-throughput reconstruction algorithms will enable the acquisition of the aforementioned data.
- What is the role of self-avoidance in wiring optimization? Is self-avoidance a necessary and sufficient condition for growing optimal trees? The work done in this thesis provides the first step to answer these questions, but the development of more cell-types needs to be studied in order to general principles to emerge.
- Is there a canonical growth programme of dendrite patterning? What are the differences in the developmental stages of sensory dendrites compared with neurons located in associative areas of the nervous system? Certain stages of dendrite elaboration shared across cell-types located in different areas of the nervous system have been reported (Yoong et al., 2019). However, a fully general theory of developmental stages regulating the dendritic differentiation remains elusive (**Figure 5.3**).

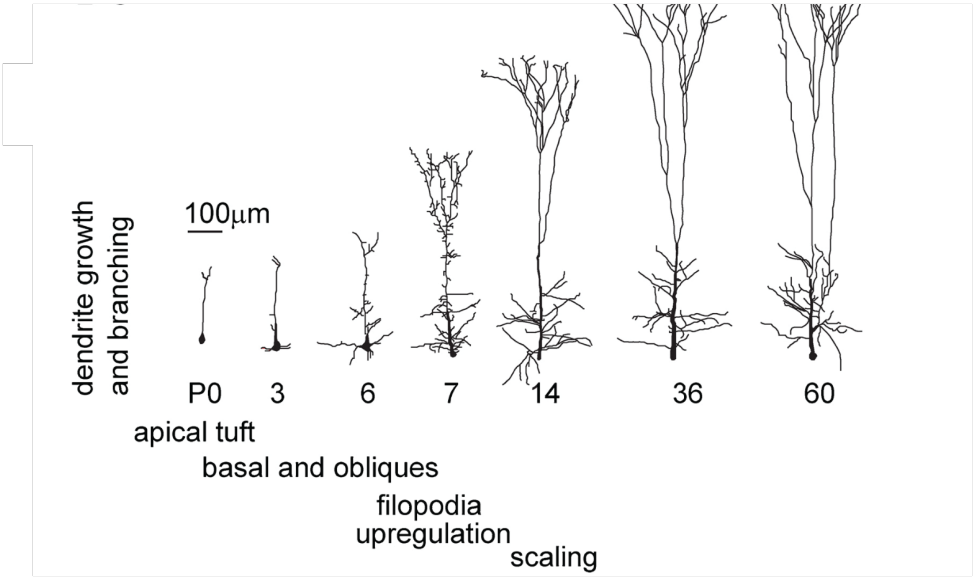

Figure 5.3: **Differentiation of rat cortical pyramidal neurons.**
Stages of morphogenesis of the dendrite arbor of rat cortical pyramidal neurons. Similar to the ones from c1vpda cells: initial stem polarisation, dendrite growth and branching, and scaling. Time in days postnatal (modified from Yoong et al. (2019)).

5.2.3 Conclusion and Future Work

Taken together, our results demonstrate that a specialised dendritic tree pattern can be obtained due to the correct temporal sequence of developmental stages. Interestingly, evidence can be found that similar stages and strategies may be preserved across different neuron types (Gao et al., 2000; Sugimura et al., 2003; Baltruschat et al.) and animal models (Yoong et al., 2019). The flexible usage of such self-organisational programs provides developmental resilience and robustness to perturbations in the growth medium (Hiesinger and Hassan, 2018). It also possibly avoids the encoding of a deterministic morphogenetic program that may be less costly to implement genetically (Hiesinger and Hassan, 2018). In the future, it will be interesting to elucidate the precise genetic transcriptional program underpinning these developmental stages of the c1vpda cells (Grueber et al., 2003a; Jinushi-Nakao et al., 2007) and on a higher scale to understand to what extent similar self-organising processes and mechanisms are implicated in the formation of other cell types (Ryglewski et al., 2017; Özel et al., 2015), neuronal networks (Hassan and Hiesinger, 2015) and even in the emergence of non-neuronal branching organs (Hannezo et al., 2017).

Chapter 6

Methods

6.1 Experimental Model and Imaging Details

6.1.1 *Drosophila* Larvae

Time-lapse images of c1vpda sensory neurons in the embryo, L1, L2 and L3 I used *2-21-Gal4, UAS-mCD8::GFP* homozygous, as in (Grueber et al., 2003a). To image the L1 c1vpda sensory neurons during locomotion, I used a dual line *w-; Gal4221, UAS-GCaMP6m/cyo;UAS-tdTomato/MKRS* of to image the calcium signal and to image the dendritic tree.

6.1.2 *In Vivo* Calcium Imaging

Functional images were acquired with a Zeiss LSM 800 Confocal Microscope (`https://www.zeiss.com`). Images were acquired[1] at a temporal resolution of $0.2s$ per frame and with $40\times$ oil objective with a voxel size of ($1.3284\mu m \times 1.3284\mu m \times 1\mu m$). Forward crawling imaging trials were performed in 25 cells (A1–A6 segments) from 6 wandering L1 larvae. Every imaging session lasted for $40s$. The animals were imaged while immersed within a high viscosity ringer solution in 1.1% agarose.

To quantify the body wall contraction, a triplet of adjacent c1vpda cell somata on the anterior–posterior axis, were manually tracked during crawling behaviour, using the *ImajeJ* `Mtrack2` plug-in (Meijering et al., 2012) from *Fiji* (Schindelin et al., 2012). The contraction rate was calculated using *Matlab* (`www.mathworks.com`) as the normalised sum of the Euclidean distances between the x and y coordinates of the central cell and the x and y coordinates of the anterior and posterior cells over time (**Figure C.1**).

The regions of interest (ROIs) were first defined manually, using the `ROI` functionality from *Fiji*. Afterwards, I automatically generated tighter contours using the

[1] Images were acquired by Lothar Baltruschat at the German Center for Neurodegenerative Diseases in Bonn

"`Defaultdark`" parameter from the `roiManager` menu (**Figure C.1**). Every ROI was defined on the red channel ($mCD8 - mCherry$), ensuring that the posterior Ca^{++} was done exactly on the c1vpda dendrite's membrane. Equipped with the ROIs, the intensity values of $GCaMP6f$ and $tdTomato$ were then extracted for each time point and then exported from *Fiji*. The analysis of the fluorescence signals was performed using custom made code in *Matlab* (`www.mathworks.com`). The $GCaMP6F$ signal was normalised with the $CD2 - mCherry$ signal and the ratio $\frac{\text{GCaMP6F}}{\text{tdTomato}}$ was used to calculate $\frac{\Delta F}{F}$. To link Ca^{++} dynamics to the contraction of body wall experienced during crawling behaviour, I plotted the contraction rate against the $\frac{\Delta F}{F}$. However, before averaging the signal, I first realigned the Ca^{++} traces accordingly to the maximum segment contraction in order to avoid averaging artefacts across trials.

6.1.3 Geometrical Model of Curvature

We[2] started by assuming a marginal case for which the larva's cuticle folding can be approximated by the surface of a cylinder with radius R (**Figure D.1A**). The orientation of the branch is then defined by the tilting angle θ between the cylinder axis of symmetry and the central axis of each branch. The tilting angle varies from $\theta = \frac{\pi}{2}$ for a branch spreading in the anteroposterior axis, to $\theta = 0$ for a branch spreading dorsally. Starting from an initial branch with $\theta = \frac{\pi}{2}$ and length $L = 2\pi R$, we kept the branch length constant and calculated the curvature increase of the branch for different tilting angles $0 \leq \theta \leq \frac{\pi}{2}$.

We approximated the shape of a tilted branch, which follows an elliptical profile with diameters $a = R = \frac{L}{2\pi}$ and $b = \frac{a}{\sin\theta}$ on the cylinder, with a circular branch with a radius of curvature $R_c = 0.5\,(a + b)$ resulting in $\frac{1}{\sin\theta} = \frac{4\pi R_c}{L}1$ (see **Figure D.1B**). An initial straight branch of radius r has two principal curvatures $c_1 = 0$ and $c_2 = \frac{1}{r}$. Upon bending, the branch around the cylindrical body with radius $R \gg r$ the second principal curvature is almost constant. Therefore, we computed the relative increase in the first principal curvature $c1$ to represent the curvature variation. The curvature increase is rescaled with respect to its maximal value for a perpendicular branch to the body's axes with $\theta = \frac{\pi}{2}$.

It is then shown that curvature is a steadily rising function of the angle θ, varying from zero for an unbendend branch with $\theta = 0$ (see **Figure D.1A**, bottom branch), to one, for a fully bended, i.e., cicular, branch with $\theta = \frac{\pi}{2}$ (see **Figure D.1A**, left most branch; and **Figure 4.4B**).

[2]The geometrical model of curvature was developed in strict collaboration with Amirhoushang Bahrami at the Max Planck Institute of Biophysics in Frankfurt am Main

6.1.4 Time-Lapse Imaging

In the embryonic stages (7 animals), 28 cells (A1–A6 segments) were imaged at $5mins$ resolution between $16hrs$ AEL and around $24hrs$ AEL (**Figure 4.1A**), for periods ranging from $30mins$ to $6hrs$. Image stacks from the time series were reconstructed at $30mins$ and $1hrs$ intervals. After hatching, 20 cells (5 animals; A1–A6 segments) were imaged at time points $30hrs$ AEL, $50hrs$ AEL and $72hrs$ AEL, to cover the instar stages of larval development.

Before embryos were collected, adult male and female flies were caged and exposed to moisturised yeast powder on apple agar at $25°C$ and embryos were collected after $30mins$. Until the imaging session started, the embryos were kept in the incubator at $25°C$ and 60% relative humidity on apple agar to prevent them from drying out. Before the imaging session started, the embryos were dechorionated with mild bleach for $3.5mins$. After being selected, were rinsed using a stream of H2O from a squeeze bottle.

L1, L2 and L3 larvae were imaged under a custom made chamber (as in Baltruschat et al., in preparation) to curtail contact-based damage to the epidermis of the larvae. In between imaging sessions, every animal was kept at $25°C$ at 60% relative humidity in a separate $500\mu l$ Eppendorf tube, which was filled with $200\mu l$ fly food.

Images were acquired with a Zeiss LSM 800 Confocal Microscope (`https://www.zeiss.com`). For embryos, I used a $63\times$ oil objective and voxel size ($0.2196\mu m \times 0.2196\mu m \times 1\mu m$) for 7 time series, and for the remaining 21 time series I used a $40\times$ oil objective with voxel size ($0.3459\mu m \times 0.3459\mu m \times 1\mu m$). During the L1 stage ($30hrs$ AEL), I used a $40\times$ oil objective and voxel sizes ($0.4465\mu m \times 0.4465\mu m \times 1\mu m$) and ($0.3907\mu m \times 0.3907\mu m \times 1\mu m$). When the image stacks using these voxel sizes were blurred I increased the resolution to ($0.3907\mu m \times 0.3907\mu m \times 0.5635\mu m$). For L2 stages ($50hrs$ AEL), I used a $40\times$ oil objective and a wide range of voxel sizes – ($0.5209\mu m \times 0.5209\mu m \times 1\mu m$), ($0.4465\mu m \times 0.4465\mu m \times 1\mu m$), ($0.3907\mu m \times 0.3907\mu m \times 1\mu m$) and ($0.2841\mu m \times 0.2841\mu m \times 1\mu m$) to assure high-resolution images for all cases. Finally, to acquire images during L3 stage ($72hrs$ AEL), I used a $20\times$ oil objective and voxel sizes ($0.8335\mu m \times 0.8335\mu m \times 1.5406\mu m$) and ($0.7144\mu m \times 0.7144\mu m \times 1\mu m$).

6.2 Quantification and Statistical Analysis

6.2.1 Dendrite Morphometric Analysis

All morphometry analysis and stack reconstructions were performed in *Matlab* (`www.mathworks.com`) using our own software package, the *TREES Toolbox* (`www.treestoolbox.org`). See below for details on the individual functions. In the following, italic function names with `_tree` suffix are *TREES Toolbox* functions.

6.2.2 Stack Reconstructions

Image stacks from the confocal microscope were imported in the *TREES Toolbox* environment and manual reconstructions of all apical dendrites were performed individually ($N = 165$) using the dedicated reconstruction user interface `cgui_tree`. During the reconstruction process, I resampled (`resample_tree`) the dendritic trees, to $0.1\mu m$ for morphologies with the total length smaller than $400\mu m$ and to $1\mu m$ for cells with the total length above $400\mu m$.

6.2.3 Wiring Optimisation

To verify if c1vpda structure minimise wire ($N = 165$) I verified if the branch points (n), total length (L) and surface area of the spanning field (S) obeyed the following scaling law $L \approx \pi^{-\frac{1}{2}} \cdot S^{\frac{1}{2}} \cdot N^{\frac{1}{2}}$ (Cuntz et al., 2012). The previously mentioned morphometrics were calculated using the functions `B_tree`, `len_tree` and `span_tree` respectively, from the *TREES Toolbox* (*Matlab*). In order to facilitate the visualisation and comparison between dendritic trees from different developmental stages, all reconstructions were scaled to the same surface area ($100\mu m^2$) by using the function `scaleS_tree` (*TREES Toolbox*). Additionally, in order to further validate that c1vpda dendritic morphologies scale as expected by optimal wiring principles, I implemented simplified models of dendritic trees based on MST algorithm (`MST_tree`; $bf = 0$) (Cuntz et al., 2010). First, I generated MSTs to connect randomly distributed targets in a surface area of $100\mu m^2$. Targets were added as required to match the number of branch points of synthetic morphologies to the ones of real cells. Finally, the number of branches points and total length of the resulting synthetic trees were compared with the ones from real dendrites.

6.2.4 Perpendicularity and Curvature Quantification

In order to compute the angle distribution and curvature increase of the side branches of c1vpda cells I wrote three custom *TREES Toolbox* functions: `PB_c1_tree`, `BLO_c1_tree` and `perpendicularity_c1_tree`. Time-lapse imaging in the embryo did not allow me to differentiate between the limits of the body walls of the segments and the imaged cells. Therefore, I measured the angles and curvature increase of the segments of a given dendrite in relation to the MS of the tree as a proxy for the body wall direction. I, therefore, needed an unbiased procedure to reorient all the reconstructions in the same axis.

Thus, I wrote the *TREES Toolbox* function `PB_c1_tree` that automatically finds the c1vpda MS and rotates the entire dendrite to align the MS and $y-$axis (**Figure B.1**). For a particular cell of interest the algorithm was initialised by finding the last node from the longest path (`pvec_tree` function) and rotating the tree (`rot_tree` function) until the last node was approximately aligned vertically ($\pm 1\mu m$) with the root at position (0,

0).

Afterwards, a bounding box around the dendrite was computed using the `polyshape` and `boundingbox` functions (Matlab). The closest nodes of the tree to the top left and top right were then identified (`pdist`, Matlab function; see **Figure B.1**). The first shared branch point between those two corners was then defined to be the last node of the MS (using `ipar_tree` function). Finally, the tree was rotated again until the new MS tip was approximately vertically aligned with the root at position $(0, 0)$ (**Figure B.1**A). The previous steps were repeated until no new last node was found between two consecutive iterations (**Figure B.1**B).

After finding the MS of a given tree and taking into account assumption 3, I partitioned the tree into all the lateral subtrees that emerged from the MS and I ordered the branches of every subtree according to their length using the `BLO_c1_tree` function. This new *TREES Toolbox* function returns the Branch Length order (blo) values for each branch by first taking the longest path from the root of the subtree and defining it as $blo = 1$. It then all the longest paths that branch off from this initial path and labels them as $blo = 2$ (see **Figure 4.3**). Finally, the angles and curvature values of all nodes of all the subtrees were computed using the new *TREES Toolbox* function `perpendicularity_c1_tree`.

6.2.5 List of Morphometrics

A collection of 49 branching statistics were calculated to quantify each dendrite reconstruction. Next, I enumerate those morphometrics and their respective TREES Toolbox function:

1. **Minimal branch order of terminals** – functions: `BO_tree` and `T_tree`.
2. **Mean branch order of terminals** – function: `BO_tree` and `T_tree`.
3. **Standard deviation of the branch order of terminals** – functions: `BO_tree` and `T_tree`.
4. **Mean Van Pelt asymmetry index**, – function: `asym_tree`, option: -v (Uylings and Van Pelt, 2002,).
5. **Standard deviation of the Van Pelt asymmetry index** – function: `asym_tree`, option: -v.
6. **Total dendrite length** – function: `len_tree`.
7. **Mean diameter** – function: `mean` (`tree.D`).
8. **Standard deviation of the diameter** – function: `std` (`tree.D`).

9. **Mean tapering ratio at branch points** – function: `B_tree` and `ratio_tree`.
10. **Standard deviation of the tapering ratio at branch points** – function: `B_tree` and `ratio_tree`.
11. **Total membrane surface** – function: `surf_tree`.
12. **Total volume** – function: `vol_tree`.
13. **Mean isoneuronal distance of terminals** – function: `isoneuronal_tree`.
14. **Minimal isoneuronal distance of terminals** – function: `isoneuronal_tree`.
15. **Maximal Euclidean distance to the root** – function: `eucl_tree`.
16. **Mean Euclidean distance to the root** – function: `eucl_tree`.
17. **Standard deviation of Euclidean distance to the root** – function: `eucl_tree`.
18. **Mean Euclidean compactness** – functions: `eucl_tree` and `BO_tree`.
19. **Standard deviation of the Euclidean compactness** – function: `eucl_tree` and `BO_tree`.
20. **Maximal path distance to the root** – function: `Pvec_tree`.
21. **Mean path distance to the root** – function: `Pvec_tree`.
22. **Standard deviation of path distance to the root** – function: `Pvec_tree` .
23. **Mean path compactness** – function: `Pvec_tree` and `BO_tree`.
24. **Standard deviation of the path compactness** – functions: `path_tree` and `BO_tree`.
25. **Mean Tortuosity** – function: `turt_c1_tree`.
26. **Standard deviation of the tortuosity** – function: `turt_c1_tree`.
27. **Mean branching angle** – function: `angleB_tree`.
28. **Standard deviation of the branching angle** – function: `angleB_tree`.
29. **Surface of spanning field** – function: `span_tree`.
30. **Cable density** – functions: `len_tree` and `span_tree`.
31. **space-filling** – function: `theta_tree` (Baltruschat et al.).
32. **Dendritic field width** – function: (`PB_c1_tree`).
33. **Dendritic field height** – function: (`PB_c1_tree`).

34. **Dendritic field ratio** – function: (`PB_c1_tree`).
35. **MS ratio** – function: (`PB_c1_tree`).
36. **Total number of terminals** – function: `T_tree`.
37. **Terminals lateral density** – function: `T_tree` and `PB_c1_tree`.
38. **Perpendicularity of side branches** – function: `perpendicularity_tree`.
39. **Minimal branch length** – function: `perpendicularity_tree`.
40. **Mean branch length** – function: `perpendicularity_tree`.
41. **Standard deviation of branch length** – function: `perpendicularity_tree`.
42. **Maximal branch length** – function: `perpendicularity_tree`.
43. **Minimal length over radius ratio** – functions: `tree.D` ./ `len_tree`.
44. **Maximum length over radius ratio** – function: `tree.D` ./ `len_tree`.
45. **Scaled length** – function: `scaleS_tree`.

6.2.6 Single Branch Tracking

Both branch points and terminals of the pruning dataset ($N = 9$) of c1vpda cells during pruning were registered using `ui_tlbp_tree` (*TREES Toolbox*), a dedicated user interface as described previously (Baltruschat et al., in preparation), in order to track branch dynamics between $17.5hrs - 21.5hrs$ AEL. Custom written *Matlab* scripts tracked the terminal branch dynamics across time in $1hrs$ time intervals. The analysis partitioned the terminal branches into 5 distinct groups based on their dynamics between each time interval: newly formed branches, retracting branches, extending branches, pruned branches and stable branches that do not change in length, or the changes were below the resolution of the microscope.

6.2.7 Synthetic Pruning Simulations

For a given c1vpda time series ($n = 9$) during pruning, I selected the reconstructions when the number of branch points was maximal, i.e., before pruning, and when the number of branch points was minimal after pruning. Afterwards, I computed the difference in number of branch points between the aforementioned trees using the `B_tree` function (*TREES Toolbox*).

Then, using the `B_tree`, `T_tree` and `dissect_tree` functions (*TREES Toolbox*) I generated a set of all terminal branches belonging to a given tree before pruning, defined as the piece of dendrite cable between a given termination point and the immediately

preceding branch point on its path to the soma. Afterwards, I pruned the same number of branches from the tree as the number of branch points difference, by applying four different pruning schemes: small branches first, lower angle branches first, higher branch length first and random pruning

6.2.8 Generative Growth Model With Random Pruning

The generative pruning growth model (`growth_c1_tree`) is an extension of the `growth_tree` function from the *TREES Toolbox*, as described in Baltruschat et al., in preparation. The pruning model was fit to replicate the morphometrics of real dendritic reconstructions during embryonic differentiation. The model reproduces the growth dynamics of real cells by iteratively adding new branches on a tree at a given time point to produce the tree in the next time point. An additional pruning step was applied to the synthetic trees generated by this growth function to replicate the pruning phase dynamics of the c1vpda cells (see **Figure E.1** for simulations without pruning).

The algorithm started by selecting the reconstruction when the number of branch points was maximal, i.e., before pruning. Then it computed the mean branch rate (B_r) of all cells per time interval ($15mins$), between the time point when the imaging experiment started ($16hrs$ AEL), and the time point before pruning ($19.5hrs$ AEL). To incorporate the initial main stem polarisation described in real cells, the growth was simulated starting with an existing real initial main stem. The main stem of a given tree was found by applying the function `PB_c1_tree` (new *TREES Toolbox* function) on a selected tree. After stripping the main stem from the real morphology, the algorithm extracted the contour of the dendritic spanning field of the initial tree using the function `boundary` (*Matlab* function), with parameter $\alpha = 1$ and positioned the main stems inside the corresponding dendritic field of the tree before pruning. This spanning area defined the geometry where the simulations are performed.

At each iteration, the surface area was probed with $N = 100,000$ random target points. For each target point, the shortest Euclidean distance to the tree was detected and the resulting distances were capped at a maximal growth range radius of $r = 2.5\mu m$, before pruning ($19.5hrs$ AEL) and $r = 1.81\mu m$ after pruning. These radii were defined as the average growth rate of new branches until and after pruning respectively (from **Figure 4.5C**, left panel). Then, a target point was chosen at random with a preference for points with a larger Euclidean distance (noise parameter $k = 0.5$) to enable space-filling. The selected target point was then connected to the closest point on the tree minimising cable length and path length cost with a $bf = 0.225$ (see model in Baltruschat et al., in preparation). At each iteration the synthetic trees grew at rate B_r, between $16 - 19.5hrs$ AEL for the case of the pruning models, and between $16 - 22.5hrs$ AEL for the case of the model without pruning. The simulations stopped when time point

$22.5hrs$ AEL was reached.

Concomitantly with the noisy growth step, the model entered a phase of dynamic pruning at time points $16.5, 17.5, 18.5, 19.5, 20.5, 21.5hrs$ AEL, taking into account the $1hr$ resolution of the time-lapse data. Evidence from the single branch tracking data was used to constrain the model pruning steps. The pruning rate and distribution of branches per class data was then divided and averaged into bins with the corresponding bin edges: $\leq 17.5 \leq 18.5 \leq 19.5 \leq 20.5 \leq 21.5$ (**Figure 4.5C**, right panel). At each of the aforementioned time points, terminals are selected at random for their tips to be retracted. The percentage of branches selected for retraction was defined as the combined percentage of retracting and pruned branches at the corresponding time bin in the real data. Each tip of the selected terminals is pruned in the same amount as the average cable length pruned per branch in the real cells, in that time bin. If the amount of cable to be pruned surpassed the terminal length the branch was removed from the tree. Moreover, a proportion of new branches were added to the existing tree equalling the percentage of newly formed branches at the same time bin in the real data. The simulated results were then analysed and compared with the morphometrics from the real cells as explained in the Results section.

6.2.9 Data Analysis

Statistical tests and all data analysis were performed using *Matlab* (`www.mathworks.com`) and they were implemented in custom made code. Statistical parameters including the exact value of the sample size and precision measures ($mean \pm SEM$ or $mean \pm SD$) are reported in the figures and the text. All statistical evaluations were done empirically by means of bootstrap hypothesis testing to avoid any assumptions of normal distributions. All p values were reported as: * $p < 0.05$, ** $p < 0.01$, *** $p < 0.001$.

Bibliography

T. Abrahamsson, L. Cathala, K. Matsui, R. Shigemoto, and D. A. DiGregorio. Thin Dendrites of Cerebellar Interneurons Confer Sublinear Synaptic Integration and a Gradient of Short-Term Plasticity. *Neuron*, 73(6):1159–1172, 2012. doi: 10.1016/j.neuron.2012.01.027.

H. Agmon-Snir, C. E. Carr, and J. Rinzel. The role of dendrites in auditory coincidence detection. *Nature*, 393(6682):268–272, 1998. doi: 10.1038/30505.

A. Akhmanova and M. O. Steinmetz. Control of microtubule organization and dynamics: two ends in the limelight. *Nature Reviews Molecular Cell Biology*, 16(12):711–726, 2015. doi: 10.1038/nrm4084.

O. Akin, B. T. Bajar, M. F. Keles, M. A. Frye, and S. L. Zipursky. Cell-type-Specific Patterned Stimulus-Independent Neuronal Activity in the Drosophila Visual System during Synapse Formation. *Neuron*, 101(5):894–904, 2019. doi: 10.1016/j.neuron.2019.01.008.

M. J. Allen, T. A. Godenschwege, M. A. Tanouye, and P. Phelan. Making an escape: Development and function of the Drosophila giant fibre system. *Seminars in Cell and Developmental Biology*, 17(1):31–41, 2006. doi: 10.1016/j.semcdb.2005.11.011.

M. J. Almeida-Carvalho, D. Berh, A. Braun, Y.-c. Chen, K. Eichler, C. Eschbach, P. M. J. Fritsch, B. Gerber, N. Hoyer, X. Jiang, J. Kleber, C. Klämbt, C. König, M. Louis, B. Michels, A. Miroschnikow, C. Mirth, D. Miura, T. Niewalda, N. Otto, E. Paisios, M. J. Pankratz, M. Petersen, N. Ramsperger, N. Randel, B. Risse, T. Saumweber, P. Schlegel, M. Schleyer, P. Soba, S. G. Sprecher, T. Tanimura, A. S. Thum, N. Toshima, J. W. Truman, A. Yarali, and M. Zlatic. The Ol 1 mpiad: concordance of behavioural faculties of stage 1 and stage 3 Drosophila larvae. *The Journal of Experimental Biology*, 220(13):2452–2475, 2017. doi: 10.1242/jeb.156646.

G. A. Ascoli and J. L. Krichmar. L-neuron: A modeling tool for the efficient generation and parsimonious description of dendritic morphology. *Neurocomputing*, 32-33:1003–1011, 2000. doi: 10.1016/S0925-2312(00)00272-1.

G. A. Ascoli, D. E. Donohue, and M. Halavi. NeuroMorpho.Org: A central resource for neuronal morphologies, 2007.

M. Ashburner. Life Cycle. In *Drosophila: A Laboratory Handbook*, chapter 6, pages 122–206. Cold Spring Harbor Laboratory, Cold Spring Harbor, 2 edition, 2005.

L. Baltruschat, G. Tavosanis, H. Cuntz, C. Author, and H. Cuntz. A developmental stretch-and-fill process that optimises dendritic wiring. *bioRxiv*.

L. Beaulieu-Laroche, E. H. Toloza, M. S. van der Goes, M. Lafourcade, D. Barnagian, Z. M. Williams, E. N. Eskandar, M. P. Frosch, S. S. Cash, and M. T. Harnett. Enhanced Dendritic Compartmentalization in Human Cortical Neurons. *Cell*, 175(3):643–651.e14, 2018. doi: 10.1016/j.cell.2018.08.045.

H. J. Bellen, C. Tong, and H. Tsuda. 100 years of Drosophila research and its impact on vertebrate neuroscience: A history lesson for the future. *Nature Reviews Neuroscience*, 11(7):514–522, 2010. doi: 10.1038/nrn2839.

M. Bota and L. W. Swanson. The neuron classification problem. *Brain Research Reviews*, 56(1):79–88, 2007. doi: 10.1016/j.brainresrev.2007.05.005.

K. M. Brown, T. a. Gillette, and G. a. Ascoli. Quantifying neuronal size: Summing up trees and splitting the branch difference. *Seminars in Cell and Developmental Biology*, 19(6):485–493, 2008. doi: 10.1016/j.semcdb.2008.08.005.

N. Brunel, V. Hakim, and M. J. Richardson. Single neuron dynamics and computation, 2014.

R. E. Burke and W. B. Marks. Some Approaches to Quantitative Dendritic Morphology. pages 27–47. Humana Press, Totowa, New Jersey, 2002.

J. A. Campos-Ortega and V. Hartenstein. Stages of Drosophila Developement. In *The Embryonic Development of Drosophila Melanogaster*, chapter 2, pages 9–101. 1997.

C. E. Carr, S. Iyer, D. Soares, R. Kalluri, and J. Z. Simon. Are Neurons Adapted for Specific Computations? Examples from Temporal Coding in the Auditory System. In J. van Hemmen and T. Sejnowski, editors, *23 Problems in Systems Neuroscience*, chapter 12, pages 245–265. Oxford University Press, New York City, 1 edition, 2006.

M. S. Cembrowski and V. Menon. Continuous Variation within Cell Types of the Nervous System. *Trends in Neurosciences*, 41(6):337–348, 2018. doi: 10.1016/j.tins.2018.02.010.

E. P. Cervantes, C. H. Comin, R. M. C. Junior, and L. D. F. Costa. Morphological Neuron Classification Based on Dendritic Tree Hierarchy. *Neuroinformatics*, 17(1):147–161, 2018. doi: 10.1007/s12021-018-9388-7.

H. Chen, H. Xiao, T. Liu, and H. Peng. SmartTracing: self-learning-based Neuron reconstruction. *Brain Informatics*, 2(3):135–144, 2015. doi: 10.1007/s40708-015-0018-y.

L. E. Cheng, W. Song, L. L. Looger, L. Y. Jan, and Y. N. Jan. The Role of the TRP Channel NompC in Drosophila Larval and Adult Locomotion. *Neuron*, 67(3):373–380, 2010. doi: 10.1016/j.neuron.2010.07.004.

M. A. Chesarone and B. L. Goode. Actin nucleation and elongation factors: mechanisms and interplay. *Current Opinion in Cell Biology*, 21(1):28–37, 2009. doi: 10.1016/j.ceb.2008.12.001.

D. B. Chklovskii. Synaptic connectivity and neuronal morphology: two sides of the same coin. *Neuron*, 43(5):609–17, sep 2004. doi: 10.1016/j.neuron.2004.08.012.

H. T. Cline. Dendritic arbor development and synaptogenesis. *Current Opinion in Neurobiology*, 11:118–126, 2001.

C. H. Coles and F. Bradke. Coordinating Neuronal Actin-Microtubule Dynamics. *Current Biology*, 25(15):677–691, 2015. doi: 10.1016/j.cub.2015.06.020.

T. Copf. Impairments in dendrite morphogenesis as etiology for neurodevelopmental disorders and implications for therapeutic treatments. *Neuroscience and Biobehavioral Reviews*, 68:946–978, 2016. doi: 10.1016/j.neubiorev.2016.04.008.

M. M. Corty, B. J. Matthews, and W. B. Grueber. Molecules and mechanisms of dendrite development in Drosophila. *Development*, 136(7):1049–1061, 2009. doi: 10.1242/dev.014423.

F. Costa and Edson Tadeu Manoel Monteiro. A Percolation Approach to Neural Morphometry and Connectivity. *Neuroinformatics volume*, (1):65–80, 2003.

M. Crozatier and A. Vincent. Control of multidendritic neuron differentiation in Drosophila: The role of Collier. *Developmental Biology*, 315(1):232–242, 2008. doi: 10.1016/j.ydbio.2007.12.030.

H. Cuntz, J. Haag, and A. Borst. Neural image processing by dendritic networks. *PNAS*, 100(19): 11082–11085, sep 2003. doi: 10.1073/pnas.1830705100.

H. Cuntz, F. Forstner, J. Haag, and A. Borst. The morphological identity of insect dendrites. *PLoS Computational Biology*, 4(12):e1000251, dec 2008. doi: 10.1371/journal.pcbi.1000251.

H. Cuntz, F. Forstner, A. Borst, and M. Häusser. One rule to grow them all: A general theory of neuronal branching and its practical application. *PLoS Computational Biology*, 6(8), 2010. doi: 10.1371/journal.pcbi.1000877.

H. Cuntz, F. Forstner, A. Borst, and M. Häusser. The TREES toolbox—probing the basis of axonal and dendritic branching. *Neuroinformatics*, 9(1):91–96, mar 2011. doi: 10.1007/s12021-010-9093-7.

H. Cuntz, A. Mathy, and M. Häusser. A scaling law derived from optimal dendritic wiring. *Proceedings of the National Academy of Sciences*, 109(27):11014–11018, 2012. doi: 10.1073/pnas.1200430109.

H. Cuntz, M. W. Remme, and B. Torben-Nielsen. *The Computing Dendrite*, volume 11. Springer, 2014. doi: 10.1007/978-1-4614-8094-5.

M. E. Dailey and S. J. Smith. The Dynamics of Dendritic Hippocampal Slices Structure in Developing. *The Journal of Neuroscience*, 16(9):2983–2994, 1996.

P. Dayan and L. F. Abbott. *Theoretical Neuroscience: Computational and Mathematical Modeling of Neural Systems*. The MIT Press, Cambridge, Massachusetts, 1 edition, 2001.

E. De Schutter. Introduction. In E. De Schutter, editor, *Computational Modeling Methods for Neuroscientists*, chapter 1, pages IX–XII. The MIT Press, Cambridge, Massachusetts, 1 edition, 2009.

C. Delandre, R. Amikura, and A. W. Moore. Microtubule nucleation and organization in dendrites. *Cell Cycle*, 15(13):1685–1692, 2016. doi: 10.1080/15384101.2016.1172158.

W. Denk, K. L. Briggman, and M. Helmstaedter. Structural neurobiology: missing link to a mechanistic understanding of neural computation. *Nature reviews. Neuroscience*, 13(5):351–8, 2012. doi: 10.1038/nrn3169.

R. B. Dewell and F. Gabbiani. Linking dendritic processing to computation and behavior in invertebrates. In M. Häusser, N. Spruston, and G. J. Stuart, editors, *Dendrites*, chapter 23. Oxford University Press, 2017.

X. Dong, K. Shen, and H. E. Bülow. Intrinsic and Extrinsic Mechanisms of Dendritic Morphogenesis. *Annual review of physiology*, 77:271–300, 2014. doi: 10.1146/annurev-physiol-021014-071746.

D. E. Donohue and G. A. Ascoli. A comparative computer simulation of dendritic morphology. *PLoS Computational Biology*, 4(6):1–15, 2008. doi: 10.1371/journal.pcbi.1000089.

M. S. S. Dresselhaus, G. Dresselhaus, and A. Jorio. *Group Theory Application to the Physics of Condensed Matter*. Springer Science & Business Media, 1 edition, 2007.

J. P. Eberhard, A. Wanner, and G. Wittum. NeuGen: A tool for the generation of realistic morphology of cortical neurons and neural networks in 3D. *Neurocomputing*, 70(1-3):327–342, 2006. doi: 10.1016/j.neucom.2006.01.028.

K. Eichler, F. Li, A. Litwin-Kumar, Y. Park, I. Andrade, C. M. Schneider-Mizell, T. Saumweber, A. Huser, C. Eschbach, B. Gerber, R. D. Fetter, J. W. Truman, C. E. Priebe, L. F. Abbott, A. S. Thum, M. Zlatic, and A. Cardona. The complete connectome of a learning and memory centre in an insect brain. *Nature*, 548 (7666):175–182, 2017. doi: 10.1038/nature23455.

K. Emoto, R. Wong, E. Huang, and C. Hoogenraad. Introduction. In E. H. Kazuo Emoto, Rachel Wong and C. Hoogenraad, editors, *Dendrites - Development and Disease*, chapter 1, pages 3–8. Springer Japan, 1 edition, 2016. doi: 10.1007/978-4-431-56050-0.

T. Falk, D. Mai, R. Bensch, Ö. Çiçek, A. Abdulkadir, Y. Marrakchi, A. Böhm, J. Deubner, Z. Jäckel, K. Seiwald, A. Dovzhenko, O. Tietz, C. Dal Bosco, S. Walsh, D. Saltukoglu, T. L. Tay, M. Prinz, K. Palme, M. Simons, I. Diester, T. Brox, and O. Ronneberger. U-Net: deep learning for cell counting, detection, and morphometry. *Nature Methods*, 16(1):67–70, 2019. doi: 10.1038/s41592-018-0261-2.

K. Farrow, J. Haag, and A. Borst. Input organization of multifunctional motion-sensitive neurons in the blowfly. *The Journal of neuroscience : the official journal of the Society for Neuroscience*, 23(30):9805–9811, 2003.

Floreano, Dario and C. Mattiussi. *Bio-inspired artificial intelligence: theories, methods, and technologies*. MIT Press, 2008.

M. P. Forrest, E. Parnell, and P. Penzes. Dendritic structural plasticity and neuropsychiatric disease. *Nature Reviews Neuroscience*, 19(4):215–234, 2018. doi: 10.1038/nrn.2018.16.

L. Frenkel and M. Fernando Ceriani. *Recent advances in the use of Drosophila in neurobiology and neurodegeneration*, volume 99. 2011. doi: 10.1016/B978-0-12-387003-2.00005-7.

P. G. Fuerst, A. Koizumi, R. H. Masland, and R. W. Burgess. Neurite arborization and mosaic spacing in the mouse retina require DSCAM. *Nature*, 451(7177):470–474, 2008. doi: 10.1038/nature06514.

A. Fushiki, M. F. Zwart, H. Kohsaka, R. D. Fetter, A. Cardona, and A. Nose. A circuit mechanism for the propagation of waves of muscle contraction in Drosophila. *eLife*, 5:1–23, 2016. doi: 10.7554/eLife.13253.

F. Gabbiani, H. G. Krapp, C. Koch, and G. Laurent. Multiplicative computation in a visual neuron sensitive to looming. *Nature*, 420(6913):320–324, 2002. doi: 10.1038/nature01190.

S. Ganguly, O. Trottier, X. Liang, H. Bowne-Anderson, and J. Howard. Morphology of Fly Larval Class IV Dendrites Accords with a Random Branching and Contact Based Branch Deletion Model. *arXiv*, pages 1–12, 2016.

F. B. Gao, M. Kohwi, J. E. Brenman, L. Y. Jan, and Y. N. Jan. Control of dendritic field formation in Drosophila: the roles of flamingo and competition between homologous neurons. *Neuron*, 28(1):91–101, 2000. doi: 10.1016/S0896-6273(00)00088-X.

A. M. Garrett, A. Khalil, D. O. Walton, and R. W. Burgess. DSCAM promotes self-avoidance in the developing mouse retina by masking the functions of cadherin superfamily members. *Proceedings of the National Academy of Sciences of the United States of America*, 115(43):E10216–E10224, 2018. doi: 10.1073/pnas.1809430115.

W. Gerstner. *Spiking Neuron Models: Single Neurons, Populations, Plasticity*. Cambridge University Press, Cambridge, UK, 1 edition, 2002.

W. Gerstner, W. M. Kistler, R. Naud, and L. Paninski. Neuronal Dynamics. (October 2013):14–17, 2015. doi: 10.1017/CBO9781107447615.

S. F. Gilbert. The genetics of axis specification in Drosophila. In *Developmental Biology*. Sinauer Associates, Inc. Publishers, 6 edition, 2000. doi: 10.1016/0168-9525(89)90012-7.

T. M. Gomez and P. C. Letourneau. Actin dynamics in growth cone motility and navigation. *Journal of Neurochemistry*, 129(2):221–234, 2014. doi: 10.1111/jnc.12506.

N. Gompel and S. Chyb. *Atlas of Drosophila Morphology - Wild-type and Classical Mutants*. Academic Press, 1 edition, 2013. doi: 10.1016/B978-0-12-384688-4.00011-0.

I. Goodfellow, Y. Bengio, and A. Courville. Convolutional Networks. In *Deep Learning*, chapter 9, pages 330–372. MIT Press, 1 edition, 2016.

G. J. Goodhill. Theoretical Models of Neural Development, 2018.

B. Graham, A. Gillies, and D. Willshaw. *Principles of computational modelling in neuroscience*. Cambridge University Press, Cambridge, UK, 2011.

B. P. Graham and A. van Ooyen. Mathematical modelling and numerical simulation of the morphological development of neurons, 2006.

W. B. Grueber and Y. N. Jan. Dendritic development: Lessons from Drosophila and related branches. *Current Opinion in Neurobiology*, 14(1):74–82, 2004. doi: 10.1016/j.conb.2004.01.001.

W. B. Grueber and A. Sagasti. Self-avoidance and tiling: Mechanisms of dendrite and axon spacing. *Cold Spring Harbor perspectives in biology*, 2(9):1–16, 2010. doi: 10.1101/cshperspect.a001750.

W. B. Grueber, L. Y. Jan, and Y. N. Jan. Tiling of the Drosophila epidermis by multidendritic sensory neurons. *Development*, 129(12):2867–78, 2002a. doi: 10.1083/jcb.140.1.143.

W. B. Grueber, L. Y. Jan, and Y. N. Jan. Tiling of the Drosophila epidermis by multidendritic sensory neurons. *Development*, 129(12):2867–2878, 2002b.

W. B. Grueber, L. Y. Jan, and Y. N. Jan. Different levels of the homeodomain protein Cut regulate distinct dendrite branching patterns of Drosophila multidendritic neurons. *Cell*, 112(6):805–818, 2003a. doi: 10.1016/S0092-8674(03)00160-0.

W. B. Grueber, B. Ye, A. W. Moore, L. Y. Jan, and Y. N. Jan. Dendrites of distinct classes of Drosophila sensory neurons show different capacities for homotypic repulsion. *Current Biology*, 13(8):618–626, 2003b. doi: 10.1016/S0960-9822(03)00207-0.

W. B. Grueber, B. Ye, C.-H. Yang, S. Younger, K. Borden, L. Y. Jan, and Y.-N. Jan. Projections of Drosophila multidendritic neurons in the central nervous system: links with peripheral dendrite morphology. *Development*, 134(1):55–64, 2007. doi: 10.1242/dev.02666.

J. Guerguiev, T. P. Lillicrap, and B. A. Richards. Towards deep learning with segregated dendrites. *eLife*, 6:1–37, 2017. doi: 10.7554/eLife.22901.

Y. Guo, Y. Wang, W. Zhang, S. Meltzer, D. Zanini, Y. Yu, J. Li, T. Cheng, Z. Guo, Q. Wang, J. S. Jacobs, Y. Sharma, D. F. Eberl, M. C. Göpfert, L. Y. Jan, Y. N. Jan, and Z. Wang. Transmembrane channel-like (tmc) gene regulates Drosophila larval locomotion. *PNAS*, 113(26):7243–7248, 2016. doi: 10.1073/pnas.1606537113.

V. Haberle and B. Lenhard. Promoter architectures and developmental gene regulation, 2016.

M. Halavi, K. a. Hamilton, R. Parekh, and G. a. Ascoli. Digital reconstructions of neuronal morphology: three decades of research trends. *Frontiers in neuroscience*, 6(April):49, jan 2012. doi: 10.3389/fnins.2012.00049.

D. H. Hall and M. Treinin. How does morphology relate to function in sensory arbors? *Trends in Neurosciences*, 34(9):443–451, 2011. doi: https://doi.org/10.1016/j.tins.2011.07.004.

B. Han, R. Zhou, C. Xia, and X. Zhuang. Structural organization of the actin-spectrin–based membrane skeleton in dendrites and soma of neurons. *Proceedings of the National Academy of Sciences of the United States of America*, 114(32):E6678–E6685, 2017. doi: 10.1073/pnas.1705043114.

C. Han, D. Wang, P. Soba, S. Zhu, X. Lin, L. Y. Jan, and Y. N. Jan. Integrins Regulate Repulsion-Mediated Dendritic Patterning of Drosophila Sensory Neurons by Restricting Dendrites in a 2D Space. *Neuron*, 73(1):64–78, 2012. doi: 10.1016/j.neuron.2011.10.036.

E. Hannezo, C. L. Scheele, M. Moad, N. Drogo, R. Heer, R. V. Sampogna, J. van Rheenen, and B. D. Simons. A Unifying Theory of Branching Morphogenesis. *Cell*, 171(1):242–255.e27, 2017. doi: 10.1016/j.cell.2017.08.026.

B. A. Hassan and P. R. Hiesinger. Beyond Molecular Codes: Simple Rules to Wire Complex Brains. *Cell*, 163(2):285–291, 2015. doi: 10.1016/j.cell.2015.09.031.

D. Hattori, E. Demir, H. W. Kim, E. Viragh, S. L. Zipursky, and B. J. Dickson. Dscam diversity is essential for neuronal wiring and self-recognition. *Nature*, 449(7159):223–227, 2007. doi: 10.1038/nature06099.

Y. Hattori, T. Usui, D. Satoh, S. Moriyama, K. Shimono, T. Itoh, K. Shirahige, and T. Uemura. Sensory-neuron subtype-specific transcriptional programs controlling dendrite morphogenesis: Genome-wide analysis of abrupt and knot/collier. *Developmental Cell*, 27(5):530–544, 2013. doi: 10.1016/j.devcel.2013.10.024.

M. Häusser and B. Mel. Dendrites: Bug or feature? *Current Opinion in Neurobiology*, 13:372–383, 2003. doi: 10.1016/S0959-4388(03)00075-8.

M. Hausser, N. Spruston, and G. Stuart. The Future of Dendrite Research. In M. Hausser, N. Spruston, and G. Stuart, editors, *Dendrites*, chapter 25, pages 703–707. Oxford University Press, New York City, 3 edition, 2017.

L. He, S. Gulyanon, M. Mihovilovic Skanata, D. Karagyozov, E. S. Heckscher, M. Krieg, G. Tsechpenakis, M. Gershow, and W. D. Tracey. Direction Selectivity in Drosophila Proprioceptors Requires the Mechanosensory Channel Tmc. *Current Biology*, 29(6):945–956.e3, 2019. doi: 10.1016/j.cub.2019.02.025.

E. S. Heckscher, S. R. Lockery, and C. Q. Doe. Characterization of Drosophila Larval Crawling at the Level of Organism, Segment, and Somatic Body Wall Musculature. *Journal of Neuroscience*, 32(36):12460–12471, 2012. doi: 10.1523/JNEUROSCI.0222-12.2012.

W. Helfrich. Elastic properties of lipid bilayers: Theory and Possible Experiments. *Zeitschrift fur Naturforschung C*, 28:693–703, 1973.

M. Helmstaedter. Cellular-resolution connectomics: Challenges of dense neural circuit reconstruction. *Nature Methods*, 10(6):501–507, 2013. doi: 10.1038/nmeth.2476.

A. V. M. Herz, T. Gollisch, C. K. Machens, and D. Jaeger. Modeling Single-Neuron Dynamics Detail and Abstraction. *Science*, 314(5796):80–85, 2006.

P. R. Hiesinger and B. A. Hassan. The Evolution of Variability and Robustness in Neural Development. *Trends in Neurosciences*, 41(9):577–586, 2018. doi: 10.1016/j.tins.2018.05.007.

S. E. Hill, M. Parmar, K. W. Gheres, M. a. Guignet, Y. Huang, F. R. Jackson, and M. M. Rolls. Development of dendrite polarity in Drosophila neurons. *Neural Development*, 7(1):34, 2012. doi: 10.1186/1749-8104-7-34.

R. D. Hodge, T. E. Bakken, J. A. Miller, K. A. Smith, E. R. Barkan, L. T. Graybuck, J. L. Close, B. Long, N. Johansen, O. Penn, Z. Yao, J. Eggermont, T. Höllt, B. P. Levi, S. I. Shehata, B. Aevermann, A. Beller, D. Bertagnolli, K. Brouner, T. Casper, C. Cobbs, R. Dalley, N. Dee, S.-L. Ding, R. G. Ellenbogen, O. Fong, E. Garren, J. Goldy, R. P. Gwinn, D. Hirschstein, C. D. Keene, M. Keshk, A. L. Ko, K. Lathia, A. Mahfouz, Z. Maltzer, M. McGraw, T. N. Nguyen, J. Nyhus, J. G. Ojemann, A. Oldre, S. Parry, S. Reynolds, C. Rimorin, N. V. Shapovalova, S. Somasundaram, A. Szafer, E. R. Thomsen, M. Tieu, G. Quon, R. H. Scheuermann, R. Yuste, S. M. Sunkin, B. Lelieveldt, D. Feng, L. Ng, A. Bernard, M. Hawrylycz, J. W. Phillips, B. Tasic, H. Zeng, A. R. Jones, C. Koch, and E. S. Lein. Conserved cell types with divergent features in human versus mouse cortex. *Nature*, 573(7772):61–68, 2019. doi: 10.1038/s41586-019-1506-7.

C. C. Homem and J. A. Knoblich. Drosophila neuroblasts: A model for stem cell biology. *Development (Cambridge)*, 139(23):4297–4310, 2012. doi: 10.1242/dev.080515.

S. Hossain, D. Sesath Hewapathirane, and K. Haas. Dynamic morphometrics reveals contributions of dendritic growth cones and filopodia to dendritogenesis in the intact and awake embryonic brain. *Developmental Neurobiology*, 72(4):615–627, 2012. doi: 10.1002/dneu.20959.

J. Y. Hua and S. J. Smith. Neural activity and the dynamics of central nervous system development. *Nature neuroscience*, 7(4):327–332, 2004. doi: 10.1038/nn1218.

C. L. Hughes and J. B. Thomas. A sensory feedback circuit coordinates muscle activity in Drosophila. *Molecular and Cellular Neuroscience*, 35(2):383–396, 2007a. doi: 10.1016/j.mcn.2007.04.001.

C. L. Hughes and J. B. Thomas. A sensory feedback circuit coordinates muscle activity in Drosophila. *Molecular and Cellular Neuroscience*, 35(2):383–396, 2007b. doi: 10.1016/j.mcn.2007.04.001.

S. Inberg and B. Podbilewicz. Sensory experience controls dendritic structure and behavior by distinct pathways involving degenerins. *bioRxiv*, 436758, 2018. doi: http://dx.doi.org/10.1101/436758.

G. Indiveri, B. Linares-Barranco, T. J. Hamilton, A. van Schaik, R. Etienne-Cummings, T. Delbruck, S.-C. Liu, P. Dudek, P. Häfliger, S. Renaud, J. Schemmel, G. Cauwenberghs, J. Arthur, K. Hynna, F. Folowosele, S. Saighi, T. Serrano-Gotarredona, J. Wijekoon, Y. Wang, and K. Boahen. Neuromorphic silicon neuron circuits. *Frontiers in neuroscience*, 5(May):73, jan 2011. doi: 10.3389/fnins.2011.00073.

G. Jacobs, B. Claiborne, and K. Harris. Reconstruction of Neuronal Morphology. In E. D. Schutter, editor, *Computational Modeling Methods for Neuroscientists*, chapter 8, pages 211–232. The MIT Press, Cambridge, Massachusetts, 1 edition, 2009. doi: 10.7551/mitpress/9780262013277.001.0001.

Y.-N. Jan and L. Y. Jan. Branching out: mechanisms of dendritic arborization. *Nature reviews. Neuroscience*, 11(5):316–328, 2010. doi: 10.1038/nrn2854.

M. Januszewski, J. Kornfeld, P. H. Li, A. Pope, T. Blakely, L. Lindsey, J. Maitin-Shepard, M. Tyka, W. Denk, and V. Jain. High-precision automated reconstruction of neurons with flood-filling networks. *Nature Methods*, 15(8):605–610, 2018. doi: 10.1038/s41592-018-0049-4.

S. Jinushi-Nakao, R. Arvind, R. Amikura, E. Kinameri, A. W. Liu, and A. W. Moore. Knot/Collier and Cut Control Different Aspects of Dendrite Cytoskeleton and Synergize to Define Final Arbor Shape. *Neuron*, 56(6):963–978, 2007. doi: 10.1016/j.neuron.2007.10.031.

J. Jost. *Mathematical Methods in Biology and Neurobiology*. Springer, 1 edition, 2007.

L. Kanari, P. Dłotko, M. Scolamiero, R. Levi, J. Shillcock, K. Hess, and H. Markram. A Topological Representation of Branching Neuronal Morphologies. *Neuroinformatics*, 16(1):3–13, 2018. doi: 10.1007/s12021-017-9341-1.

E. R. Kandel, J. H. Schwartz, and T. M. Jessell. *Principles of Neural Science*. McGraw-Hill Education, 2012.

H. Kasai, M. Fukuda, S. Watanabe, A. Hayashi-Takagi, and J. Noguchi. Structural dynamics of dendritic spines in memory and cognition. *Trends in Neurosciences*, 33(3):P121–129, 2010. doi: https://doi.org/10.1016/j.tins.2010.01.001.

S. Katta, M. Krieg, and M. B. Goodman. Feeling Force: Physical and Physiological Principles Enabling Sensory Mechanotransduction. *Annual Review of Cell and Developmental Biology*, 31(1):347–371, 2015. doi: 10.1146/annurev-cellbio-100913-013426.

D. P. Kiehart, J. M. Crawford, A. Aristotelous, S. Venakides, and G. S. Edwards. Cell Sheet Morphogenesis: Dorsal Closure in Drosophila melanogaster as a Model System. *Annual Review of Cell and Developmental Biology*, 33(1):169–202, 2017. doi: 10.1146/annurev-cellbio-111315-125357.

M. D. Kim, Y. J. Lily, and N. J. Yuh. The bHLH-PAS protein spineless is necessary for the diversification of dendrite morphology of Drosophila dendritic arborization neurons. *Genes and Development*, 20(20):2806–2819, 2006. doi: 10.1101/gad.1459706.

M. E. Kim, B. R. Shrestha, R. Blazeski, C. A. Mason, and W. B. Grueber. Integrins Establish Dendrite-Substrate Relationships that Promote Dendritic Self-Avoidance and Patterning in Drosophila Sensory Neurons. *Neuron*, 73(1):79–91, 2012a. doi: 10.1016/j.neuron.2011.10.033.

Y. Kim, R. Sinclair, N. Chindapol, J. A. Kaandorp, and E. de Schutter. Geometric theory predicts bifurcations in minimal wiring cost trees in biology are flat. *PLoS Computational Biology*, 8(4), 2012b. doi: 10.1371/journal.pcbi.1002474.

H. Kimura, T. Usui, A. Tsubouchi, and T. Uemura. Potential dual molecular interaction of the Drosophila 7-pass transmembrane cadherin Flamingo in dendritic morphogenesis. *Journal of Cell Science*, 119(6):1118–1129, 2006. doi: 10.1242/jcs.02832.

T. Kobayashi, K. Terajima, M. Nozumi, M. Igarashi, and K. Akazawa. A stochastic model of neuronal growth cone guidance regulated by multiple sensors. *Journal of Theoretical Biology*, 266(4):712–722, 2010. doi: 10.1016/j.jtbi.2010.07.036.

C. Koch and I. Segev. The role of single neurons in information processing. *Nature Neuroscience*, 3(11s):1171–1177, nov 2000. doi: 10.1038/81444.

R. A. Koene, B. Tijms, P. Van Hees, F. Postma, A. De Ridder, G. J. Ramakers, J. Van Pelt, and A. Van Ooyen. NETMORPH: A framework for the stochastic generation of large scale neuronal networks with realistic neuron morphologies. *Neuroinformatics*, 7(3):195–210, 2009. doi: 10.1007/s12021-009-9052-3.

J. Kohl, A. D. Ostrovsky, S. Frechter, and G. S. Jefferis. A Bidirectional Circuit Switch Reroutes Pheromone Signals in Male and Female Brains. *Cell*, 155(7):1610–1623, 2013. doi: 10.1016/j.cell.2013.11.025.

A. Konietzny, J. Bär, and M. Mikhaylova. Dendritic Actin Cytoskeleton: Structure, Functions, and Regulations. *Frontiers in Cellular Neuroscience*, 11(May):1–10, 2017. doi: 10.3389/fncel.2017.00147.

J. Kornfeld and W. Denk. Progress and remaining challenges in high-throughput volume electron microscopy, 2018.

M. Krieg, A. R. Dunn, and M. B. Goodman. Mechanical control of the sense of touch by β-spectrin. Supplementary Material. *Nature cell biology*, 16(3):224–33, 2014. doi: 10.1038/ncb2915.

J. K. Krottje and A. V. Ooyen. A mathematical framework for modeling axon guidance. *Bulletin of Mathematical Biology*, 69(1):3–31, 2007. doi: 10.1007/s11538-006-9142-4.

A. V. Kuznetsov. Comparison of active transport in neuronal axons and dendrites. *Mathematical Biosciences*, 228(2):195–202, 2010. doi: 10.1016/j.mbs.2010.10.003.

S. Lawrence Zipursky and W. B. Grueber. The Molecular Basis of Self-Avoidance. *Annual Review of Neuroscience*, 36(1):547–568, 2013. doi: 10.1146/annurev-neuro-062111-150414.

Y. Lecun, Y. Bengio, and G. Hinton. Deep learning. *Nature*, 521(7553):436–444, 2015. doi: 10.1038/nature14539.

J. L. Lefebvre, J. R. Sanes, and J. N. Kay. Development of Dendritic Form and Function. *Annual Review of Cell and Developmental Biology*, 31(1):741–777, 2015. doi: 10.1146/annurev-cellbio-100913-013020.

J. Lefevre, K. M. Short, T. O. Lamberton, O. Michos, D. Graf, I. M. Smyth, and N. A. Hamilton. Branching morphogenesis in the developing kidney is governed by rules that pattern the ureteric tree. *Development*, 144:4377–4385, 2017. doi: 10.1242/dev.153874.

G. LeMasson, S. Przedborski, and L. F. Abbott. A Computational Model of Motor Neuron Degeneration. *Neuron*, 83(4):975–988, 2014. doi: 10.1016/j.neuron.2014.07.001.

M. Leptin. Gastrulation in Drosophila: the logic and the cellular mechanisms. *The EMBO Journal*, 18(12):3187–3192, 1999.

G. H. Li, C. De Qin, and L. W. Wang. Computer model of growth cone behavior and neuronal morphogenesis. *Journal of Theoretical Biology*, 174(4):381–389, 1995. doi: 10.1006/jtbi.1995.0106.

W. Li, F. Wang, L. Menut, and F. B. Gao. BTB/POZ-zinc finger protein abrupt suppresses dendritic branching in a neuronal subtype-specific and dosage-dependent manner. *Neuron*, 43(6):823–834, 2004. doi: 10.1016/j.neuron.2004.08.040.

X. Liang and J. Howard. Structural Biology: Piezo Senses Tension through Curvature, 2018.

X. Liang, J. Madrid, R. Gärtner, J. M. Verbavatz, C. Schiklenk, M. Wilsch-Bräuninger, A. Bogdanova, F. Stenger, A. Voigt, and J. Howard. A NOMPC-dependent membrane-microtubule connector is a candidate for the gating spring in fly mechanoreceptors. *Current Biology*, 23(9):755–763, 2013. doi: 10.1016/j.cub.2013.03.065.

X. Liang, J. Madrid, and J. Howard. The microtubule-based cytoskeleton is a component of a mechanical signaling pathway in fly campaniform receptors. *Biophysical Journal*, 107(12):2767–2774, 2014. doi: 10.1016/j.bpj.2014.10.052.

X. Liang, Z. Liu, and L. Sun. *Mechanosensory Transduction in Drosophila Melanogaster*. Springer Nature, Singapore, 1 edition, 2017.

M. London and M. Häusser. Dendritic computation. *Annual review of neuroscience*, 28:503–32, jan 2005. doi: 10.1146/annurev.neuro.28.061604.135703.

A. Luczak. Spatial embedding of neuronal trees modeled by diffusive growth. *Journal of Neuroscience Methods*, 157:132–141, 2006. doi: 10.1016/j.jneumeth.2006.03.024.

Z. F. Mainen and T. J. Sejnowski. Influence of dendritic structure on firing pattern in model neocortical neurons. *Nature*, 382(6589):363–6, jul 1996. doi: 10.1038/382363a0.

B. J. Matthews, M. E. Kim, J. J. Flanagan, D. Hattori, J. C. Clemens, S. Zipursky, and W. B. Grueber. Dendrite Self-Avoidance Is Controlled by Dscam. *Cell*, 129(3):593–604, 2007. doi: 10.1016/j.cell.2007.04.013.

W. S. McCulloch and W. Pitts. A logical calculus of the ideas immanent in nervous activity. *The Bulletin of Mathematical Biophysics*, 5(4):115–133, 1943. doi: 10.1007/BF02478259.

E. Meijering, O. Dzyubachyk, and I. Smal. Methods for cell and particle tracking. In *Methods in Enzymology*, volume 504, pages 183–200. 2012. doi: 10.1016/B978-0-12-391857-4.00009-4.

S. Meltzer, S. Yadav, J. Lee, P. Soba, S. H. Younger, P. Jin, W. Zhang, J. Parrish, L. Y. Jan, and Y. N. Jan. Epidermis-Derived Semaphorin Promotes Dendrite Self-Avoidance by Regulating Dendrite-Substrate Adhesion in Drosophila Sensory Neurons. *Neuron*, 89(4):741–755, 2016. doi: 10.1016/j.neuron.2016.01.020.

H. Memelli, B. Torben-Nielsen, and J. Kozloskiy. Self-referential forces are suffcient to explain different dendritic morphologies. *Frontiers in Neuroinformatics*, 6:1, 2013. doi: 10.3389/fninf.2013.00001.

G. Mitchison. Axonal trees and cortical architecture. *Trends in Neurosciences*, 15(4):122–126, 1992. doi: 10.1016/0166-2236(92)90352-9.

S. E. Mohr. *First in Fly: Drosophila Research and Biological Discovery*. Harvard University Press, Cambridge, Massachusetts, 1 edition, 2018.

M. F. Moody. *Structural Biology Using Electrons and X-rays: An Introduction for Biologists*. Academic Press, 1 edition, 2011.

S. Nanda, R. Das, S. Bhattacharjee, D. N. Cox, and G. A. Ascoli. Morphological determinants of dendritic arborization neurons in Drosophila larva. *Brain Structure and Function*, 223(3):1107–1120, 2018. doi: 10.1007/s00429-017-1541-9.

V. Nithianandam and C.-T. Chien. Actin blobs prefigure dendrite branching sites. *The Journal of cell biology*, page jcb.201711136, 2018. doi: 10.1083/jcb.201711136.

S. Okasha. *Philosophy of Science: Very Short Introduction*. Oxford University Press, Oxford, UK, 2016.

M. N. Özel, M. Langen, B. A. Hassan, and P. R. Hiesinger. Filopodial dynamics and growth cone stabilization in Drosophila visual circuit development. *eLife*, 4:1–21, 2015. doi: 10.7554/elife.10721.

Y. Park, V. Filippov, S. S. Gill, and M. E. Adams. Deletion of the ecdysis-triggering hormone gene leads to lethal ecdysis deficiency. *Development*, 129(2):493–503, 2002.

J. Z. Parrish, M. D. Kim, Y. J. Lily, and N. J. Yuh. Genome-wide analyses identify transcription factors required for proper morphogenesis of Drosophila sensory neuron dendrites. *Genes and Development*, 20 (7):820–835, 2006. doi: 10.1101/gad.1391006.

J. Z. Parrish, P. Xu, C. C. Kim, L. Y. Jan, and Y. N. Jan. The microRNA bantam Functions in Epithelial Cells to Regulate Scaling Growth of Dendrite Arbors in Drosophila Sensory Neurons. *Neuron*, 63(6): 788–802, 2009. doi: 10.1016/j.neuron.2009.08.006.

H. Peng, A. Bria, Z. Zhou, G. Iannello, and F. Long. Extensible visualization and analysis for multidimensional images using Vaa3D. *Nature Protocols*, 9(1):193–208, 2014. doi: 10.1038/nprot.2014.011.

Y. Peng, J. Lee, K. Rowland, Y. Wen, H. Hua, N. Carlson, S. Lavania, J. Z. Parrish, and M. D. Kim. Regulation of dendrite growth and maintenance by exocytosis. *Journal of Cell Science*, 128(23):4279–4292, 2015. doi: 10.1242/jcs.174771.

S. Polavaram, T. A. Gillette, R. Parekh, and G. A. Ascoli. Statistical analysis and data mining of digital reconstructions of dendritic morphologies. *Front Neuroanat*, 8(December):138, 2014. doi: 10.3389/fnana.2014.00138[doi].

J. F. Poulin, B. Tasic, J. Hjerling-Leffler, J. M. Trimarchi, and R. Awatramani. Disentangling neural cell diversity using single-cell transcriptomics. *Nature Neuroscience*, 19(9):1131–1141, 2016. doi: 10.1038/nn.4366.

R. C. Powell. *Symmetry, Group Theory, and the Physical Properties of Crystals*. Springer, 1 edition, 2010.

S. V. Puram and A. Bonni. Cell-intrinsic drivers of dendrite morphogenesis. *Development*, 140(23):4657–71, 2013. doi: 10.1242/dev.087676.

S. Ramon y Cajal. *Histology of the Nervous System of Man and Vertebrates*. Oxford University Press, Oxford, UK, 1 edition, 1995.

R. Real, M. Peter, A. Trabalza, S. Khan, M. A. Smith, J. Dopp, S. J. Barnes, A. Momoh, A. Strano, E. Volpi, G. Knott, F. J. Livesey, and V. De Paola. In vivo modeling of human neuron dynamics and down syndrome. *Science*, 362(6416), 2018. doi: 10.1126/science.aau1810.

B. A. Richards, T. P. Lillicrap, P. Beaudoin, Y. Bengio, R. Bogacz, A. Christensen, C. Clopath, R. P. Costa, A. de Berker, S. Ganguli, C. J. Gillon, D. Hafner, A. Kepecs, N. Kriegeskorte, P. Latham, G. W. Lindsay, K. D. Miller, R. Naud, C. C. Pack, P. Poirazi, P. Roelfsema, J. Sacramento, A. Saxe, B. Scellier, A. C. Schapiro, W. Senn, G. Wayne, D. Yamins, F. Zenke, J. Zylberberg, D. Therien, and K. P. Kording. A deep learning framework for neuroscience. *Nature Neuroscience*, 22(11):1761–1770, 2019. doi: 10.1038/s41593-019-0520-2.

M. Rivera-alba, H. Peng, G. G. D. Polavieja, and D. B. Chklovskii. Wiring economy can account for cell body placement across species and brain areas. *Current Biology*, 24(3):R109–R110, 2014. doi: 10.1016/j.cub.2013.12.012.

H. Robert E. Erosional development of streams and their drainage basins: hydro-physical approach to quantitative morphology. *Geological Society of America Bulletin*, 56(3):275–370, 1945.

S. Ryglewski, F. Vonhoff, K. Scheckel, and C. Duch. Intra-neuronal Competition for Synaptic Partners Conserves the Amount of Dendritic Building Material. *Neuron*, 93(3):632–645.e6, 2017. doi: 10.1016/j.neuron.2016.12.043.

C. Santiago and G. J. Bashaw. Transcription factors and effectors that regulate neuronal morphology. *Development*, 141(24):4667–4680, 2014. doi: 10.1242/dev.110817.

K. Saotome, S. E. Murthy, J. M. Kefauver, T. Whitwam, A. Patapoutian, and A. B. Ward. Structure of the mechanically activated ion channel Piezo1. *Nature*, 554(7693):481–486, 2017. doi: 10.1038/nature25453.

A. Schierwagen. Neuronal morphology: Shape characteristics and models. *Neurophysiology*, 40(4):310–315, 2008. doi: 10.1007/s11062-009-9054-7.

J. Schindelin, I. Arganda-Carreras, E. Frise, V. Kaynig, M. Longair, T. Pietzsch, S. Preibisch, C. Rueden, S. Saalfeld, B. Schmid, J. Y. Tinevez, D. J. White, V. Hartenstein, K. Eliceiri, P. Tomancak, and A. Cardona. Fiji: An open-source platform for biological-image analysis. *Nature Methods*, 9(7):676–682, 2012. doi: 10.1038/nmeth.2019.

P. Schlegel, M. Costa, and G. S. Jefferis. Learning from connectomics on the fly, 2017.

F. Schöck and N. Perrimon. Cellular processes associated with germ band retraction in Drosophila. *Developmental Biology*, 248(1):29–39, 2002. doi: 10.1006/dbio.2002.0698.

M. Schröter, O. Paulsen, and E. T. Bullmore. Micro-connectomics: probing the organization of neuronal networks at the cellular scale. *Nature Reviews Neuroscience*, 18(3):131–146, 2017. doi: 10.1038/nrn.2016.182.

E. K. Scott and L. Luo. How do dendrites take their shape? *Nature neuroscience*, 4(4):359–365, 2001. doi: 10.1038/86006.

I. Segev, J. Rinzel, and G. M. Shepherd. *The Theoretical Foundations of Dendritic Function: The Selected Papers of Wilfrid Rall with Commentaries*. The MIT Press, Cambridge, Massachusetts, 1 edition, 1994.

K. Shimono, A. Fujimoto, T. Tsuyama, M. Yamamoto-Kochi, M. Sato, Y. Hattori, K. Sugimura, T. Usui, K.-i. Kimura, and T. Uemura. Multidendritic sensory neurons in the adult Drosophila abdomen: origins, dendritic morphology, and segment- and age-dependent programmed cell death. *Neural development*, 4 (1):37, 2009. doi: 10.1186/1749-8104-4-37.

R. A. Silver. Neuronal arithmetic. *Nature reviews. Neuroscience*, 11(7):474–489, 2010. doi: 10.1038/nrn2864.

A. B. Simmons, S. J. Bloomsburg, J. M. Sukeena, C. J. Miller, Y. Ortega-Burgos, B. G. Borghuis, and P. G. Fuerst. DSCAM-mediated control of dendritic and axonal arbor outgrowth enforces tiling and inhibits synaptic plasticity. *Proceedings of the National Academy of Sciences*, page 201713548, 2017. doi: 10.1073/pnas.1713548114.

A. Singhania and W. B. Grueber. Development of the embryonic and larval peripheral nervous system of Drosophila. *Wiley interdisciplinary reviews. Developmental biology*, 3(3):193–210, 2015. doi: 10.1002/wdev.135.

J. Snider, A. Pillai, and C. F. Stevens. A Universal Property of Axonal and Dendritic Arbors. *Neuron*, 66 (1):45–56, 2010. doi: 10.1016/j.neuron.2010.02.013.

P. Soba, S. Zhu, K. Emoto, S. Younger, S. J. Yang, H. H. Yu, T. Lee, L. Y. Jan, and Y. N. Jan. Drosophila Sensory Neurons Require Dscam for Dendritic Self-Avoidance and Proper Dendritic Field Organization. *Neuron*, 54(3):403–416, 2007. doi: 10.1016/j.neuron.2007.03.029.

O. Sporns. *Networks of the Brain*. The MIT Press, Cambridge, Massachusetts, 1 edition, 2011.

N. Spruston. Pyramidal neurons: dendritic structure and synaptic integration. *Nature reviews. Neuroscience*, 9(3):206–21, mar 2008. doi: 10.1038/nrn2286.

A. Stepanyants and D. B. Chklovskii. Neurogeometry and potential synaptic connectivity. *Trends in neurosciences*, 28(7):387–94, jul 2005. doi: 10.1016/j.tins.2005.05.006.

A. Stepanyants, G. Tamas, and D. B. Chklovskii. Class-specific features of neuronal wiring. *Neuron*, 43(2): 251–259, 2004. doi: 10.1016/j.neuron.2004.06.013.

P. Sterling and S. Laughlin. *Neural Design*. MIT Press, Cambridge, Massachusetts, 1 edition, 2015.

G. J. Stuart and N. Spruston. Dendritic integration: 60 years of progress. *Nature Neuroscience*, 18(12): 1713–1721, 2015. doi: 10.1038/nn.4157.

K. Sugimura, M. Yamamoto, R. Niwa, D. Satoh, S. Goto, M. Taniguchi, S. Hayashi, and T. Uemura. Distinct developmental modes and lesion-induced reactions of dendrites of two classes of Drosophila sensory neurons. *The Journal of neuroscience*, 23(9):3752–3760, 2003. doi: 23/9/3752[pii].

K. Sugimura, D. Satoh, P. Estes, S. Crews, and T. Uemura. Development of morphological diversity of dendrites in Drosophila by the BTB-zinc finger protein abrupt. *Neuron*, 43(6):809–822, 2004. doi: 10.1016/j.neuron.2004.08.016.

U. Sümbül, S. Song, K. McCulloch, M. Becker, B. Lin, J. R. Sanes, R. H. Masland, and H. S. Seung. A genetic and computational approach to structurally classify neuronal types. *Nature Communications*, 5: 3512, 2014. doi: 10.1038/ncomms4512.

D. M. Suter and K. E. Miller. The emerging role of forces in axonal elongation. *Progress in Neurobiology*, 94 (2):91–101, 2011. doi: 10.1016/j.pneurobio.2011.04.002.

P. Szekely, H. Sheftel, A. Mayo, and U. Alon. Evolutionary Tradeoffs between Economy and Effectiveness in Biological Homeostasis Systems. *PLoS Computational Biology*, 9(8), 2013. doi: 10.1371/journal.pcbi.1003163.

W. Tadros, S. Xu, O. Akin, C. H. Yi, G. J. eun Shin, S. S. Millard, and S. L. Zipursky. Dscam Proteins Direct Dendritic Targeting through Adhesion. *Neuron*, 89(3):480–493, 2016. doi: 10.1016/j.neuron.2015.12.026.

B. Tasic, V. Menon, T. N. Nguyen, T. K. Kim, T. Jarsky, Z. Yao, B. Levi, L. T. Gray, S. A. Sorensen, T. Dolbeare, D. Bertagnolli, J. Goldy, N. Shapovalova, S. Parry, C. Lee, K. Smith, A. Bernard, L. Madisen, S. M. Sunkin, M. Hawrylycz, C. Koch, and H. Zeng. Adult mouse cortical cell taxonomy revealed by single cell transcriptomics. *Nature Neuroscience*, 19(2):335–346, 2016. doi: 10.1038/nn.4216.

B. Torben-Nielsen and E. De Schutter. Context-aware modeling of neuronal morphologies. *Frontiers in neuroanatomy*, 8:92, 2014. doi: 10.3389/fnana.2014.00092.

L. O. Trussell. Cellular mechanisms for preservation of timing in central auditory pathways. *Current Opinion in Neurobiology*, 7(4):487–492, 1997. doi: 10.1016/S0959-4388(97)80027-X.

M. S. Tyler. Development of the Fruit Fly. In *Devlopmental Biology. A Guide for Experimental Study*, chapter 8, pages 85–106. Sinauer Associates, Inc. Publishers, Sunderland, MA, 2000. doi: 10.1002/ajmg.1320590229.

H. B. Uylings and J. Van Pelt. Measures for quantifying dendritic arborizations. *Network: Computation in Neural Systems*, 13(3):397–414, 2002. doi: 10.1088/0954-898X_13_3_309.

R. D. Vaadia, W. Li, V. Voleti, A. Singhania, E. M. C. Hillman, and W. B. Grueber. Characterization of proprioceptive system dynamics in behaving Drosophila larvae using high-speed volumetric microscopy. *Current Biology*, 29(6):935–944, mar 2019. doi: 10.1016/j.cub.2019.01.060.

L. van der Maaten. Visualizing Data using t-SNE. *Journal of Machine Learning Research*, 9:2579–2605, 2008. doi: 10.1007/s10479-011-0841-3.

R. a. J. van Elburg and A. van Ooyen. Impact of dendritic size and dendritic topology on burst firing in pyramidal cells. *PLoS computational biology*, 6(5), may 2010. doi: 10.1371/journal.pcbi.1000781.

D. C. Van Essen. A tension-based theory of morphogenesis and compact wiring in the central nervous system. *Nature*, 385(6614):313–318, 1997. doi: 10.1038/385313a0.

A. van Ooyen. Formation of Dendritic Branching Patterns. In A. van Ooyen, editor, *Modeling neural development*, chapter 4, pages 75–93. MIT Press, Cambridge, Massachusetts, 2003.

A. van Ooyen. Using theoretical models to analyse neural development. *Nature reviews. Neuroscience*, 12 (6):311–26, 2011. doi: 10.1038/nrn3031.

A. Van Ooyen and D. J. Willshaw. Competition for neurotrophic factor in the development of nerve connections. *Proceedings of the Royal Society B: Biological Sciences*, 266(1422):883–892, 1999. doi: 10.1098/rspb.1999.0719.

A. Van Ooyen and D. J. Willshaw. Development of nerve connections under the control of neurotrophic factors: Parallels with consumer-resource systems in population biology. *Journal of Theoretical Biology*, 206(2):195–210, 2000. doi: 10.1006/jtbi.2000.2114.

A. Van Ooyen, B. P. Graham, and G. J.a. Ramakers. Competition for tubulin between growing neurites during development. *Neurocomputing*, 38-40:73–78, 2001. doi: 10.1016/S0925-2312(01)00487-8.

A. Van Ooyen, A. Carnell, S. De Ridder, B. Tarigan, H. D. Mansvelder, F. Bijma, M. De Gunst, and J. Van Pelt. Independently outgrowing neurons and geometry-based synapse formation produce networks with realistic synaptic connectivity. *PLoS ONE*, 9(1), 2014. doi: 10.1371/journal.pone.0085858.

M. van Veen and J. van Pelt. A model for outgrowth of branching neurites. *Journal of Theoretical Biology*, 159(1):1–23, 1992. doi: 10.1016/S0022-5193(05)80764-7.

L. Vanherpe, L. Kanari, G. Atenekeng, J. Palacios, and J. Shillcock. Framework for efficient synthesis of spatially embedded morphologies. *Physical Review E*, 94(2):1–9, 2016. doi: 10.1103/PhysRevE.94.023315.

A. VanHook and A. Letsou. Head involution in Drosophila: Genetic and morphogenetic connections to dorsal closure, 2008.

M. Vijayalakshmi. Drosophila melanogaster-Life Cycle. Technical report, 2012.

W. P. Volker Hartenstein, Shana Spindler and S. Fung. The Development of the Drosophila Larval Brain. In G. M. Technau, editor, *Brain Development in Drosophila melanogaster*, pages 1–29. Springer New York, New York, New York, USA, 1 edition, 2008. doi: https://doi.org/10.1007/978-0-387-78261-4.

H. Wang, Y. Rivenson, Y. Jin, Z. Wei, R. Gao, H. Günaydın, L. A. Bentolila, C. Kural, and A. Ozcan. Deep learning enables cross-modality super-resolution in fluorescence microscopy. *Nature Methods*, 16(1): 103–110, 2019. doi: 10.1038/s41592-018-0239-0.

Q. Wen, A. Stepanyants, G. N. Elston, A. Y. Grosberg, and D. B. Chklovskii. Maximization of the connectivity repertoire as a statistical principle governing the shapes of dendritic arbors. *Proceedings of the National Academy of Sciences of the United States of America*, 106(30):12536–41, jul 2009. doi: 10.1073/pnas.0901530106.

D. W. Williams and J. W. Truman. Mechanisms of dendritic elaboration of sensory neurons in Drosophila : Insights from in vivo time lapse. *Journal of Neuroscience*, 24(7):1541–1550, 2004. doi: 10.1523/JNEUROSCI.4521-03.2004.

L. Wolpert, R. Beddington, T. Jessell, P. Lawrence, E. Meyerowitz, and J. Smith. Development of the Nervous System. In L. Wolpert, editor, *Principles of Development*, chapter 11, pages 375–417. Oxford University Press, New York City, 2 edition, 2002.

C. Yalgin, S. Ebrahimi, C. Delandre, L. F. Yoong, S. Akimoto, H. Tran, R. Amikura, R. Spokony, B. Torben-nielsen, K. P. White, and A. W. Moore. Centrosomin represses dendrite branching by orienting microtubule nucleation. *Nature Neuroscience*, 18(10):1437–1445, 2015. doi: 10.1038/nn.4099.

D. L. Yamins and J. J. DiCarlo. Using goal-driven deep learning models to understand sensory cortex. *Nature Neuroscience*, 19(3):356–365, 2016. doi: 10.1038/nn.4244.

Z. Yan, W. Zhang, Y. He, D. Gorczyca, Y. Xiang, L. E. Cheng, S. Meltzer, L. Y. Jan, and Y. N. Jan. Drosophila NOMPC is a mechanotransduction channel subunit for gentle-touch sensation. *Nature*, 493(7431):221–225, 2012. doi: 10.1038/nature11685.

J. Yeon, J. Kim, D.-Y. Kim, H. Kim, J. Kim, E. J. Du, K. Kang, H.-H. Lim, D. Moon, and K. Kim. A sensory-motor neuron type mediates proprioceptive coordination of steering in C. elegans via two TRPC channels. *PLOS Biology*, 16(6):e2004929, 2018. doi: 10.1371/journal.pbio.2004929.

L. F. Yoong, Y. J. Pai, and A. W. Moore. Stages and transitions in dendrite arbor differentiation, 2019.

H. Zeng and J. R. Sanes. Neuronal cell-type classification: challenges, opportunities and the path forward. *Nature Reviews Neuroscience*, 18(9):530–546, 2017. doi: 10.1038/nrn.2017.85.

Q. Zhao, H. Zhou, S. Chi, Y. Wang, J. Wang, J. Geng, K. Wu, W. Liu, T. Zhang, M.-Q. Dong, J. Want, X. Li, and B. Xiao. Structure and mechanogating mechanism of the Piezo1 channel. *Nature*, 554(7693):1–17, 2016. doi: 10.1038/nature20555.

J. Zheng and M. C. Trudeau. *Handbook of Ion Channels*. CRC Press LLC, 1 edition, 2016. doi: 10.1201/b18027.

Z. Zheng, J. S. Lauritzen, E. Perlman, S. Saalfeld, R. D. Fetter, and D. D. Bock Correspondence. A Complete Electron Microscopy Volume of the Brain of Adult Drosophila melanogaster. *Cell*, 174(3):1–14, 2018. doi: 10.1016/j.cell.2018.06.019.

Appendix A

Scaling Relations

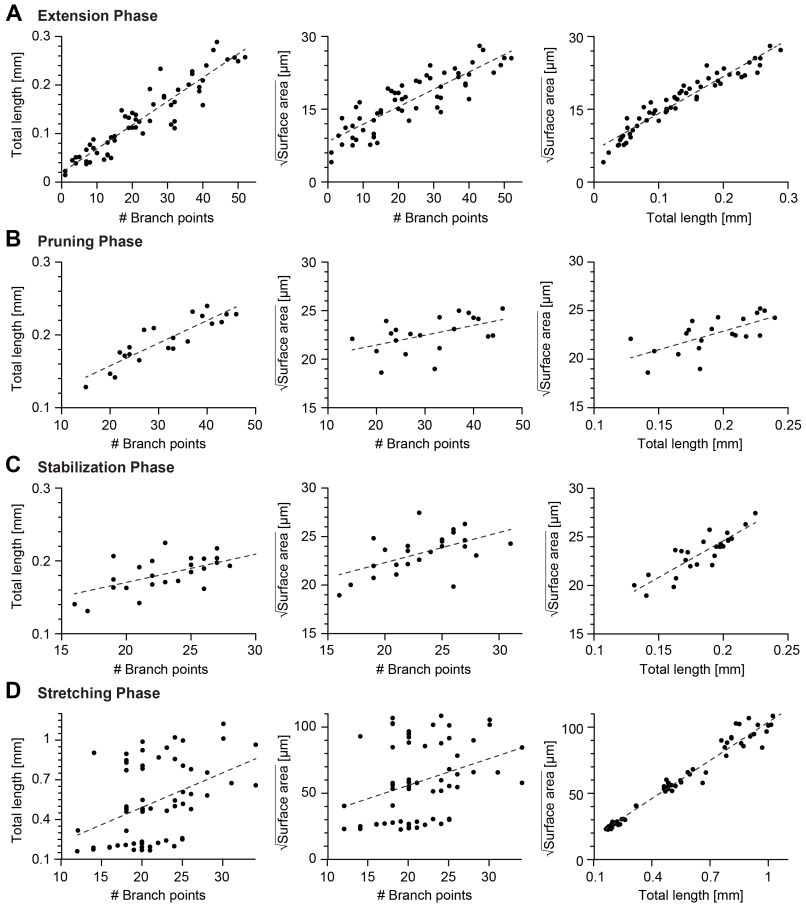

Figure A.1: **Morphological Scaling Relations During Development.**
A–D, Linear fits of the number of branch points vs total cable length, number of branch points vs the square root of the dendrite surface area (middle) and total cable length vs the square root of the dendrite surface area (right) during the extension, pruning, stabilization and scaling phases. In all panels, each black dot represents one reconstruction (overall $n = 165$) black dashed lines represent the best-fit.

Appendix B

Alignment Algorithm

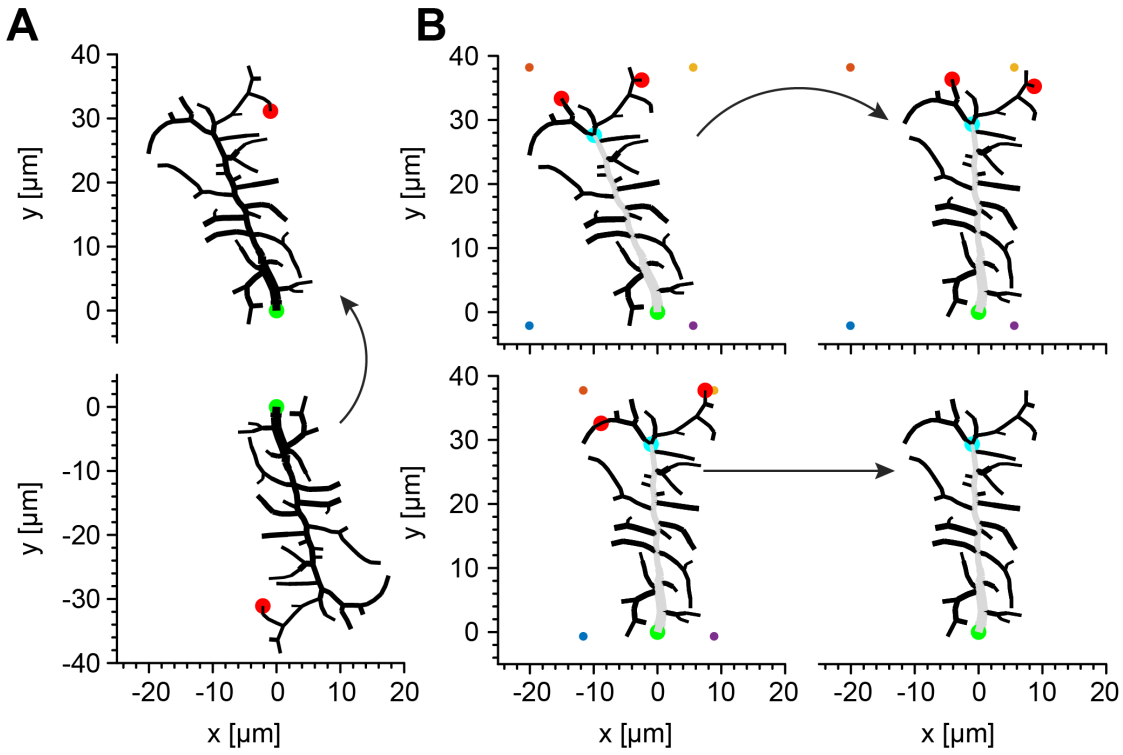

Figure B.1: **Illustration of the Alignment Algorithm.**

A, First, the algorithm translates the reconstruction of an arbitrary dendritic tree (bottom) by setting the root to x- and y-coordinates $(0, 0)$ and rotates it until the terminal of the longest path of the tree (red circle) is set to x-coordinate (0) and the y-coordinate is set to a positive value. **B**, At each new iteration a bounding box (coloured dots) is generated around the dendritic tree and the closest node to the top left corner, and to the top right corner are found (red cirlcles). The first common branch point in the paths of these nodes is defined as the provisional last node of the primary branch (light blue circle) and the tree is rotated until this node is set to x-coordinate (0). This procedure is repeated until the branch point of the primary branch in the current iteration is the same as the one in the previous iteration. In all panels, green circles represent the root of the dendritic tree and gray nodes represent the primary branch.

Appendix C

Calcium Imaging

(Continued on the following page due to figure size.)

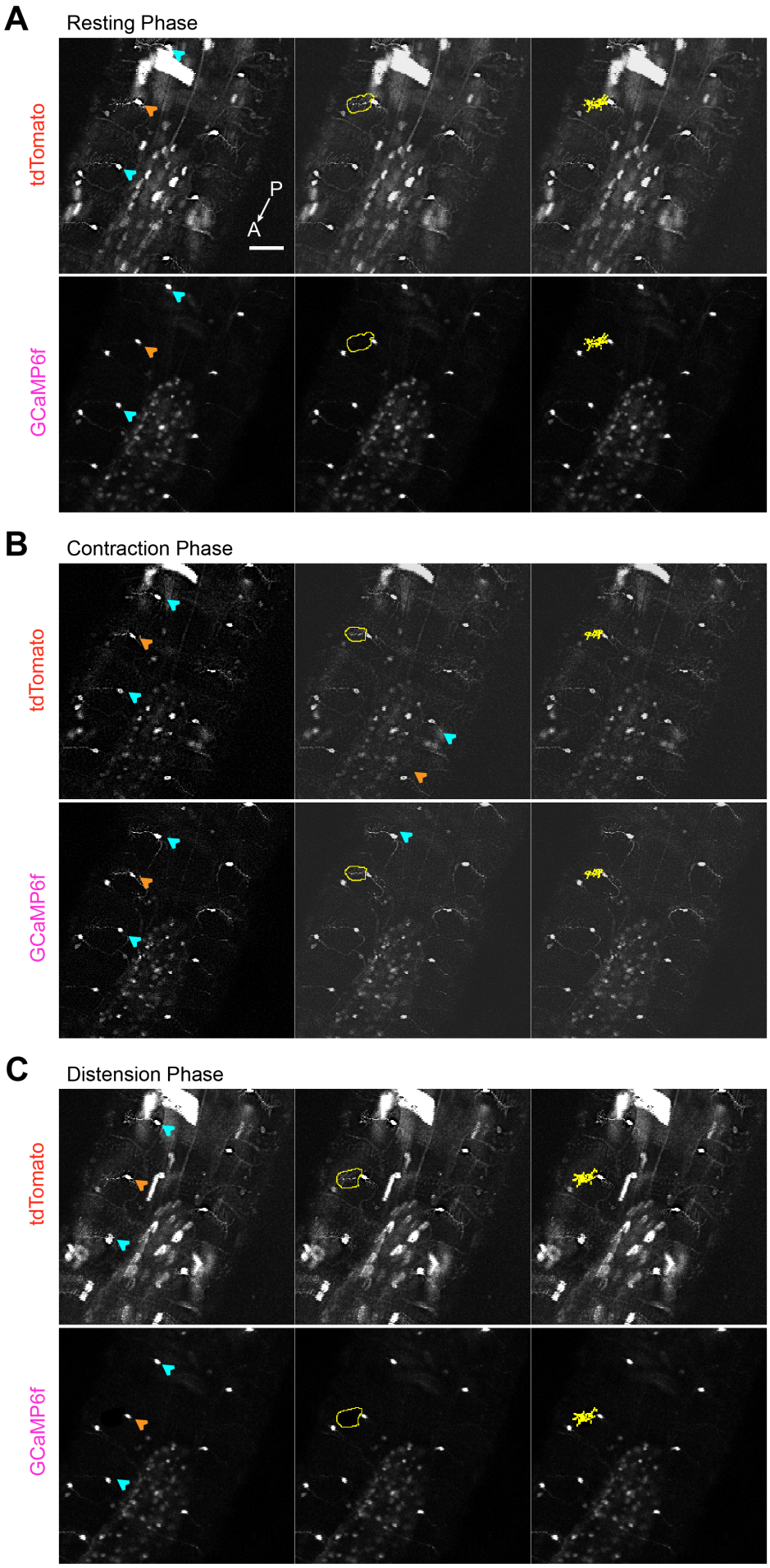

Figure C.1: **Functional Imaging During Forward Crawling.** (Continued on the following page.)

Figure C.1: Representative images of c1vpda cells using a dual line CD2-mCherry (top panels) and GCaMP6 (Bottom panels), showing the ventral view of the larval body during resting phase. The GCaMP6 signal was extracted from cell indicated by the orange arrow (left Panels). Illustrative rough ROI's (middle panels) used to generate the tight ROI's around the cells dendrites (rightmost panels). In **B**, images showing increased GCaMP6 activity in c1vpda dendrites during contraction, but in **C**, GCaMP6 activity decreased back to baseline during distension. Scale bar, $50\mu m$.

Appendix D

Curvature Quantification

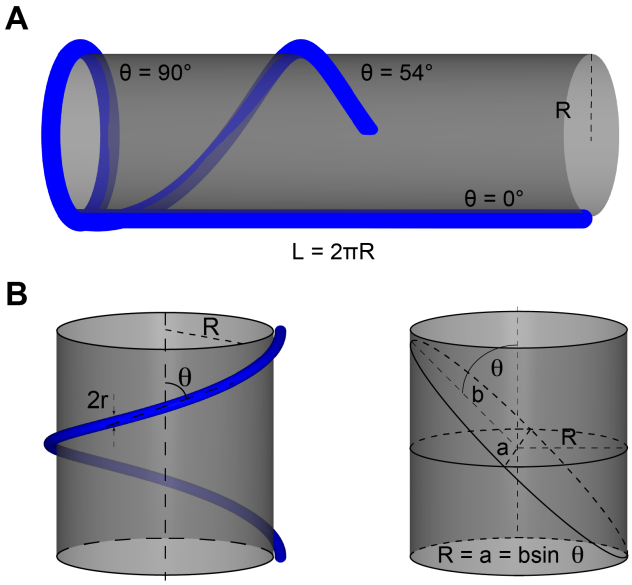

Figure D.1: **Tubular Structure Elliptical Profile Approximation to Circular Profiles.**
A, Sketch of tubular structures with different tilting angles deformed when wrapped around a cylindrical surface. **B**, Representation of tubular structure with diameter $2r$ with tilting angle θ wrapped around a cylinder with radius R (top panel). Illustrative elliptical profile of a tubular structure wrapped around a cylinder. b and a represent the radii of the ellipse.

Appendix E

No Pruning Model Simulations

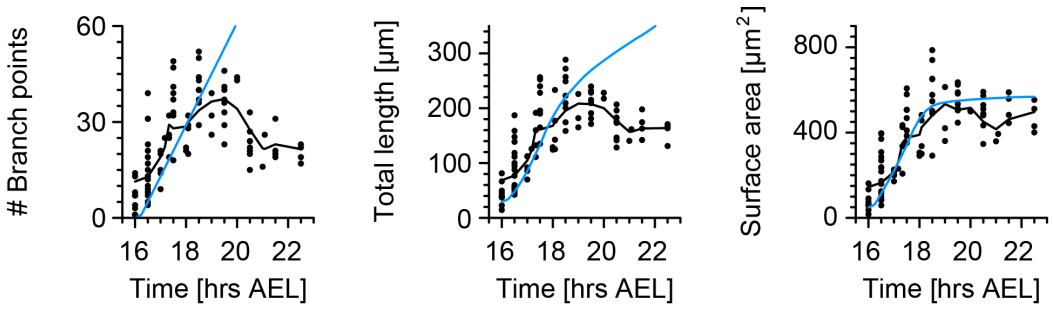

Figure E.1: **Growth Model Without Pruning Key Morphometrics Time Course.**
Growth model without pruning does not replicate c1vpda dendrite growth. Time course of the number of branch points (left), total length of dendrite cable (middle) and surface area (right) during embryonic development. Same arrangement and same data as in **Figure 4.6B** but for the growth model without pruning.